Control of Molecular Orientation in Solution-Cast Films of Cellulose Esters and Its Application to Optical Functional Films

KULTIDA SONGSURANG

Japan Advanced Institute of Science and Technology

Control of Molecular Orientation in Solution-Cast Films of Cellulose Esters and Its Application to Optical Functional Films

by

KULTIDA SONGSURANG

Submitted to
Japan Advanced Institute of Science and Technology
in partial fulfillment of the requirements
for the degree of
Doctor of philosophy

Supervisor: **Prof. Dr. Masayuki Yamaguchi**

School of Materials Science
Japan Advanced Institute of Science and Technology

March 2014

Referee-in-chief : **Professor Dr. Masayuki Yamaguchi**
Japan Advanced Institute of Science and Technology

Referees : **Professor Dr. Noriyoshi Matsumi**
Japan Advanced Institute of Science and Technology

Associate Professor Tatsuo Kaneko
Japan Advanced Institute of Science and Technology

Associate Professor Toshiaki Taniike
Japan Advanced Institute of Science and Technology

Professor Dr. Akihiro Tagaya
Keio University

Preface

Cellulose is the most abundant natural biopolymer and is readily available from renewable resources. Esterified cellulose is a highly flexible material as its properties can be varied by controlling the type and amount of the ester substituents during the chemical manufacturing process. Some cellulose esters have been applied as optical films for decades by virtue of their excellent properties such as high transparency and heat resistance. The cellulose ester used is mainly cellulose acetate, while the applications are rather limited to photographic films and protective films.

In this study, in-plane and out-of-planes birefringences in various types of cellulose esters including those prepared by solution-cast method was examined. Birefringence is an important property that defines the optical behavior of optical films. The information on the molecular orientation and the birefringence of a solution-cast film for cellulose triacetate were investigated. Incorporation of low-mass compound was also proposed as a mean to control three-dimensional orientation birefringence in cellulose esters. Moreover, effects of the type and amount of ester groups were investigated. It is expected that this thesis will contribute to a profound understanding regarding the mechanism for in-plane and out-of-plane birefringences in cellulose esters. This would open up possibilities of developing biopolymer-based optical films with birefringence suited for various functions in optical devices.

Kultida Songsurang

Contents

Chapter 1

General Introduction

1.1 Introduction

In recent years, conventional plastics have been widely used, which caused severe environmental problems with the increase in their waste. With mounting the environmental and legislative pressure to reduce plastic and packaging wastes, there has been an increased demand for biodegradable or biomass-based plastics that are compatible with the environment. Therefore, alternative materials that can be biodegraded emerge as the time and more environmentally friendly requires [1,2].

Cellulose is the most abundant biomass material in nature, and possesses some promising properties such as mechanical robustness, biocompatibility, biodegradability, low toxicity, and low cost [3,4]. Thus, cellulose has been widely applied in various fields such as food packaging, adhesive tape, membrane and various others [5]. Conversion of cellulose to its organic esters affords materials that are processable into various useful forms such as three dimensional objects, fibers and coating solutions [6-8]. One of the most important applications of cellulose esters is optical films such as polarizer protective films and retardation (compensation) films due to their excellent characteristic properties such as surface smoothness, homogeneity of thickness, high transparency, and high heat

resistance [5,9-13].

Optical films frequently exhibit birefringence as a result of processing operations such as injection-molding, extrusion, and drawing result from the orientation of polymeric chains forced in the flow direction [14]. As optical films usually deal with polarized light, *e.g*., in liquid crystal display (LCD) application, using a film with irregular birefringence degrades the performance of the optical devices [15,16]. Thus, it is necessary for optical films to have a certain birefringence characteristic when dealing with polarized light. Furthermore, the required birefringence characteristic differs according to its application. In the application as polarizer protective films, the films cover a polarizing film to protect it from mechanical damage, moisture and oxidation. In order to keep the polarizing condition of the light after passing through the polarizer, the films have to be free from birefringence. While, a retardation film, the films is placed on the liquid crystal cell and/ or polarizers to widen the viewing angle requires a specific orientation birefringence that increases with increasing wavelength [12,17].

Conventionally, optical films in LCD application are produced using solution-cast method, in which solvent is evaporated to obtain a film, to avoid the occurrence of irregular birefringence associated with extrusion process [10,18]. Therefore, the information on the molecular orientation and the birefringence of a solution-cast film are significantly important.

For optical anisotropic films, three refractive indices, n_x, n_y and n_z, along three principal axes have to be taken into consideration. The *x*-axis is the direction showing the maximum refractive index within the film plane in general, the *y*-axis is the direction

perpendicular to the *x*-axis within the film plane, and the z-axis is the thickness direction and is normal to the *x*–*y* plane.

It is well known that a solution-cast method provides films without molecular orientation in the film plane, *i.e.* $n_x = n_y$ [19]. This is the reason why a solution-cast film is preferably employed for a protective film rather than a melt-extruded one. However, the other component of birefringence, namely out-of-plane birefringence, is generally not zero. Therefore, it has to be precisely controlled to provide a high quality display.

In order to achieve a film with a controlled birefringence by solution-cast method, a modification of the polymeric material is necessary. Up to now, several methods such as polymer blending [20-22] or or a low-mass compound blending [23,24], copolymerization techniques [25], and anisotropic crystal doping [26] have been proposed to control the birefringence in polymeric materials, either for polarizer protection films or retardation films. These methods will be discussed further in this chapter.

This chapter covers the background information for this study. Firstly, fundamental information on the polymeric material dealt in this study, *i.e.*, cellulose esters is presented. Subsequently, descriptions of birefringence in polymeric materials are provided followed by explanation on optical films. Lastly, the justification and objective of the study will be described.

1.2 Cellulose Esters

1.2.1 Molecular Structure of Cellulose

Cellulose constitutes the most abundant and renewable polymer resource available worldwide. It is estimated that by photosynthesis, 10^{11}–10^{12} tons of cellulose are synthesized annually in a relatively pure form or combined with lignin and other polysaccharides in the cell wall of woody plants [27]. Cellulose is an organic compound with containing repeated cellobiose (disaccharide) segments with the formula of $(C_6H_{10}O_5)_n$. In nature, cellulose chains have a degree of polymerization (DP) of approximately 5,000 cellobiose units in wood cellulose and 7,500 in natural cotton cellulose [28].

Cellulose is a polydisperse linear homopolymers, consisting of β-1-4-glycosidic linked D-glucopyranose units. Figure 1.1 shows the molecular structure of cellulose as a carbohydrate polymer generated from repeating β- D-glucopyranose molecules that are covalently linked through acetal functions between the equatorial OH group of C_4 and the C_1 carbon atom (β-1,4-glucan), which is, in principle, the manner in which cellulose is biogenetically formed [29]. As a result, cellulose is an extensive, linear-chain polymer with a large number of hydroxy groups (three per anhydroglucose (AGU) unit) present in the thermodynamically preferred $^4C_1$ conformation. To accommodate the preferred bond angles of the acetal oxygen bridges, every second AGU ring is rotated 180° in the plane. In this manner, two adjacent structural units define the disaccharide cellobiose.

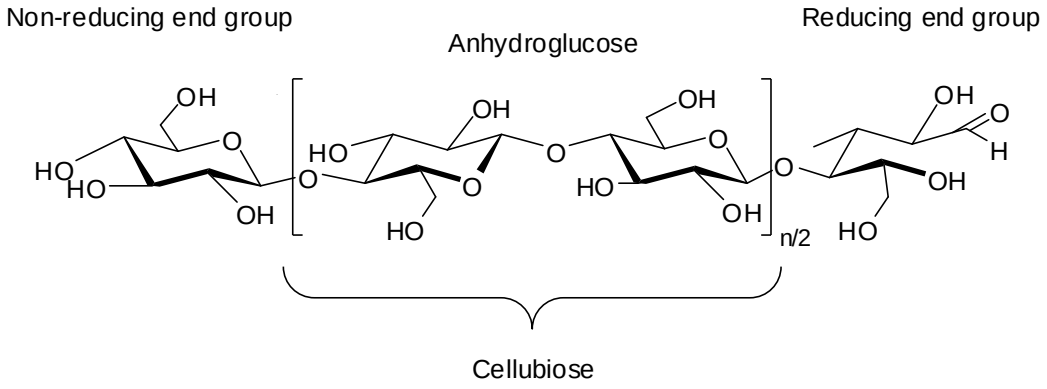

Figure 1.1 Chemical structure of cellulose [30]

Native cellulose does not exhibit thermoplasticity, due to strong intermolecular and intramolecular hydrogen bonding. It is poorly soluble in common solvents and is not melt-processable as it decomposes before undergoes melt flow. Conversion of cellulose to its esters affords materials that are processible into various useful forms. In fact, thermoplastic properties observed in common cellulosic plastics such as cellulose triacetate and cellulose acetate propionate, results from the esterification of cellulose [5,31,32].

1.2.2 Esterification of Cellulose

Organic cellulose esters, as modified cellulose, have gained special technical importance due to their wide range of properties. The esterification is performed in order to improve processability and to produce cellulose derivatives which can be tailored for specific industrial applications [33]. The existence of hydroxyl groups in cellulose chains allows for substitution groups to be incorporated into the cellulose chains by processes such as esterification or etherification [34]. For the esterification process,

the hydroxyl groups of cellulose are partially or fully reacted with carboxylic acids or other acylating agents to produce a cellulose ester.

During the formation of any particular cellulose derivatives, two reactions occur: a substitution reaction at the hydroxyl groups, and a glycosidic bond cleavage reaction. The physical and chemistry properties of cellulose derivatives are determined largely by the degree of substitution (DS) and the degree of polymerization (DP) [35]. The term degree of substitution is used to denote the extent of a reaction and is defined as the average of hydroxyl groups substituted out of the three available in the glucopyranose units and range from 0 to 3. Higher degrees of substitution, or reaction conditions which disrupt the crystalline regions, can be used to reduce interchain hydrogen bonding and force the chains apart. This results in a cellulose derivative that is soluble in common solvents, and capable for extrusion to form filaments or other structures [36].

Properties that are most strongly affected by changing the degree of substitution are the solubility, swelling and thermoplasticity. The thermoplasticity is increased by the substitution of non-polar groups, where the thermoplasticity increases with increasing the chain length of the substituent groups [35,37]. This is because the individual chains are forced further apart. For materials to be used for casting films, molding plastics and spraying lacquers, a reduced viscosity which is obtained by a lower degree of polymerization is required [36]. On the other hand, if the mechanical properties are important in the final product, a suitable degree of polymerization is required to balance between good processability while attaining acceptable mechanical properties.

1.2.3 Cellulose Esters of Acetic, Propionic and Butyric Acid

A cellulose ester (with all hydroxyl groups are replaced by acetyl groups) is called cellulose triacetate (CTA). (Fig. 1.2) CTA differs to cellulose diacetate (CDA) as during the manufacture of cellulose triacetate, the cellulose is completely acetylated whereas in regular cellulose diacetate, it is only partially acetylated [35,38]. According to the definition by the Federal Trade Commission, CTA refers to a cellulose ester with no less than 92 percent of the hydroxyl groups acetylated [39]. Cellulose triacetate is non toxic, odorless, tasteless and low flammable.

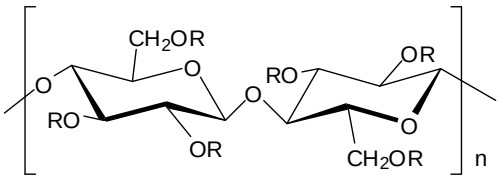

R = $COCH_3$ (CTA)
R = $COCH_3$, $COCH_2CH_3$ (CAP)
R = $COCH_3$, $COCH_2CH_2CH_3$ (CAB)

Figure 1.2 Chemical structure of some cellulose esters.

CTA is one of the most important cellulose esters in the cellulose acetate family. CTA is applied in various forms such as fiber, membrane and film. As a film, CTA shows a relatively high moisture regain, high degree of heat resistance, high transparency, low birefringence and moderate mechanical strength and has been widely used as photographic film and protective film for polarizing plate for decades [10,40,41].

Cellulose acetate propionate (CAP) and cellulose acetate butyrate (CAB) are two of the most important mixed cellulose esters currently available. In CAP and CAB, the acetyl group is grafted to the same cellulose backbone, with the propionyl or butyryl groups, respectively (Fig. 1.2). Thus, they confer additional properties compared to the homo-substituted cellulose esters. They have found many commercial uses as the

properties of the esters can be changed within certain limits to fit special purposes [42,43]. Compared to monocellulose esters such as cellulose acetate (CA), CAB and CAP have a number of advantages, such as excellent solubility, structural stability, light and weather resistance, good leveling, high gloss retention, good transparency, high moisture resistance and a low glass transition temperature [30,44,45]. They are widely used in the paint industry for top grade cars and furniture, as well as printing ink.

1.3 Birefringence

1.3.1 Refractive Index

Refractive index is an intrinsic property of materials, which governs the velocity of light in a given material. Refractive index, n can be expressed by

$$n = c/v \tag{1.1}$$

where c is light velocity in vacuum, and v is light velocity in a given body [46]. In other words, light transmits slower in a body with a high refractive index than that with a low refractive index (Fig. 1.3). A light moving in a polymeric material with a refractive index of 1.5 is 1.5 times slower than a light moving in a vacuum.

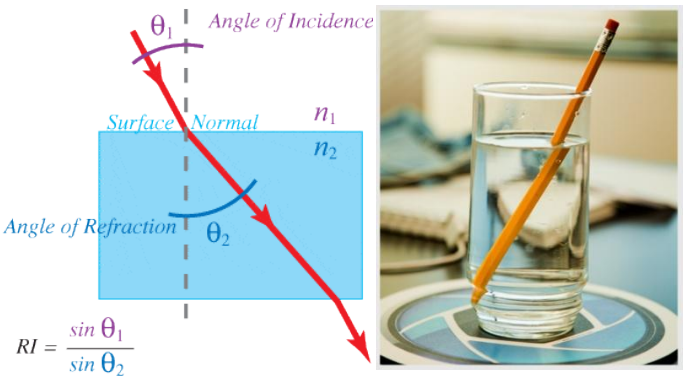

Figure 1.3 A phenomenon of refractive index difference.

Light is an electromagnetic wave with both electric and magnetic field components that oscillate in phase perpendicular to each other and perpendicular to the direction of wave propagation [47,48]. As a light ray passes through a material having highly polarizable molecular structure, electron polarization having the same frequency to the oscillating electric field of the light occurs. For example, electron polarization of the π-electron in the benzene rings of polystyrene as light ray passes. As the light progresses, electron polarization propagates to the neighboring benzene ring and the process continues. As the process involves innumerous benzene rings present in the material, the light velocity becomes slower compared when it travels in vacuum [49,50].

The refractive index, n in a material is related to the volume and electron density. The relation between refractive index and molecular structure is based on the Lorentz-Lorenz equation and can be expressed by the equations below [51-53]:

$$\frac{n^2-1}{n^2+2}=\frac{4}{3}\pi N\alpha\equiv\frac{[R]}{V}\equiv\phi \tag{1.2}$$

$$n=\sqrt{\frac{2\phi+1}{1-\phi}} \tag{1.3}$$

where N is the number of molecules per unit volume, α is polarizability, $[R]$ is molecular refraction, and V is molecular volume ($V = M/\rho$, where M is molecular mass and ρ is density). Furthermore, incorporation of any of these molecules: aromatic ring, element from halogen group (except fluorine) or sulfur into a material increases its refractive index, while incorporation of fluorine decreases it [54,55].

1.3.2 Birefringence in Polymers

Birefringence is defined as the double refraction of light when it passes through a transparent and anisotropic material [56,57]. It also refers to the difference between two refractive indices in anisotropic materials [58,59]. The structure of a birefringent material is such that it has an axis of symmetry called optical axis, with no equivalent axis in the plane perpendicular to it. When light travels on the optical axis of anisotropic crystals, it behaves in a manner similar to the interaction with isotropic crystals, and passes through at a single velocity [60,61].

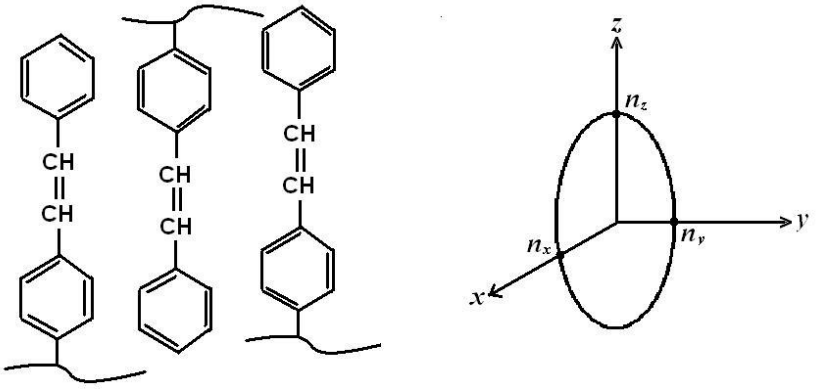

Figure 1.5 Polarizability ellipsoid of stilbene structure

However, when light travels on a non-equivalent axis, it is refracted into two rays; each polarized with the vibration directions oriented mutually perpendicular to one another and traveling at different velocities [50,62]. Light with linear polarizations parallel and perpendicular to the optical axis has different indices of refraction, denoted as n_e and n_o where the suffixes stand for extraordinary and ordinary, respectively. The difference in refractive index, or birefringence, Δn between the extraordinary and ordinary rays traveling through an anisotropic crystal is a measurable quantity, and can be

expressed by the equation [59,63,64]:

$$\Delta n = n_e - n_o \tag{1.4}$$

Birefringence in polymers can be explained by using polarizability ellipsoid model. The refractive index of a light when the polarization plane, *i.e.*, electric field plane is parallel to *x*, *y* or *z*-axis, is given as n_x, n_y and n_z respectively. The polarizability ellipsoid of stilbene groups oriented in longitudinal (*z*-axis) direction due to their conjugate bonding is shown in Fig. 1.5. The polarizability anisotropy in *z*-axis is higher than that in *x* or *y*-axis direction ($n_z > n_x = n_y$).

If a birefringent polymer receives an incident light from an oblique direction as shown in Fig. 1.6(a), the birefringence can be expressed by the cross-sectional surface of polarizability ellipsoid that contain the cut perpendicularly to the wave propagation direction at the origin. The incident light polarization wave will be separated into two; one in the direction of largest polarizability, and another one perpendicular to it. The refractive index of these two polarization waves is represented by the long and short axes of the cross-sectional surface and denoted as n_e and n_o in the Fig. 1.6(a). The birefringence Δn, when the incident light comes from this particular direction can be expressed by the equation 1.4 above. In this case, $n_z > n_e > n_x$, $n_x = n_o$.

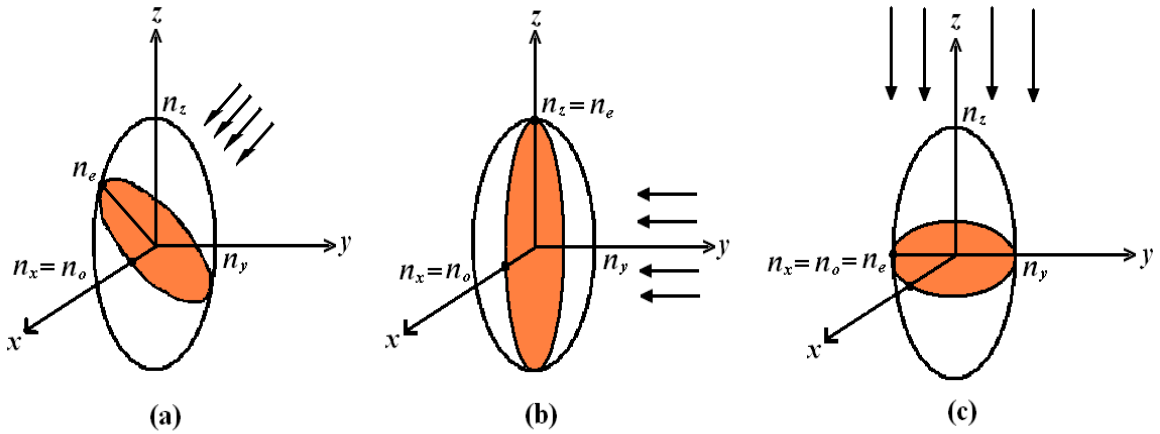

Figure 1.6 Birefringence and its directional dependence

On the other hand, if the incident light comes from the *y*-axis direction, birefringence can be represented by the cross-sectional surface shown in Fig. 1.6(b) and expressed as

$$\Delta n = n_e - n_o = n_z - n_x \tag{1.5}$$

which is the highest value of birefringence possible in this case. Furthermore, if the incident light comes from a direction parallel to the *z*-axis as shown in Fig. 1.6(c), which is parallel to the long axis of the polarizability ellipsoid, the birefringence becomes

$$\Delta n = n_e - n_o = 0 \tag{1.6}$$

which means no birefringence occurs.

The diagram when a linearly polarized light passing through a birefringent material at 45 degree angle to the *z*-axis is illustrated in Fig. 1.7. As a polarized light enters a birefringent material, it is decomposed into two polarization waves with a plane parallel to *y* and *z*-axis respectively. Upon exiting the material, the polarization waves recombine into a single ray but with a different optical characteristic, which is determined

by the phase difference or phase retardation of the two polarization waves. In an isotropic material, there is no phase retardation; hence the polarization of the exiting light is equal to that of the entering light as shown in Fig. 1.7(a). For an anisotropic material with a phase retardation of a quarter wavelength (λ/4), the exiting light will be transformed into a circularly polarized light as shown in Fig. 1.7(b) [65,66]. Moreover, a half wavelength (λ/2) of phase retardation will produce a linearly polarized light but with an angle of -45 degree to the *z*-axis. Retardation, *R* is an important parameter in the design of optical films and given as the product of birefringence, Δ*n* and film thickness, *d* [67-69]:

$$R = d\Delta n \tag{1.7}$$

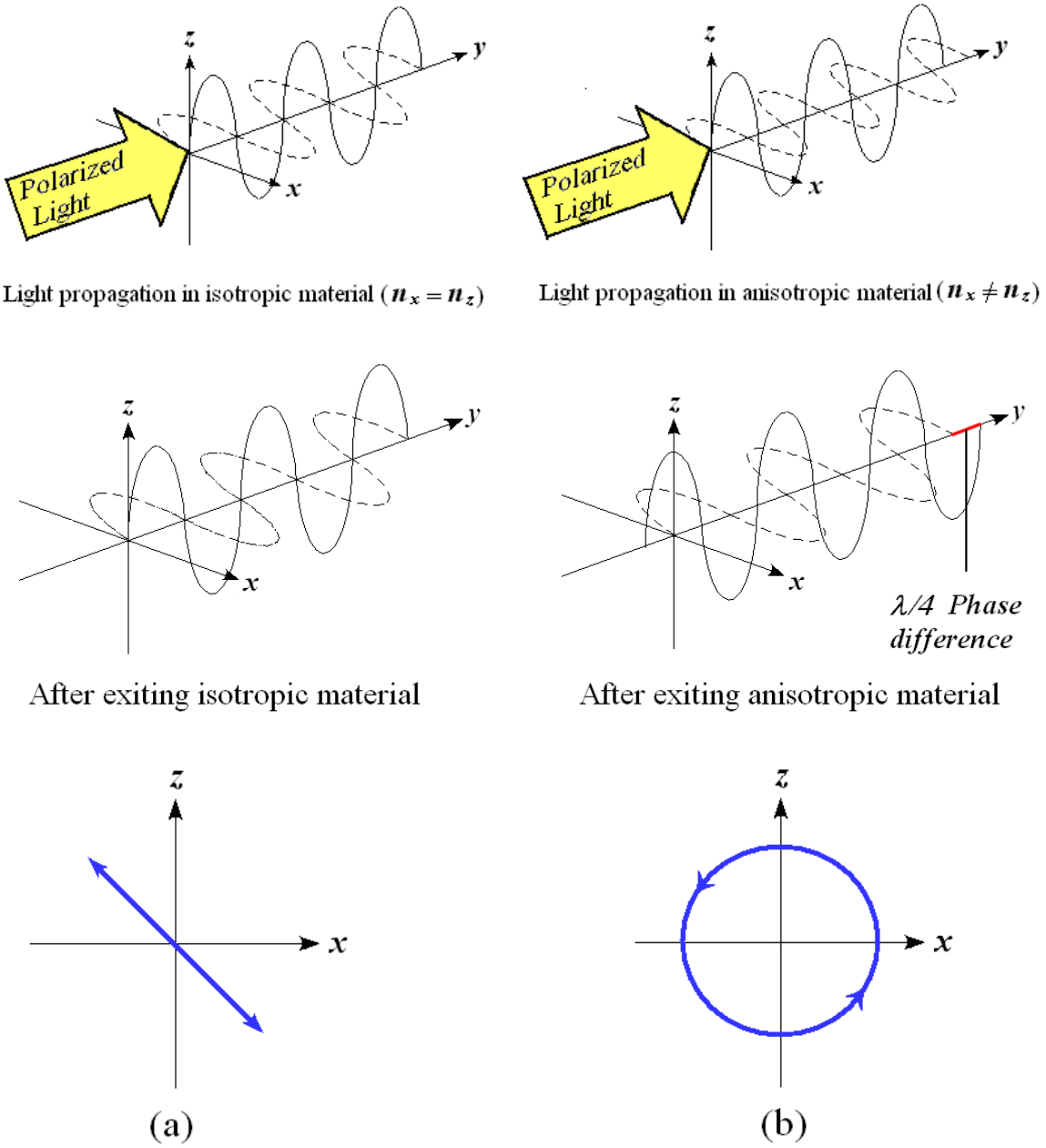

Figure 1.7 Polarized light properties with isotropic and anisotropic materials

1.3.3 In-plane and Out-of-plane Birefringence

Many optical materials as well as oriented polymer films exhibit physical properties which are different in different directions. When a beam of light enters such anisotropic medium, it is, in general, divided into two parts which are refracted in different directions. This optical anisotropy is often referred to as birefringence or double refraction.

Birefringence is an intrinsic property of many optical materials, and may also be induced by external forces applied to the material. The induced birefringence may be temporary, as when the material is oscillated, or the birefringence may be residual, as may happen when, for example, the material undergoes thermal stress during production of the material.

Retardation represents the integrated effect of birefringence acting along the path of a light beam that traverses a sample of the optical material. If the incident light beam is linearly polarized, the two orthogonal components of the polarized light will exit the sample with a phase difference, called the retardation. The fundamental unit of retardation is length, such as nanometers (nm). It is frequently convenient, however, to express retardation in units of phase angle (waves, radians, or degrees), which is proportional to the retardation (nm) divided by the wavelength of the light (nm). An "average" birefringence for a sample is sometimes computed by dividing the measured retardation magnitude by the thickness of the sample.

The two orthogonal, polarized beam components mentioned above are parallel to two orthogonal axes associated with the optical material, which axes are referred to as

the “fast axis” and the “slow axis.” The fast axis is the axis of the material that aligns with the faster moving component of the polarized light through the sample. Therefore, a complete description of the retardation of a sample along a given optical path requires specifying both the magnitude of the retardation and the relative angular orientation of the fast (or slow) axis of the sample.

The need for precise measurement of birefringence properties has become increasingly important in a number of technical applications. For instance, it is important to specify linear birefringence in optical elements that are used in high-precision instruments employed in semiconductor and other industries.

According to previous study [70], birefringence measurement system, hereby incorporated by reference, discloses methods and apparatus for measuring birefringence of a sample using a light beam that is directed through the sample at a normal (zero-degree) incidence angle relative to the surface of the sample. As a result, the determination of the sample’s birefringence is “in-plane,” meaning that the determination essentially represents the difference between the indices of refraction of two orthogonal axes in a plane of the sample, that plane being normal to the incident light beam.

The effect of birefringence on displayed visible light (such effects occurring, for example, when the light passes through an optical film or coating) may be to reduce contrast or alter colors. Also, with many materials, such as those used with liquid crystal display (LCD) panels, the extent or magnitude of birefringence is a function of the incident angle of the light under consideration. For example, increasing (from normal)

the viewing angle of a LCD panel will increase the birefringence effect on the light emanating from the panel and, without compensation, reduce the perceived quality of the visible light by reducing contrast and/or altering colors.

Transparent polymer films have been developed for use with LCD panels for the purpose of compensating for the just noted birefringence variations attributable to viewing angle. In short, these films possess birefringence characteristics that compensate for the birefringence of the LCD panel and thus provide a wide viewing angle without significant loss of contrast or color.

It is important to properly characterize the birefringence of such films, and other optical materials, in planes that are parallel to the normal (zero-degree) angle of incidence. This birefringence measure can be referred to as "vertical" or "out-of-plane" birefringence. One can consider the notion of in-plane and out-of-plane birefringences in terms of a Cartesian coordinate system. Accordingly, if the normal-incidence light is considered to travel in a direction parallel to the *z*-axis of such a coordinate system, the in-plane birefringence occurs in the *x*-*y* plane of the sample. Out-of-plane birefringence is in a plane perpendicular to the in-plane birefringence, thus occurring in the *x*-*z* or *y*-*z* plane.

Moreover, birefringence is produced in polymeric films by stretching [71-73]. Unstretched films are isotropic as the polymeric chains are randomly orientated and show no difference of refractive index irrespective of direction. The residue birefringence produced in films stretched at high temperature and subsequently quenched is called orientation birefringence. The polymeric chains which are forced to

orientate at a specific direction by stretching at high temperature are frozen by quenching. In other words, orientation birefringence is resulted from the frozen state of the molecular orientation upon being quenched [74]. On the other hand, birefringence that is observed upon bending or stretching of polymeric materials in a glassy state is called photoelastic birefringence [75,76].

Monomer units that constitute long polymeric chains, to a lesser or greater extent, do have polarizability anisotropy [77]. At certain direction from the tangential line of the long chains, the polarizability becomes largest. Fig. 1.8 shows monomers having the highest polarizability in the direction perpendicular to the main chains. When the polymeric chains are in random positions, the polarizability anisotropy of the monomer units cancels each others, thus the overall polarizability anisotropy becomes zero as shown in Fig. 1.8(a) [78,79]. Upon being stretched, polymeric chains are orientated in a particular direction, and the macroscopic view of monomer units shows a particular direction of orientation, hence the observed polarizability anisotropy as shown in Fig. 1.8(b).

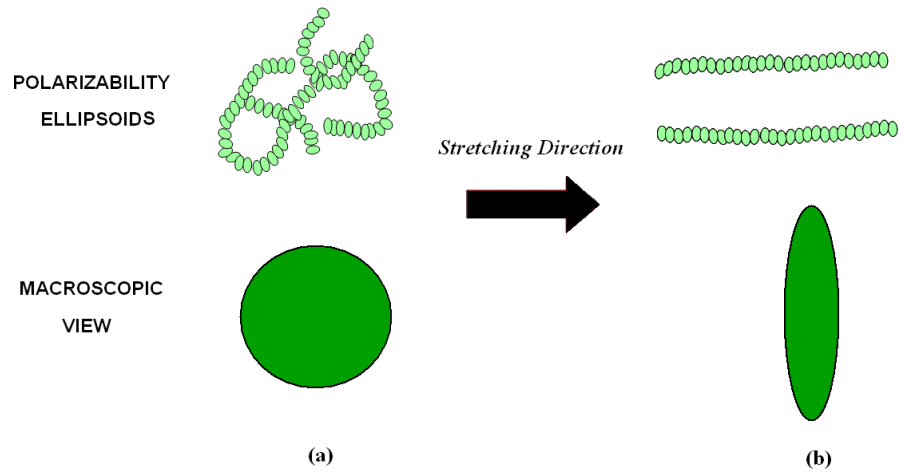

Figure 1.8 Birefringence associated with the orientation of polymeric chains

Generally, the orientation birefringence resulted from the orientation of polymeric chains can be expressed by the equation below [59,64,80]:

$$\Delta n = n_{//} - n_{\perp} \tag{1.8}$$

where $n_{//}$ and $n_{\perp}$ are refractive index parallel and perpendicular to the stretching direction, respectively. $n_{//}$ and $n_{\perp}$ correspond to the n_e and n_o in the equation 1.4-1.6 above.

Intrinsic birefringence, n^0 has been used as an indicator for orientation birefringence. It is defined as the birefringence when polymeric chains are completely orientated and can be expressed as [81,82]:

$$\Delta n = \Delta n^0 F \tag{1.9}$$

where F represents orientation factor. The intrinsic birefringence is determined by the size of the structural unit and its degree of anisotropy. Furthermore, intrinsic birefringence can be given by the following equation [46,83]:

$$\Delta n^0 = \frac{2\pi}{9}.\frac{\left(\bar{n}^2+2\right)^2}{\bar{n}}.\frac{\rho}{M}.N_A\Delta\alpha \tag{1.10}$$

$$\Delta\alpha = \alpha_x - \frac{\alpha_y + \alpha_z}{2} \tag{1.11}$$

where ρ is density, N_A is Avogadro's number, $\bar{n}$ is average refractive index, M is molecular mass per unit molecule and α is polarizability for each direction.

As for the orientation factor F, it is related to the angle that a segment makes with the stretching axis θ as below [84,85]:

$$F = \frac{3\left\langle \cos^2\theta \right\rangle - 1}{2} \tag{1.12}$$

Furthermore, the orientation factor can be expressed by the dichroic ratio D ($\equiv A_{||}/A_{\perp}$) as follows [86,87]:

$$F = \frac{D-1}{D+2} \cdot \frac{2\cot^2 \alpha + 1}{2\cot^2 \alpha - 1} \tag{1.13}$$

where α is the angle between the transition moment vector $\boldsymbol{M}$ of the absorbing group and the chain axis as shown in Fig. 1.9 [88]. The dichroic ratio can be measured using infrared spectrometer of which $A_{||}$ and $A_{\perp}$ are the absorbance at a particular band for linearly polarized light, polarized parallelly and perpendicularly to the stretching direction, respectively.

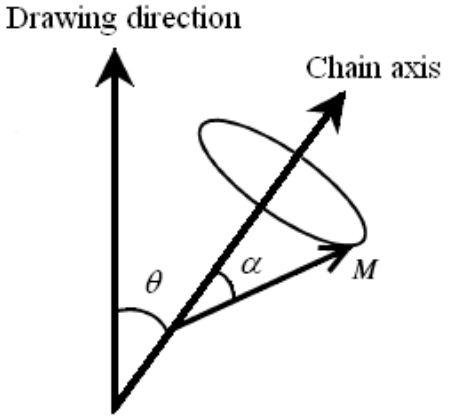

Figure 1.9 Schematic representation for molecular chain axis and transition moment vector $\boldsymbol{M}$.

1.3.4 Birefringence Analyzer

The molecular orientation using birefringence measured using a refractometer or a polarization microscope has long been performed. However, these measurement methods are rather time and effort consuming [89,90]. Furthermore, it was rather

difficult to measure with a sufficient accuracy. In this study, the birefringence of stretched films is measured by a birefringence analyzer namely KOBRA-WPR from Oji Scientific Instruments, Inc. Using this device, birefringence can be measured as a function of wavelength by using multiple color filters. The image of the device and the schematic diagram of measurement mechanism are shown in Fig. 1.10 below.

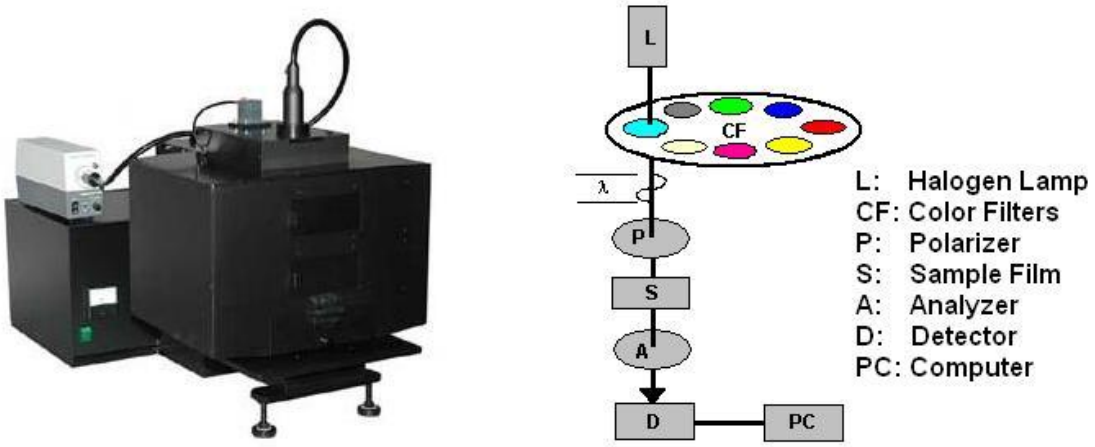

Figure 1.10 A birefringence analyzer and its measurement mechanism diagram.

The birefringence analyzer is basically a polarization analysis device that uses parallel nicols rotating method. A pair of polarizing plates which acts as light polarizer and analyzer is set to the upper and lower sides of a sample. A single wavelength light flux is irradiated from the polarizer side, and then goes through the sample while the sample stage is rotated around the optical axis while maintaining the polarizer and analyzer at parallel nicols. Phase retardation is measured from the information of angular dependence of penetration light intensity [91].

1.4 Optical Polymeric Films

1.4.1 Optical Film in Liquid Crystal Display Application

Optical films generally require high clarity, high transmittance throughout the visible light of spectrum, homogeneity in appearance, high surface smoothness and uniformity in thickness [10,12]. Furthermore, resistance in dimensional change upon changing temperature and humidity within normal use ranges are also required [5]. The term 'film' refers to a generally planar structure typically having a thickness substantially smaller *i.e.*, at least 10 times than its width and length.

In LCD applications, there are many types of optical films such as polarizing film, protective film, brightness enhancement film, diffusion film and retardation film [92,93]. Each film has different function in the LCD assembly, thus requires different physical and optical characteristic. For example, brightness enhancing films are used to improve brightness, hence allows the electronic product to operate more efficiently by using less power to light the display, thereby reducing the power consumption and extending the lifetime of the product. The film is required to have index of refraction that is related to the brightness gain.

A polarizing plate protective film is used to prevent the polarizing plate from shrinking and to prevent the iodine or dyes, which are used as polarizing elements, from evaporation [10,94]. The protective film must show high transparency and low birefringence so that the polarized light will not be disturbed [10,95]. It also should have certain permeability for vaporized water so that water vapor from the adhesive used to pile up the polarizing element and the protective film is allowed to evaporate. A retardation film

is used to improve the picture quality and viewing angle of LCD. It should show a consistent retardation over a wideband of visible light, which requires a control of birefringence dispersion over a wideband of visible light [12,15,92].

1.4.2 Retardation Film

Many LCDs are equipped with a retardation film. Since LCD is a monitor device that utilizes polarized lights, polarizing plates are placed at the back and forth of a liquid crystal cell. However, when a linearly polarized light passes through a liquid crystal cell, it will be transformed into various types of elliptically polarized light, which depends on the wavelength. This resulted in degeneration of contrast at certain view angle, the so-called limited viewing angle [96]. By inserting retardation films, the elliptically polarized light will be compensated back to a linearly polarized light. This enables the polarization plates to act as a simple yet effective switch (Fig. 1.11).

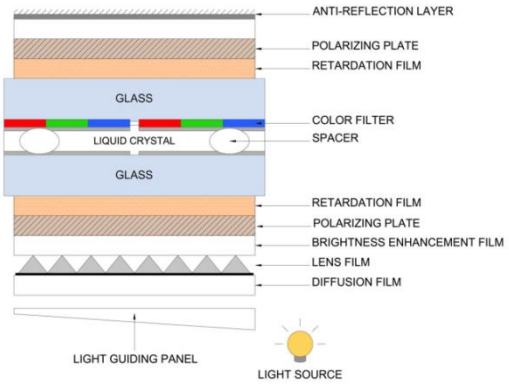

Figure 1.11 The structure of liquid crystal display panel. [97]

Generally, polymers show a decrease of birefringence with increasing wavelength as shown in Fig. 1.12(a). [15,98] The relationship between birefringence and wavelength can be predicted from the following relations such as Sellmeier (eq. 1.14) equation

[99,100], which express the wavelength dispersion of refractive index for conventional polymers.

$$\Delta n(\lambda) = A' + \frac{B'}{\lambda^2 - \lambda_{ab}^2} \tag{1.14}$$

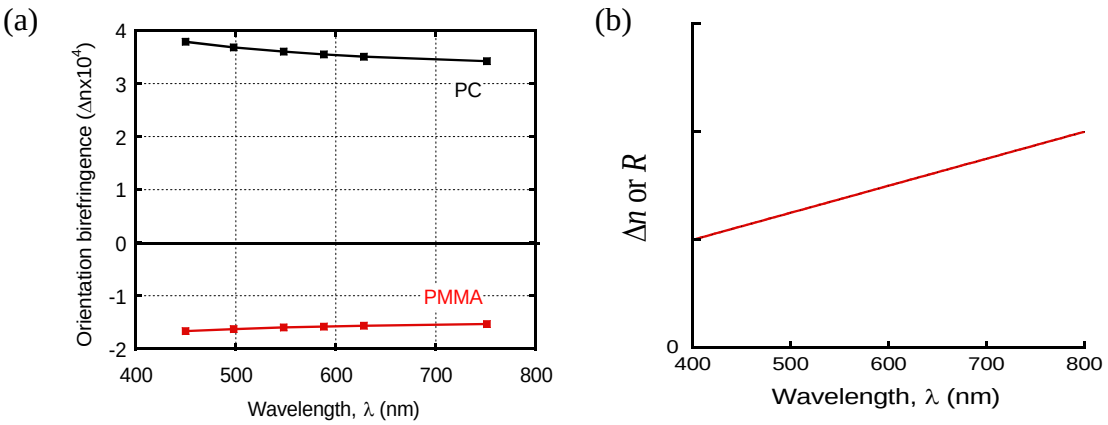

Figure 1.12 Wavelength dispersion of birefringence for (a) polycarbonate (PC) and polymethyl methacrylate (PMMA), and (b) an ideal quarter-wavelength retardation plate.

For a film to function as a retardation film, it has to show a consistent retardation value, *e.g*. quarter wavelength (λ/4) as in the case of quarter-wavelength retardation plate over a wide-band of visible light [15,101,102]. As a retardation is given by the product of birefringence and film thickness (eq. 1.7), a film must show an increase in birefringence with increasing wavelength in order to be used as retardation film as shown in Fig. 1.12(b). The wavelength dispersion of which the birefringence increases with increasing wavelength is called 'extraordinary dispersion' [12,25,98].

Industrially, extraordinary dispersion of birefringence is obtained by piling together two or more films having different birefringence characteristic, with their fast axis are set to be perpendicular to each other (Fig. 1.13) [22,103]. However, as two or

more films are used to produce the required retardation property, the adhesion process is rather complicated and costly. Thus, having a single material that shows extraordinary dispersion of birefringence is desirable as the cost production and thickness could be reduced.

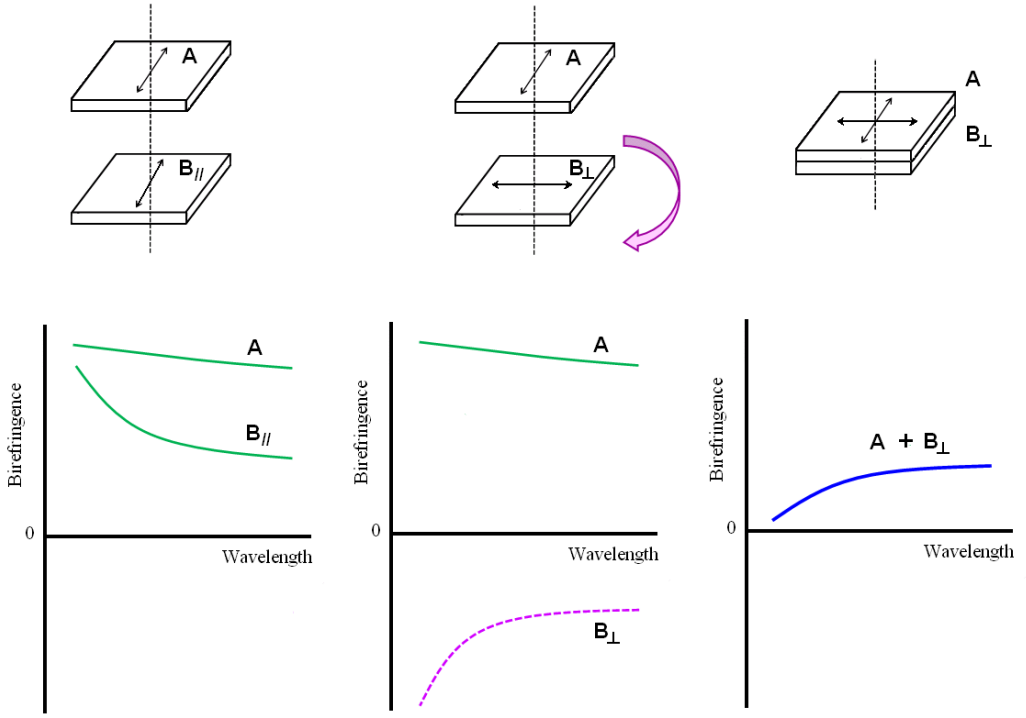

Figure 1.13 Combination of two films to produce extraordinary dispersion of birefringence.

1.4.3 Optical Film Fabrication

1.4.3.1 Solution-Cast Method

Solution-cast method is the oldest technology in polymer films manufacturing. It was developed more than hundred years ago driven by the needs of the emerging photographic industry. Nowadays, the solution-cast method is becoming increasingly attractive for the production of films with extremely high quality requirements such as

engineering plastics, optical films, medical films and sheet forming for electronic applications. The advantages of this method include uniform thickness distribution, maximum optical purity and extremely low haze. The optical orientation is virtually isotropic and the films have excellent flatness and dimensional stability [95].

For solution-cast method, the polymeric material used has to be soluble in a volatile solvent. Firstly, a solid polymer which can be available in various geometrical shapes such as flakes, granules or powder, is dissolved in a solvent and stirred to prepare a dope. The dope is subsequently cast onto a moving belt before going through evaporation and drying process. Industrially, the geometry of the stirrer, as well as the shear rate and the dope temperature need to be carefully controlled as they influence the quality of the dissolution process, hence the final film. Solution-cast method in general is more expensive than extrusion because (i) the production speed is slower since it involves the solvent diffusion process, (ii) the extra cost for solvent recovery, and (iii) the need to invest in facilities for handling solvents and dope solutions [104,105].

1.4.3.2 Extrusion Method

Extrusion is a high volume manufacturing process in which a raw polymeric material is melted and formed into a continuous profile. In addition to preparing raw stock such as sheet for thermoforming and pellets for injection molding, extrusion is used to produce numerous end-use products such as film, tubing, wire insulation and a variety of profiles. [106-108] For film fabrication, the main advantages of extrusion method as compared to the solution-cast method are (i) capable to manufacture in high volumes (ii) shorter lead times and (iii) does not involve solvent evaporation.

In the extrusion of plastics, raw polymeric material is fed from a top mounted hopper into the barrel of the extruder. The material enters through the feed throat, which is an opening near the rear of the barrel and comes into contact with the screw. The rotating screw forces the raw polymer forward into the barrel which is heated to the desired melt temperature of the molten plastic. In most processes, a heating profile is set for the barrel in which three or more independent heater zones gradually increase the temperature of the barrel from the rear to the front. This allows the plastic beads to melt gradually as they are pushed through the barrel and lowers the risk of overheating which may cause degradation in the polymer. Extra heat is contributed by the intense pressure and friction taking place inside the barrel. By the time the plastic reaches the front of the screw, it is completely melted. In most extruders, the temperature is monitored and kept below the set value by cooling fans. The pumping action of the screw forces the molten polymer through an orifice with a specially designed cross section, called a die where the polymer is shaped into a desired form. Eventually the polymer exits the die and enters a cooling apparatus, which usually uses air or water to solidify the shaped polymer [109].

For products such as plastic sheet or film, the cooling is achieved by pulling through a set of cooling rolls also known as calendering [110]. The cooling rolls are usually three or four in number. The rolling speed has to be controlled as to allow an adequate contact time to dissipate the heat present in the extruded plastic. In sheet and film extrusion, these rolls not only deliver the necessary cooling but also determine sheet thickness and surface texture.

1.5 Solution-Cast Films

1.5.1 Processing

There are several sorts of polymer films for the optical use. In order to produce such a polymer film, a casting die is usually used to cast a dope onto a support, the cast dope is peeled as the polymer film from the support, and then wound as the polymer film after a drying process. This method is called a solution-cast method and a representative method for producing the polymer film.

The cast film process is an important industrial operation to produce thin polymeric film products, mainly for packaging, magnetic tape or coating applications. An extensive range of viscoelastic polymeric materials have been used in the cast film process by manufactures according to various product uses, for example poly(ethylene terephthalate) (PET), polystyrene (PS), polypropylene (PP), low-density polyethylene (LDPE) and high density polyethylene (HDPE). The cast film process can be performed under a wide range of processing conditions. Figure 1.14 provides a schematic of the cast film process. The elongational flow between the extrusion die and chill roll, which is usually called as air gap, plays a major role in the final film properties, because flow induced orientation or crystallization and profiles of film thickness and width are formed in this stage and it also provides initial conditions for all subsequent processing. Therefore, similar with most studies, we focus on the steady flow of air gap stage. The molten polymeric melt is extruded through a slit die and immediately stretched with a constant take-up velocity by a rotational chill roll. In practice, the die is designed to provide a constant exit velocity and uniform thickness in order to produce a film with uniform thickness [11]. During the process, the film width decreases along the transverse

direction and this phenomenon is called the neck-in defect. The film thickness at the chill roll is thicker at the edge than in the middle, which is called as edge bead phenomenon, and the thicker portion will be trimmed out. It is known empirically that neck-in and edge bead are the same problem, *i.e.*, a small neck-in value leads to a wide edge bead area, which will be trimmed. In order to produce a film with a small neck-in value and uniform thickness, it is important to clarify the relationship between the neck-in phenomenon and the viscoelastic flow behavior of polymer melts in the cast film process [112].

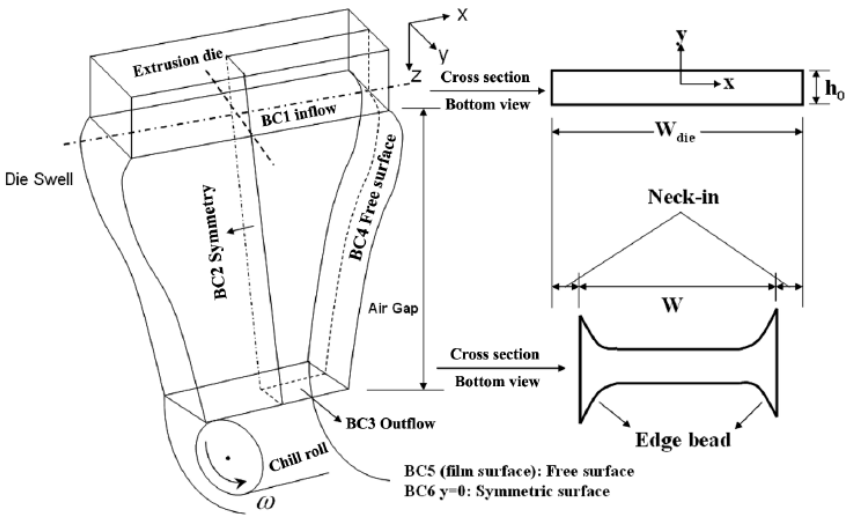

Figure 1.14 Schematic of the three-dimensional cast film process [112].

1.5.2 Principal advantages and drawbacks of solution-cast films

The main advantage of solution-cast technology is caused by the unique process drying a liquid on a surface without applying further mechanical or thermal stress. Additionally, dope handling and filtration offer a variety of specific features for the final product. Advantages are:

- Homogeneous thickness distribution

- Highest optical purity, free of gels or specks
- Excellent transparency, low haze
- Isotropic orientation, low optical retardation, excellent flatness
- Processing of thermally or mechanically sensitive components is feasible
- Possibility of production of high-temperature resistant films from non-melting but soluble raw materials

There are constraints on the types of polymer films for which solution-cast technology must or cannot be used. Relatively few materials can be processed into films by both methods: slot extrusion and solution-cast method. In these cases, a cost-performance comparison decides. Very thin films cannot be produced by extrusion without stretching, very thick films are very costly to produce by solution-cast method and lamination. In general, solution-cast method products are more expensive than extruded film to manufacture for several reasons:

- Slow production speed depending on a slow solvent diffusion process
- Extra energy costs of solvent recovery
- Investments in facilities for handling solvents and dope solutions

1.6 Control of Birefringence in Polymeric Films

Control of birefringence in optical polymeric films over a wideband of visible light is necessary to enable their function in a particular application as different application requires different birefringence property. As discussed previously, for the application as polarizer protective films, zero birefringence is required, while for

retardation films, the so-called extraordinary dispersion of birefringence is required. The various methods that have been proposed to control birefringence in polymeric films will be discussed in the following sub-chapters.

1.6.1 Polymer Blending Technique

Polymer blend method is a well-known method employed to control birefringence in polymers. It was firstly revealed by Hahn and Wendorff [113] that a miscible binary blend of poly(methyl methacrylate) PMMA and poly(vinylidene fluoride) PVDF, two polymers with opposite sign of intrinsic birefringence, shows no birefringence at a specific blend ratio irrespective of the molecular orientation. The mechanism of which the opposite polarizability cancels each other is illustrated in Fig. 1.15. Furthermore, it is important to note that the factor of miscibility is greatly important as it affects transparency, which is a critical property for optical films.

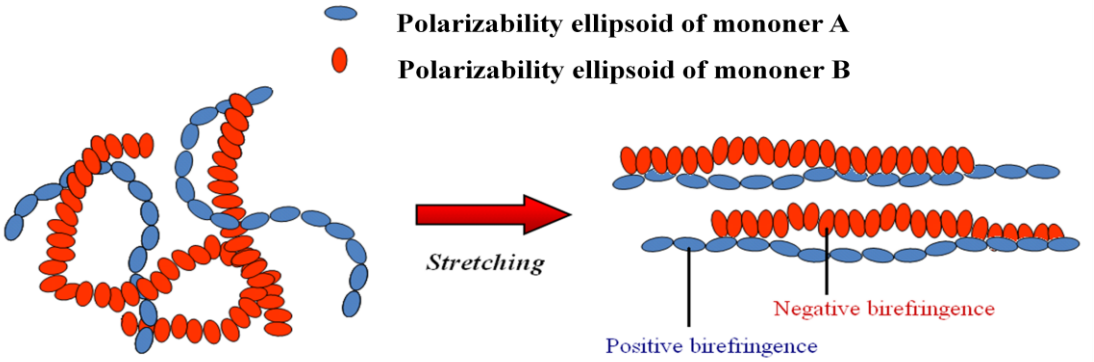

Figure 1.15 Illustration of birefringence offset in a miscible polymer blend.

Using the polymer blend method, Yamaguchi and Masuzawa [114] have made some studies to create zero-birefringence in cellulose acetate propionate (CAP). They found that poly(vinyl acetate) (PVAc) and CAP are miscible and show opposite signs of

birefringence. Consequently, at a specific blend ratio, the blend does not show orientation birefringence even after stretching. In another study [115], they found that PMMA and poly(epichlorohydrin) (PECH) also reduce the orientation birefringence of CAP by the same mechanism illustrated in the in Fig. 1.15 above.

Meanwhile, Uchiyama and Yatabe [20,21] have successfully controlled the wavelength dispersion using binary blend composed of poly(2,6-dimethyl-1,4-phenylene oxide) (PPO) and atactic polystyrene (PS). In the blend system, PS shows negative birefringence with strong wavelength dependence, whereas PPO exhibits positive one with weak wavelength dependence. Although individually both polymers show ordinary wavelength dispersion, their blends at certain blend compositions show extraordinary wavelength dispersion as the summation of the contributions from both polymers. This can be expressed by the equation for birefringence in a multi-component system as discussed by Stein et al. as follows [116] :

$$\Delta n = \Delta n_F + \sum_i \phi_i \Delta n_i \qquad (1.15)$$

where *i* refers to *i*-th component, ϕ_i is the volume fraction, and Δn_F is the birefringence arising from form or deformation effects, which is negligible for cellulose-esters owing to the homogeneous structure.

Kuboyama et al. [22,117] have managed to control the wavelength dispersion of miscible blend comprised of polynorbornene (NB) and poly(styrene-*co*-maleic anhydride) (SMA) by adjusting the blend composition and stretching conditions. NB has positive birefringence with weak wavelength dispersion, while SMA has negative birefringence with strong wavelength dispersion as shown in Fig. 1.16. They found that

the reversal in sign of birefringence between positive and negative occurred between the compositions of NB/SMA of 60/40 and 50/50. Furthermore, the blend shows positive birefringence with extraordinary wavelength dispersion when the content of NB is around 60 - 70 wt%.

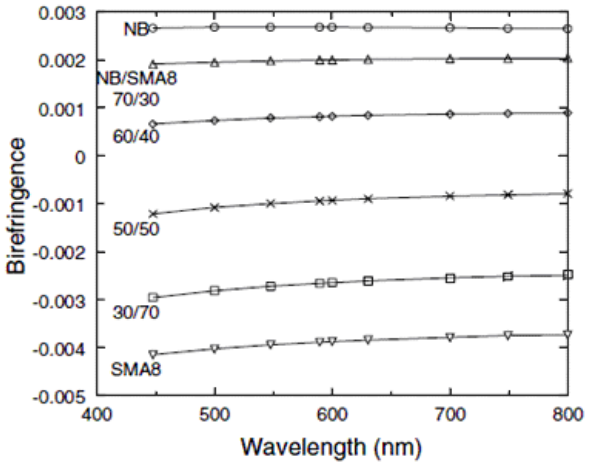

Figure 1.16 Wavelength dispersion of various NB/SMA blend compositions. [22]

1.6.2 Copolymerization Technique

The polymer blending technique, in which negative and positive birefringence homopolymers are blended, is a useful method to control birefringence in polymers. However, in practice, it is difficult to completely blend two polymers during injection-molding or extrusion, and thus difficult to achieve the transparency and homogeneity required for use in high performance optical devices as the blends tend to phase separate into regions, thus leading to scattering [118,119]. The random copolymerization method [120-122] was proposed in order to solve this problem by creating chemical bonding between the negative and positive birefringent monomers.

Iwata et al. [120] have developed the random copolymerization technique, in

which the two monomers have opposite polarizability anisotropy to each other, to obtain a zero-birefringence polymer. (Fig. 1.17) In the study, methyl methacrylate (MMA) was used as negative birefringent monomer while 2,2,2-trifluoroethyl methacrylate (3FMA) was used as positive birefringent monomer. They found that poly(MMA-*co*-3FMA) copolymer synthesized with a composition of MMA/3FMA (45/65) showed no birefringence for any draw ratio.

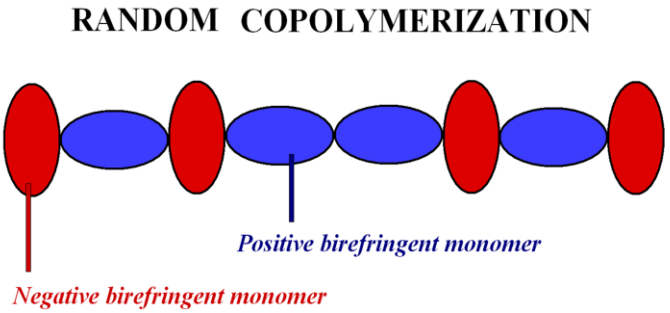

Figure 1.17 Schematic diagram of polarizability ellipsoids for compensating the birefringence by copolymerization.

Uchiyama and Yatabe [25] have studied the wavelength dispersion of a copolymer as a function of monomer content employing two monomers; 2,2-bis(4-hydroxyphenyl) propane (BPA) and 9,9-bis(4-hydroxy-3-methylphenyl) fluorine (BMPF). The birefringence in the visible region is positive for the former and negative for the latter. (Fig. 1.18) The existence of positive and negative birefringence units in the copolymer is indispensable to achieve extraordinary dispersion of birefringence as demonstrated in their study. Moreover, they found that the wavelength dispersion of the copolymer films can be controlled by the copolymerization ratio.

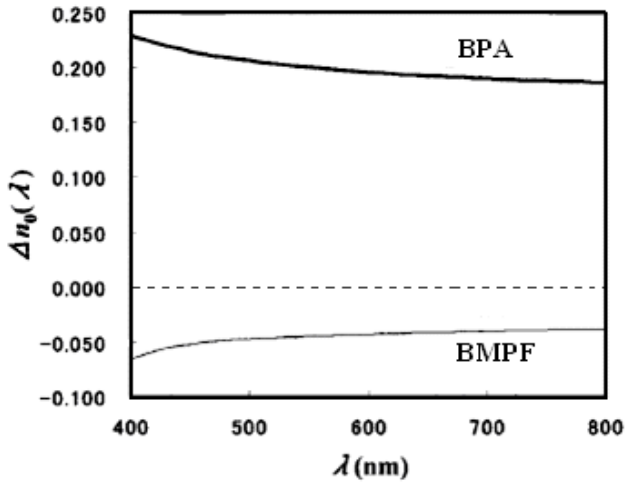

Figure 1.18 Intrinsic birefringence (Δn_0) dispersion of BPA and BMPF homopolymers. [25]

1.6.3 Anisotropic Molecule/Crystal Doping Technique

The random copolymerization method approach has been somewhat successful in solving the phase separation problem associated to the blending technique. However, the typical optical, mechanical and thermal properties of most copolymers synthesized by this method are significantly different from their corresponding homopolymers, because the mixing ratio of the minority component is usually more than 10 wt%. Anisotropic molecule doping method has been proposed to avoid this problem [123-125].

In the anisotropic molecule doping method, molecules that have anisotropic polarizability and a rodlike shape are chosen and doped into the polymers. When the polymer chains are oriented in processing, the molecules are also oriented because of their rodlike shape. Tagaya et al. [125] have managed to compensate the negative

orientation birefringence of PMMA by doping rodlike anisotropic molecules with positive polarizability anisotropy such as *trans*-stilbene and diphenylacetylene.

Ohkita et al. [126] have successfully developed a zero birefringence polymer by adding needlelike crystals having polarizability anisotropy opposite to the host polymer. (Fig. 1.19) In the study, strontium carbonate ($SrCO_3$) crystals with a length of about 200 nm and width of about 20 nm were doped into a copolymer of methyl methacrylate (MMA) and benzyl methacrylate (BzMA). The surface of the crystal was modified using a titanate-based coupling agent in order to disperse the crystals more homogeneously in the polymer.

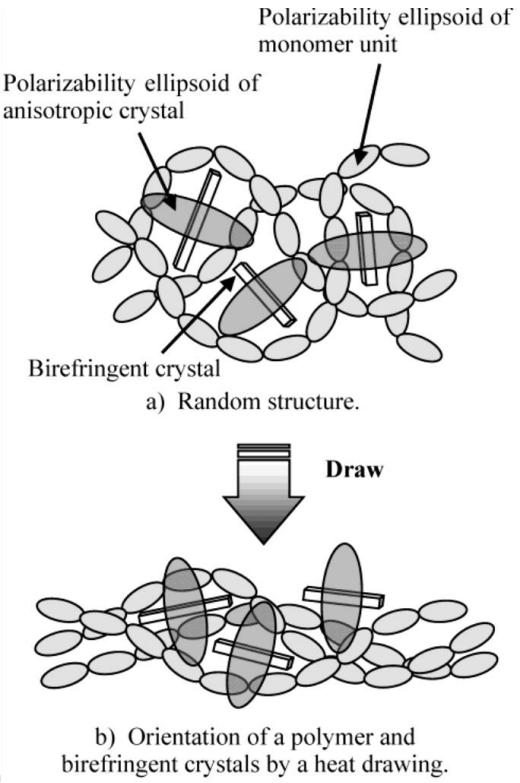

Figure 1.19 Mechanism of the compensation of orientational birefringence by the anisotropic crystal doping technique [126]

1.7 Objectives of the Study

Cellulose esters are biomass derived materials with great potential as optical films. Besides their relatively low cost, cellulose esters also possess excellent physical properties suitable for optical film application such as high transparency and excellent heat resistance. However, to fulfill that purpose, it is necessary for films of cellulose esters to show birefringence characteristic required for the particular application such as zero birefringence for polarizer protective films and extraordinary wavelength dispersion for retardation films.

Despite the potential exhibited by cellulose esters, most of the reported studies on the control of orientation birefringence deal with a more conventional polymer such as PMMA. Therefore, there is serious lack of study that deals with cellulose esters or any biomass-derived polymer on this subject.

The main objective of this research is to study the control mechanism of orientation birefringence in cellulose esters. At first, the information on the molecular orientation and the birefringence of a solution-cast film for cellulose triacetate was investigated.

Furthermore, the effects of low-mass compound (LMC) addition on the in-plane and out-of-plane birefringence before and after stretching of cellulose esters were studied. Plasticizers such as tricresyl phosphate (TCP) and triphenyl phosphate (TPP) and 4-cyano-4'-pentylbiphenyl (5CB) were added to cellulose esters such as cellulose triacetate (CTA) and cellulose acetate propionate (CAP). Then their viscoelastic properties and wavelength dispersion of birefringence were studied. Lastly, the effects of the type and

amount of the substituent ester groups on the in-plane and out-of-plane birefringence and its wavelength dispersion were investigated.

Through this research, it is expected that a better understanding regarding the mechanism for in-plane and out-of-plane birefringences in cellulose esters can be achieved. This would open up possibilities of developing biopolymer-based optical films with birefringence suited for various functions in optical devices.

References

[1] Shen L.; Worrell, E.; Patel, M. *Biofuel Bioprod. Bior.* **2010**, *4*, 25-40.

[2] Hui, P. *Renewable and Sustainable Energy Reviews* **2011**, *15*, 3454-3463.

[3] Koshijima, T. In *Functional Cellulose* [機能性セルロース]; CMC Publishing Co. Ltd.: Tokyo, 2003; pp 1-7.

[4] Ioelovich, M. *BioResources* **2008**, *3*, 1403-1418.

[5] Edgar, K. J.; Buchanan, C. M.; Debenham, J. S.; Rundquist, P. A.; Seiler, B. D.; Shelton, M. C.; Tindall, D. *Prog. Polym. Sci.* **2001**, *26*, 1605-1688.

[6] Silva Gomes, G. D.; Almeida, A. T. D.; Kosaka, P. M.; Rogero, S. O.; Cruz, A. S.; Ikeda, T. I.; Petri, D. F. S. *Materials Research*, **2007**, *10*, 469-474,

[7] Fu, X. Y.; Sotani, T.; Matsuyama, H. *Desalination* **2008**, *233*, 10-18.

[8] Puls, J.; Wilson, S. A.; Holter, D. *J. Polym. Environ.* **2011**, *19*, 152-165.

[9] Glasser, W. G. *Macromol. Symp.* **2004**, *208*, 371-394.

[10] Sata, H.; Maruyama, M.; Shimamoto, S. *Macromol. Sym.* **2004**, *208*, 323-333.

[11] Kamide, K. *Cellulose and cellulose derivatives*, Elsevier Science, Amsterdam, 2005.

[12] Yamaguchi, M. Optical properties of cellulose esters and their blends. In *Cellulose: Structure and Properties, Derivatives and Industrial Uses*; Lejeune, A., Deprez, T., Eds.; Nova Science Publishers, Inc.: New York, 2010, pp 325-340.

[13] Yamaguchi, M.; Lee, S.; Mohd Edeerozey, A. M.; Tsuji, M.; Yokohara, T. *Eur. Polym. J.* **2010**, *46*, 2269-2274.

[14] Koike, Y. What exactly the most transparent polymer [最も透明なポリマーとは]. In *The Cutting Edge of Transparent Plastics* [透明プラスチックの最前線]; NTS Publishing Co. Ltd.: Tokyo, 2006a, pp 5-34.

[15] Inoue, T. Control of Birefringence in Polymeric Materials [高分子材料の複屈折制御]. In *The Cutting Edge of Transparent Plastics* [透明プラスチックの最前線]; NTS Publishing Co. Ltd.: Tokyo, 2006, pp 37-61.

[16] Tagaya, A.; Ohkita, H.; Koike, Y. *Mater. Sci. Eng., C* **2006**, *26*, 966-970.

[17] Fujimura, Y. Optical Film for LCD [液晶ディスプレイ用光学フィルム]. In *Functional Polymers as Electronics Materials* [エレクトロニックス材料としての機能性高分子]; Tokyo NTS Publishing Co. Ltd.: Tokyo, 2003, pp 139-149.

[18] Kimura, T.; Yamato, M.; Endo, S.; Kimura, F.; Sata, H.; Kawasaki, H.; Shinagawa, Y. *J. Polym. Sci., Polym. Phys.* **2001**, *39*, 1942–1947.

[19] Songsurang, K.; Miyagawa, A.; Mohd Edeerozey, A. M.; Phulkerd, P.; Nobukawa, S.; Yamaguchi, M. *Cellulose* **2013**, *20*, 83-96.

[20] Uchiyama, A.; Yatabe, T. *Jpn. J. Appl. Phys.* **2003,** *42*, 3503–3507.

[21] Uchiyama, A.; Yatabe, T. *Jpn. J. Appl. Phys.* **2003,** *42*, 5665–5669.

[22] Kuboyama, K.; Kuroda, T.; Ougizawa, T. *Macromol. Sym.* **2007**, *249–250*, 641–646.

[23] Yamaguchi, M.; Okada, K.; Mohd Edeerozey, A. M.; Shiroyama, Y.; Iwasaki, T.; Okamoto, K. *Macromolecules* **2009**, *42*, 9034–9040.

[24] Mohd Edeerozey, A. M.; Tsuji, M.; Shiroyama, Y.; Yamaguchi, M, *Macromolecules* **2011**, *44*, 3942–3949.

[25] Uchiyama, A.; Yatabe, T. *Jpn. J. Appl. Phys.* **2003,** *42*, 6941–6945.

[26] Koike, Y.; Yamazaki, K.; Ohkita, H.; Tagaya, A. *Macromol. Sym.* **2006**, *235*, 64–70.

[27] O'Connell, D. W.; Birkinshaw, C.; O'Dwyer, T. F. *Bioresour. Technol.* **2008**, *99*, 6709-6724.

[28] O'Sullivan, A. C. *Cellulose* **1997**, *4*, 173-207.

[29] Marsh, J. T.; Wood, F. C. In *An Introduction to the Chemistry Cellulos*e; Chapman & Hall Ltd.: London, 1942, pp 55-60.

[30] Kontturi, E.; Tammelina, T.; Österberga, M. *Chem. Soc. Rev.* **2006**, *35*, 1287-1304.

[31] Malm, C. J.; Fordyce, C. R; Tanner, H. A. *Ind. and Eng. Chem.* **1942**, *34*, 430-435.

[32] Mohanty, A. R.; Wibowo, H.; Misra, M.; Drzal, L. T. *Polym. Eng. & Sci.* **2003**, *43*, 1151-1161.

[33] Kamel, S.; Ali, N.; Jahangir, K.; Shah, S. M.; El-Gendy, A. A. *Exp. Polym. Lett.* **2008**, *2*, 758–778.

[34] Isogai, A.; Tezuka, Y. In *Cellulose Encyclopedia* [セルロースの事典]; Asakura Shoten: Tokyo, 2008, pp 131-147.

[35] Fischer, S.; Thummler, K.; Volkert, B.; Hettrich, K.; Schmidt, I.; Fischer, K. *Macromol. Symp.* **2008**, *262*, 89–96.

[36] Ciolacu, D.; Popa, V. I. Cellulose Allomorphs – Overview and Perspectives. In *Cellulose: Structure and Properties, Derivatives and Industrial Uses*; Lejeune, A., Deprez, T., Eds.; Nova Science Publishers, Inc.: New York, 2010, pp 1-29.

[37] Wang, P. L.; Tao, B. Y. *J. Environ. Polym. Degradation* **1995**, *3*, 115-119.

[38] Cao, Y.; Wu, J.; Meng, T.; Zhang, J.; He, J.; Li, H.; Zhang, Y. *Carbohydr. Polym.* **2007**, *69*, 665-672.

[39] Federal Trade Commission. Rules and regulations under the textile fiber products identification act**.** Available from: http://www.ftc.gov/os/statutes/textile/rr-textl.htm [Accessed 16 April 2012]

[40] Teitelbaum, B. Y.; Yagfarova, T. A.; Pavlova, D. S.; Grabko, A. M.; Nuriazdanov, A. S.; Fedorina, L. A.; Krupnov, G. P. *J. Therm. Anal.* **1989**, *35*, 1709-1717.

[41] Novikov, D. V.; Varlamov, A. V.; Mnatsakanov, S. S. *Russ. J. Appl. Chem.* **2005**, *78*, 301-304.

[42] Peydecastaing, J.; Vaca-Garcia, C.; Borredon, E. *Cellulose*, **2011**, *18*, 1023-1031.

[43] Cannon, C. R.; Park, B.; Cantor, P. A. U.S. Patent, 3,585,126, 1971.

[44] Landry, C. J. T.; Teegarden, D. M.; Edgar, K. J.; Kelley, S.S. U.S. Patent, 5,302,637, 1994.

[45] Shogren, R. *J. Polym. Environ.* **1997**, *5*, 91-95.

[46] Koike, Y. In *Optical Properties of Polymeric Materials* [高分子の光物性]; Kyouritsu Publishing Co. Ltd.: Tokyo, 1994, pp 1-27.

[47] Serway, R. A.; Faughn, J. S.; Vuille, C. In *College Physics*; Cengage Learning Inc.: California, USA, 2009, pp 714-720.

[48] Winn, W. In *Introduction to Understandable Physics: Electricity, Magnetism and Light*; Author House: Indiana, USA, 2010, pp 25(1-6).

[49] Andrews, R. D. Thermoplastic Materials with Limited Elasticity. In *Elasticity, Plasticity and Structure of Matter*; De Decker, H. K.; Houwink, R., Eds.; Cambridge University Press: London, 1971, pp 157-160.

[50] Lekishvili, N.; Nadareishvili, N.; Zaikov, G.; Khananashvili, L. In *New Concepts in Polymer Science: Polymers and Polymeric Materials for Fiber and Gradient Optics*; Ridderprint: The Netherlands, 2002, pp 8-11.

[51] Van De Hulst, H. C. In *Light Scattering by Small Particles*. Dover Publications Inc.: New York, 1981, pp 36-38.

[52] Hamza, A. A.; Fouda, I. M.; Kabeel, M. A.; Shabana, H. M. *Polymer Testing* **1989**, *8*, 201-212.

[53] Yun, J. H.; Kuboyama, K.; Ougizawa, T. *Polymer* **2006**, *47*, 1715-1721.

[54] Li, C.; Li, Z.; Liu, J. G.; Zhao, X. J.; Yang, H. X.; Yang, S. Y. *Polymer* **2010**, *51*, 3851-3858.

[55] Seto, R.; Kojima, T.; Hosokawa, K.; Koyama, Y.; Konishi, G.; Takata, T. *Polymer* **2010**, *51*, 4744-4749.

[56] Stoiber, R. E.; Morse, S. A. In *Crystal Identification with the Polarizing Microscope*; Chapman & Hall: New York, 1994, pp 14-31.

[57] New, G. In *Introduction to Non Linear Optics*; Cambridge University Press: New York, 2011, pp 45-48.

[58] Pethrick, R. A. In *Polymer Structure Characterization: From Nano to Macro Organization*; The Royal Society of Chemistry Publishing: Cambridge, 2007, pp 130-132.

[59] Shafiee, H. ; Tagaya, A.; Koike, Y. *J. Polym. Sci. Part B: Polym. Phys.* **2010**, *48*, 2029–2037.

[60] Slayter, E. M.; Slayter, H. S. In *Light and Electro Microscopy*; Cambridge University Press: Cambridge, 1997, pp 170-175.

[61] Inoue, S. In *Collected Worls of Shinya Inoue : Microscopes, Living Cells and Dynamic Molecules*; World Scientific Publishing Co. Pte. Ltd.: Singapore, 2008, pp 875-880.

[62] Altshuler, G. B.; Tuchin, V. V. Physics Behind Light-Based Systems: Skin and Hair Follicle Interactions with Light. In *Cosmetic Applications of Laser and Light-Based Systems*; Ahluwalia, G. S., Ed.; Wiliam Andrew Inc.: New York, 2009, pp 93-95.

[63] Hardy, J. W. In *Adaptive Optics for Astronomical Telescopes*; Oxford University Press, 1998, pp 206-209.

[64] Wayne, R. In *Light and Video Microscopy*; Elsevier Inc.: California, 2009, pp 123-127.

[65] Damask, J. N.; In *Polarization Optics in Telecommunications*; Springer Science Business Media Inc.: New York, 2005, pp191-199.

[66] Bohren, C. F.; Clothiaux, E. E. In *Fundamentals of Atmospheric Radiation*; Wiley VCH: Germany, 2006, pp 360-362.

[67] Rochow, T. G.; Tucker, P. A. In *Introduction to Microscopy by Means of Light, Electrons, X Rays or Acoustics*; Plenum Press: New York, 1994, pp 123-133.

[68] Sawyer, L. C; Grubb, D. T.; Meyers, G. F. In *Polymer Microscopy*; Springer Science Business Media Inc.: New York, 2008, pp 252-254.

[69] Houck, M. M.; Siegel, J. A. In *Fundamentals of Forensic Science*; Elsevier Ltd.: Massachusetts, 2010, pp 87-90.

[70] Biggers, J. E.; Finn, K. P.; Schwartz II H. H.; McClain, Jr. R. A. **2002**, *Neural network trajectory command controller*, US Patent 6473747B1.

[71] Iyer, K. R. K.; Sreenivasan, S.; Patil, N. B. *Text. Res. J.* **1983**, *53*, 442-444.

[72] Wu, J. P.; White, J. L.; Cakmak, M. *Colloid. Polym. Sci.* **1989**, *267*, 881-888.

[73] Belfiore, L. A. In *Physical Properties of Macromolecules*; John Wiley & Sons, Inc.: New Jersey, 2010, pp 279-280.

[74] Gedde, U. W. In *Polymer Physics*; Kluwer Academic Publishers: The Netherlands, 1999, pp 211-215.

[75] Barlow, A. J.; Payne, D. N. *IEEE J. Quantum Electron* **1983**, *19*, 834-839.

[76] Machenko, O.; Kazantsev, S.; Windholz, L. In *Demonstrational Optics: Wave and Geometrical Optics*; Kluwer Academic/Plenum Publishers: New York, 2003, pp184-188.

[77] Miller, M. L. In *The Structure of Polymers*; Reinhold Publication Corp.: New York, 1966, pp 272.

[78] Wimberger-Friedl, R. *Rheol. Acta* **1991**, *30*, 329- 340.

[79] Alger, M. In *Polymer Science Dictionary*; Chapman & Hall: London, 1997, pp 352.

[80] Gupta, V. B.; Kothari, V. K. In *Manufactured Fibre Technology*; Chapman & Hall: London, 1997, pp 223-226.

[81] Van Aerle, N. A. J. M.; Tol, A. J. W. *Macromolecules* **1994**, *27*, 6520-6526.

[82] Salem, D. R. In *Structure Formation in Polymeric Fibers*; Hanser Gardner Publications Inc.: Ohio, 2000, pp 15-16.

[83] Terui, Y.; Ando, S. *J. Polym. Sci. Part B: Polym. Phys.* **2004**, *42*, 2354-2366.

[84] Piau, J. M.; Agassant, J. F. In *Rheology for Polymer Melt Processing*; Elsevier Science B.V.: Amsterdam, 1996, pp 259-260.

[85] Elias, H. G. In *An Introduction to Plastics*; Wiley-VCH GmbH & Co.: Michigan, 2003, pp 66-68.

[86] Jansen, J. A. J.; Van der Maas, J. H.; Posthuma de Boer, A. *Macromolecules* **1991**, *24*, 4278-4280.

[87] Roland, C. M. In *Viscoelastic Behavior of Rubbery Materials*; Oxford University Press Inc.: New York, 2011, pp 167.

[88] Tagaya, A.; Iwata, S.; Kawanami, E.; Tsukahara, H.; Koike, Y. *Jpn. J. Appl. Phys.* **2001**, *40*, 6117-6123.

[89] Witold, B. In *Mechanical and Thermophysical Properties of Polymer Liquid Crystals*; Chapman & Hall: London, 1998, pp 309-315.

[90] Asundi, A. K. In *MatLab for Photomechanics: A Primer*; Elsevier Science Ltd.: Oxford, 2002, pp 39-40.

[91] Ellipsoid Polarized Light Measurement Device [楕円変更測定装置], 2011. Kobra-WPR. Japan: Oji Scientific Instruments. Available from: http://www.oji-keisoku.co.jp/products/kobra/wpr.html [Accessed 22 April 2012]

[92] Lazarev, A.; Geivandov, A.; Kasianova, I. *IMID/IDMC/ASIA DISPLAY '08 Digest*, 2008, 1082-1086.

[93] Yeh, P.; Gu, C. In *Optics of Liquid Crystal Displays*; John Wiley & Sons Inc.: New Jersey, 2020, pp 2-14.

[94] Fuji Chimera Research Institute. In *Flat Panel Display Materials-Trends and Forecast 2009*; InterLingua Technology Publishing: California, 2008, pp 453.

[95] Siemann, U. *Progr. Colloid Polym.* Sci. **2005**, *130*, 1-14.

[96] Blinov, L. M.; Chigrinov, V. G. In *Electrooptic Effects in Liquid Crystal Materials*; Springer-Verlag: New York, 1994, pp 171-175.

[97] Kyocera International, Inc., 2010. Films and Layers. Available from: http://americas.kyocera.com/kicc/lcd/notes/filmlayers.html [Accessed 10 October 2013]

[98] Yamaguchi, M.; Mohd Edeerozey, A. M.; Songsurang, K.; Nobukawa, S. *Cellulose* **2012**, *19*, 601-613.

[99] Jenkins, F. A.; White, H. E. In *Fundamentals of Optics*; McGraw-Hill: New York, 1981.

[100] Weik, M. H. In *Fiber Optics Standard Dictionary*; Chapman & Hall: New York, 1997, pp 238.

[101] Uchiyama, A.; Yatabe, T. *SID '01 Digest*, 2001, 566-569.

[102] Yamaguchi, M.; Iwasaki, T.; Okada, K.; Okamoto, K. *Acta Materialia* **2009**, *57*, 823-829.

[103] Ge, Z.; Wu, S. T. In *Transreflective Liquid Crystal Displays*; John Wiley & Sons Ltd.: West Sussex, 2010, pp 8-12.

[104] Kline, G. M. In *Modern Plastics Encyclopedia and Engineer's Handbook*; Plastics Catalogue Corp., 1953, pp 353.

[105] Rosato, D. V.; Rosato, D. V.; Rosato, M. V. In *Plastic Product Materials and Process Selection Handbook*; Elsevier Ltd.: Oxford, 2004, pp 404-405.

[106] Whelan, T. In *Polymer Technology Dictionary*; Chapman & Hall: London, 1994, pp 144.

[107] Kostic, M. M.; Reifschneider, L.G. In *Encyclopedia of Chemical Processing*; Taylor & Francis, 2006, pp 633-649.

[108] Gooch, J. W. In *Encyclopedic Dictionary of Polymers*; Springer, 2010, pp 304.

[109] Mitchell, B. In *An Introduction to Materials Engineering and Science for Chemical and Materials Engineer*; John Wiley & Sons Inc.: New Jersey, 2004, pp 757-765.

[110] Abdel-Bary, E. M. In *Handbook of Plastic Films*; Rapra Technology Limited: Shrewsbury, 2003, pp 16-17.

[111] Seyfzadeh, B.; Harrison, G. M.; Carlson, C. D. *Polym. Eng. Sci.* **2005**, *45*, 443-450.

[112] Zheng, H.; Yu, W.; Zhou, C.; Zhang, H. *Fiber Polym.* **2007**, *8*, 50-59.

[113] Hahn, B. R.; Wendorff, J. H. *Polymers* **1985**, *26*, 1619-1622.

[114] Yamaguchi, M.; Masuzawa, K. *Eur. Polym. J.* **2007**, *43*, 3277-3282.

[115] Yamaguchi, M.; Masuzawa, K. *Cellulose* **2008**, *15*, 17-22Iwata, S.; Tsukahara, H.; Nihei, E.; Koike, Y. *Jpn. J. Appl. Phys.* **1996**, *35*, 3896-3901.

[116] Stein, R. S.; Onogi, S.; Sasaguri, K.; Keedy, D. A. *J. Appl. Phys.* **1963**, *34*, 80-89.

[117] Kuboyama, K.; Kuroda, T.; Ougizawa, T. *Jpn J. Polym. Sci. Tech.* **2004**, *61*, 89-94.

[118] Utracki, L. A. In *Polymer Blends Handbook*; Kluwer Academic Publishers: Dordrecht, 2002, pp 170-171.

[119] Robeson, L. M. In *Polymer Blends: A Comprehensive Review*; Hanser Gardner Publications Inc.: Ohio, 2007, pp 280-285.

[120] Iwata, S.; Tsukahara, H.; Nihei, E.; Koike, Y. *Jpn. J. Appl. Phys.* **1996**, *35*, 3896-3901.

[121] Iwata, S.; Tsukahara, H.; Nihei, E.; Koike, Y. *Appl. Opt.* **1997**, *36*, 4549-4555.

[122] Yang, W. J.; Liu, G. Z.; Wang, J. M.; Xia, D. L. *Key Eng. Mater.* **2010**, *428-429*, 111-116.

[123] Tagaya, A.; Iwata, S.; Kawanami, E.; Tsukahara, H.; Koike, Y. *Appl. Opt.* **2001**, *40*, 3677-3683 .

[124] Ohkita, H.; Ishibashi, K.; Tsurumoto, D.; Tagaya, A.; Koike, Y. *Appl. Phys. A* **2005**, *81*, 617-620.

[125] Tagaya, A.; Ohkita, H.; Harada, T.; Ishibashi, K. Koike, Y. *Macromolecules* **2006,** *39,* 3019-3023.

[126] Ohkita, H.; Tagaya, A.; Koike, Y. *Macromolecules*, **2004**, *37*, 8342-8348.

Chapter 2

Molecular Orientation of Cellulose Triacetate Prepared by a Solution-Cast Method

2.1 Introduction

With the rapid growth of optical devices these days, there is a continuing trend to develop a potential material for optical films with improved functions and good cost-performance. In particular, cellulose triacetate (CTA), one of the biomass-derived materials, has been studied intensively because of their attractive properties such as high transparency and excellent heat resistant [1-4]. It is well known that CTA films are mainly employed in liquid crystal display (LCD) at present and will be used for advanced systems such as 3D display and electro-luminescent display. CTA films are produced by a solution-cast method because melt processing is not applicable due to the severe thermal degradation beyond the melting point [1-3]. In LCD application, CTA films are used as a polarizer protective film and a retardation (compensation) film. In order to be used in such applications, birefringence control is extremely important. In the case of polarizer protective films, for example, the films have to be free from birefringence, and advanced methods to erase the birefringence have been proposed recently [3-7]. For retardation

films, specific retardation, *i.e.*, the product of birefringence and thickness, should be provided.

For optical anisotropic films, three refractive indices, n_x, n_y and n_z, along three principal axes have to be taken into consideration. The *x*-axis is a direction showing a maximum refractive index within the film plane in general, the *y*-axis is a direction perpendicular to the *x*-axis within the film plane, and the *z*-axis direction is a thickness direction and is normal to the *x*-*y* plane.

It is well known that a solution-cast method provides the film without molecular orientation in the film plane ($n_x = n_y$). This is the reason why a solution-cast film is preferably employed for a protective film rather than a melt-extruded film. However, the other component of birefringence, called out-of-plane birefringence, is typically not zero. Therefore, it has to be precisely controlled to provide a high quality display.

In this study, the in-plane birefringence (Δn_{in}) and out-of-plane birefringence (Δn_{th}) are defined by the following equations.

$$\Delta n_{in} = n_x - n_y \tag{2.1}$$

$$\Delta n_{th} = \frac{n_x + n_y}{2} - n_z \tag{2.2}$$

Based on the Kuhn and Grün model, the orientation birefringence $\Delta n(\lambda)$ of an oriented polymer is expressed in the following relation [8-12].

$$\Delta n(\lambda) = \frac{2\pi}{9} \frac{\left(\bar{n}(\lambda)^2 + 2\right)^2}{\bar{n}(\lambda)} N \, \Delta\alpha(\lambda) \left(\frac{3\left\langle \cos^2 \theta \right\rangle - 1}{2} \right) \tag{2.3}$$

where λ, $\bar{n}(\lambda)$, N, $\Delta\alpha(\lambda)$, and θ are the wavelength of light, the average refractive index, the number of chains in a unit volume, the polarizability anisotropy, and the angle that a segment makes with the stretch axis, respectively. The bracketed term $\left(3\left\langle\cos^2\theta\right\rangle-1\right)/2$ is identically equal to the Hermans orientation function [13], which is commonly denoted as F. Therefore, equation 2.3 can also be written in the following form.

$$\Delta n(\lambda)=\Delta n^0(\lambda)F \tag{2.4}$$

where $\Delta n^0(\lambda)$ is the intrinsic birefringence.

In the case of solution-cast films, the molecular orientation is caused by the stress induced by solvent removal. The alignment of polymer molecules during a solution-cast process has been investigated by several researchers [14-21]. According to these studies, polymer molecules generally tend to align in a film plane. Consequently, the in-plane refractive indices (n_x and n_y) are higher than the out-of-plane refractive index (n_z) when a material shows positive orientation birefringence. It is known to be difficult to control the out-of-plane birefringence which can affect the performance of the displays.

Sosnowski and Weber (1972) reported that the optical anisotropy in a solution-cast film of polystyrene is given by a result of the stress developed in a coated film during drying process, which makes polymer chains align in the film plane. Prest and Luca (1979) also demonstrated the same results using polystyrene, polycarbonate and poly(2,6-dimethylphenyleneoxide). They showed that the sign of birefringence depends upon the orientation of the dominating polarizable group relative to the chain backbone. Furthermore, the out-of-plane birefringence was found to be pronounced for a thin film. Prest and Luca (1979, 1980), Cohen and Reich (1981), and Machell et al. (1990) studied

the effect of polymer formulations with various casting conditions such as coating thickness, drying temperature and polymer concentration on birefringence values. They found that the out-of-plane birefringence is determined by the competition between the normal stress induced by the drying process and the Brownian motion leading to random conformation by entropic force. Therefore, it is necessary to predict the stress applied by evaporation accurately to evaluate the out-of-plane birefringence. The growth of stress in solution-cast films was studied in detail by several investigators. Croll (1979) developed a simple elastic model to predict the stress, which was modified by Lei et al. (2001). Greener and Chen (2005) calculated the out-of-plane birefringence by using the model. They found that the out-of-plane birefringence occurs when the solvent concentration is beyond a critical value. At this stage, the compression stress applied in the normal direction to the film plane starts to build up and induces molecular orientation in the film by overcoming the entropic force.

Since the intrinsic birefringence in eqs. 2.3 and 2.4 is a function of wavelength, the orientation birefringence is dependent upon the wavelength. Therefore, birefringence control is required in a wide range of visible light. In particular, the extraordinary wavelength dispersion has been desired recently because of the industrial importance for high performance retardation films such as wave plates. The property can provide a specific retardation, *e.g.*, a quarter or a half of the wavelength, in the whole visible light. However, the wavelength dispersion of most polymers is represented by the following relation called the Sellmeier equation [8].

$$\Delta n(\lambda) = A' + \frac{B'}{\lambda^2 - {\lambda_{ab}}^2} \tag{2.5}$$

where λ_{ab} is the wavelength of a vibrational absorption peak in ultraviolet region and A' and B' are the Sellmeier coefficients. The equation indicates that the absolute value of birefringence decreases with increasing the wavelength, *i.e*., ordinary wavelength dispersion.

At present, various techniques are proposed to obtain films showing extraordinary dispersion. One of the conventional methods is by piling two or more polymer films having different wavelength dispersions, in which the fast axis of one film is set to be parallel to the slow axis of the other films, as illustrated in Figure. 2.1 [4,22,23]. Although this technique is currently employed in industry to fabricate retardation films, it leads to poor cost-performance due to the complicated processing operation and results in a thick display. Therefore, it is more favorable to use a single film with extraordinary wavelength dispersion of birefringence. Blending with another polymer [24-26] or a low-mass compound [22,23], copolymerization with appropriate monomers [27], and addition of nonspherical materials having polarizability anisotropy [28] are promising techniques to provide the extraordinary dispersion.

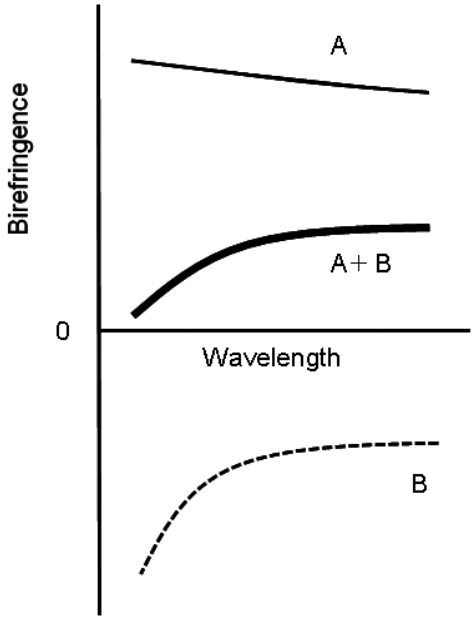

Figure 2.1 Schematic illustration of extraordinary dispersion of orientation birefringence for miscible polymer blend comprising of polymer A with positive birefringence and polymer B with negative birefringence.

In previous paper [29], it was demonstrated that cellulose acetate propionate (CAP) and cellulose acetate butyrate (CAB) having appropriate substitution of each ester group show extraordinary wavelength dispersion. Moreover, the sign of orientation birefringence of CTA is negative, whereas that of CAP and CAB is positive. It was also shown in the paper that the orientation of main chains is not important to decide the orientation birefringence. Based on these experimental results, it was deduced (but not proved directly) that the contribution of both acetyl and propionyl/butyryl groups plays an important role in the birefringence, while the contribution of the hydroxyl group is ignored. Furthermore, the photoelastic birefringence in the glassy state was also investigated and found to be positive even for CTA. The opposite sign of the stress-optical coefficient between rubbery and glassy states for CTA suggests that the origin of the birefringence is completely different as the same with that of the stress generation. Moreover, the effect of a plasticizer was

mentioned in the study. Although the species of plasticizers affects the orientation birefringence, the detailed mechanism was not clarified.

In the following paper [22], the effect of the hydroxyl group on the orientation birefringence was examined using cellulose diacetate (CDA). It was found that the hydroxyl group provides positive orientation birefringence to a great extent. The result indicates that the hydroxyl group in CAP and CAB plays an important role in the orientation birefringence, although it was not mentioned in the original paper [29]. Moreover, nematic interaction, which is a phenomenon in which low-mass compounds are forced to orient to the same direction by the alignment of polymer chains, between CTA chains and plasticizer molecules was indicated during stretching in the rubbery state, which can be applicable to control the wavelength dispersion.

It is found in this paper that the sign of the optical anisotropy of out-of-plane birefringence in a solution-cast CTA film is opposite to that of in-plane orientation birefringence in a hot-stretched one. Moreover, the wavelength dispersion of the birefringence is found to be extraordinary one for the out-of-birefringence of a cast film. The mechanism of this peculiar phenomenon is discussed in detail. Finally, the nematic interaction in a solution-cast film is also discussed using CTA films containing a specific plasticizer with large polarizability anisotropy, which will be an advanced technique to control the out-of-plane birefringence.

2.2 Experimental

2.2.1 Materials

Cellulose triacetate (CTA) was obtained from Acros Organic. The degree of substitution is 2.96, and the molecular weight M_w is 3.50×10^5 which was evaluated using a gel permeation chromatograph (Tosoh, HLC-8020) with TSK-GEL® GMHXL as polystyrene standard. The plasticizer used in this study was tricresyl phosphate (TCP) produced by Daihachi Chemical Industry. The CTA films were prepared using a solution-cast method. Both CTA and CTA/TCP (95/5 in weight) were dissolved into dichloromethane (CH_2Cl_2) and methanol (CH_3OH) in 9 to 1 weight ratio and stirred for 24 h at room temperature before casting. In order to study the effect of solvent, chloroform ($CHCl_3$) was also employed instead of dichloromethane in the same ratio. The solution containing 4 wt% of CTA was poured into a glass petri dish (80 mm dia x 15 mm H) with a flat bottom at room temperature to allow the solvent to evaporate. The thickness of the films obtained was from 50 to 300 μm, which was controlled by varying the amount of the CTA solution.

2.2.2 Measurements

Evaporation rate was measured by weight loss using an electronic balance (Mettler Toledo, AB204-S), during the drying process. Moreover, the effect of the evaporation rate was investigated by preparing various cast films dried with and without an aluminium foil over the glass petri dishes. The solution was exposed to the open atmosphere as a standard condition for evaporation process. To prepare the films at (i) slow and (ii) very slow evaporation conditions, some petri dishes containing the solution were covered with an

aluminium foil having large and small holes, respectively. The weight loss by evaporation V_e was calculated by the following equation.

$$V_e(\%) = \frac{G_0 - G(t)}{G_0} \times 100 \qquad (2.6)$$

where G_0 is the initial weight of CTA solution; $G(t)$ is the weight of CTA solution after t minutes at room temperature.

The uniaxial oriented films were also prepared by hot-stretching operation using a tensile machine with a temperature controller (UBM, DVE-3 S1000) at various draw ratios. The initial distance between the clamps was 10 mm, and the stretching rate was 0.5 mm/s. The drawn samples were quenched by cold air blowing to avoid relaxation of the molecular orientation.

The temperature dependence of oscillatory tensile moduli in the solid state was measured from 0 to 250 °C by a dynamic mechanical analyzer (UBM, E-4000) using rectangular specimens with 5 mm in width and 20 mm in length. The frequency and heating rate used were 10 Hz and 2 °C/min, respectively.

The optical properties of CTA films were measured at room temperature by a polarized optical microscope (Leica, DMLP) and an optical birefringence analyzer (Oji Scientific Instruments, KOBRA-WPR). The retardation in the thickness direction (out-of-plane birefringence) R_{th} was determined by retardation measurements at an oblique incidence angle of 40° as a function of wavelength by changing color filters. The corresponding birefringence was calculated using the film thickness measured by a digital micrometer. Prior to the measurement, the CTA films were placed in a temperature-and-humidity

control chamber (Yamato, IG420) at 25 ºC and 50% RH for one day, because the moisture in the film affects the orientation birefringence [30]. Since a small amount of the water which has strong interaction with acetyl or hydroxyl group cannot be eliminated even under a vacuum condition, this treatment is appropriate to obtain the reproducible data. The in-plane retardation (R_{in}) and out-of-plane retardation (R_{th}) are respectively defined as the following relations.

$$R_{in} = \Delta n_{in} \times d = \left(n_x - n_y\right) \times d \tag{2.7}$$

$$R_{th} = \Delta n_{th} \times d = \left(\frac{n_x + n_y}{2} - n_z \right) \times d \tag{2.8}$$

where d is the film thickness.

The refractive indices in three principal axis, such as n_x, n_y and n_z, are determined by Δn_{in} and Δn_{th}, assuming the average refractive index $\bar{n}$ is a constant irrespective of stretching. The average refractive index $\bar{n}$ was measured by an Abbe refractometer.

Attenuated total reflection (ATR) measurements using an infrared absorption spectrometer (Perkin Elmer, Spectrum 100) were performed to study the molecular orientation in CTA films. The KRS-5 was employed as an ATR crystal.

Thermal analysis was conducted by a differential scanning calorimeter (DSC) (Mettler, DSC820) under a nitrogen atmosphere. The samples were heated from room temperature to 320 °C at a heating rate of 20 °C/min. The amount of samples in an aluminum pan was about 10 mg in weight.

Wide-angle X-ray diffraction (WAXD) measurements were performed at room temperature using a powder X-ray diffractmeter (Rigaku, RINT2500) by refractive mode. Samples were mounted directly into the diffractmeter. The experiments were carried out using CuKα radiation operating at 40 kV and 30 mA at a scanning rate of 1^{o}/min over 2θ (Bragg angle) range from 10^{o} to 60^{o}.

2.3 Results and Discussion

2.3.1 Effect of film thickness

The molecular orientation in the film occurs when the relaxation time of the solution becomes longer than the characteristic time for the biaxial deformation applied by the compressional stress due to the solvent evaporation, which was quantitatively calculated by Croll (1979). Therefore, the evaporation rate has to be considered to discuss the birefringence in a solution-cast film.

Figure 2.2 (a) shows the growth curves of the weight loss in percent for the CTA solutions to obtain films with various thicknesses. Since all films are prepared using the same petri dish, the thickness is adjusted by the initial volume of the solution. As seen in the figure, the values reach to 96% eventually, suggesting that the solvent is almost fully evaporated at this process. Expectedly, it takes a longer time to prepare a thicker film. This is reasonable because the surface area of the solution is the same irrespective of the film thickness.

In Figure 2.2 (b), the weight loss in gram is plotted against the exposure time. The weight loss is proportional to the exposure time at first, and the slope is a constant for all samples. Then, the slope becomes low in the final stage, as CTA retards the solvent evaporation. Considering that the initial slope is the same for all samples, the exposing area of the solution determines the evaporation rate. The result suggests that evaporation occurs homogeneously without creating a solid film on the top of the solution. Moreover, the figures indicate that the stress applied by the reduction of the solution increases with decreasing thickness of the final film because of the rapid drying process. The distribution of molecular orientation, *i.e.*, birefringence, in the thickness direction in the film is confirmed by the polarized optical microscope. Thin films of *x*-*z* plane cut out from the cast films by an ultramicrotome are observed under crossed polars by inserting a full wave plate, as shown in Figure 2.3. It is found that a homogeneous birefringence color is detected in the whole area of the specimen, demonstrating that molecular orientation is uniform in the thickness direction. This result indicates that homogeneous deformation takes place by the solvent evaporation.

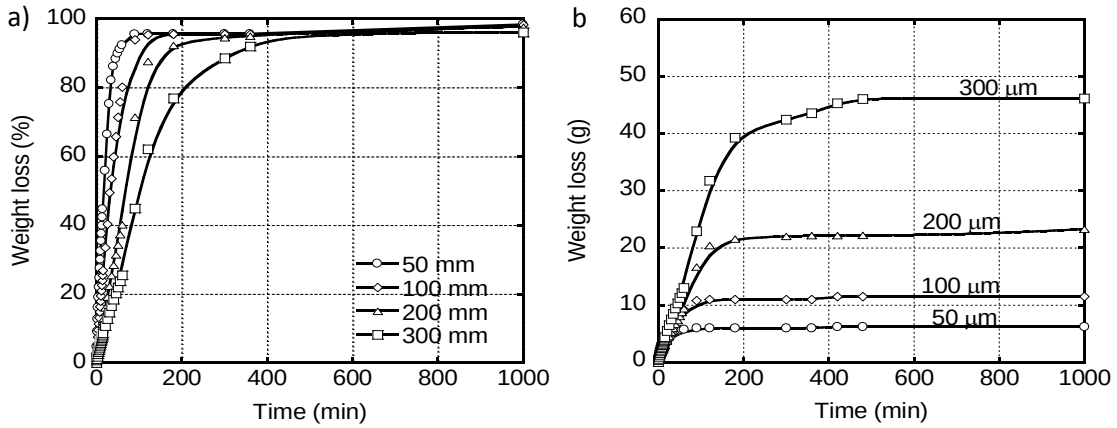

Figure 2.2 a) Growth curves of the weight loss (%) for CTA solutions to obtain films with various thicknesses, 50 μm (○), 100 μm (◊), 200 μm (Δ) and 300 μm (□); b) Growth curves of the weight loss (g) for CTA solutions to obtain films with various thicknesses,50 μm (○), 100 μm (◊), 200 μm (Δ) and 300 μm (□)

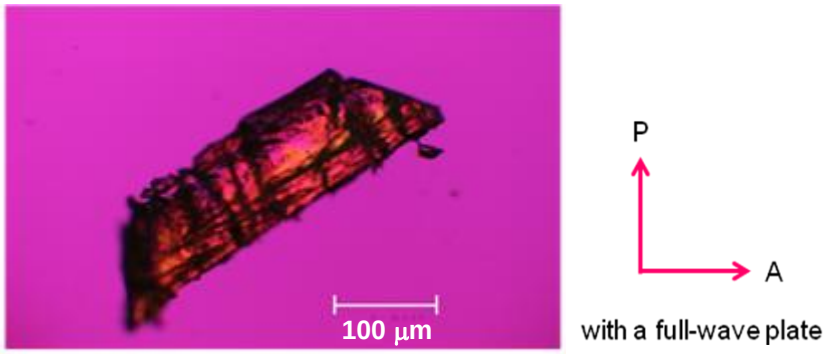

Figure 2.3 The distribution of molecular orientation, confirmed by the polarized optical microscope, in the thickness direction in the film. Crossed polar with a full-wave plate.

The wavelength dispersion of the out-of-plane birefringence is shown in Figure 2.4. It is found that the solution-cast films show positive birefringence ($n_z < n_x, n_y$) that increases with increasing wavelength, *i.e.*, extraordinary wavelength dispersion. This is an anomalous phenomenon for CTA. The in-plane birefringence is, on the other hand, negligible for all films. Generally, the orientation birefringence of CTA is determined by the contribution of acetyl and hydroxyl groups considering the previous researches at the best of our knowledge [22,29,31]. Since the direction of polarizability anisotropy associated with the acetyl group is perpendicular to the main chain, the refractive index in the oriented direction is the lowest, *i.e.*, negative orientation birefringence. Moreover, it is known that the absolute value of birefringence decreases with increasing the wavelength, *i.e.*, ordinary wavelength dispersion, for CTA, as similar to most conventional polymers [4,27,29,32]. However, the contribution of the hydroxyl group cannot be ignored, which provides positive and ordinary wavelength dispersion [22].

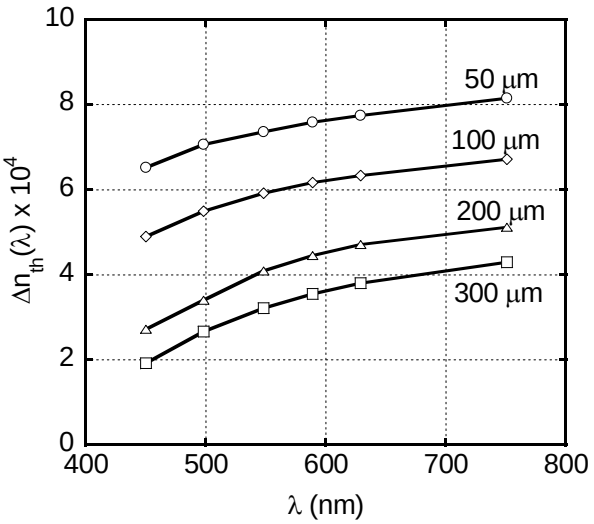

Figure 2.4 Wavelength dispersion of out-of-plane birefringence for cast films with various thicknesses; 50 μm (○), 100 μm (◊), 200 μm (Δ) and 300 μm (□).

Figure 2.4 also demonstrates that the birefringence decreases with increasing film thickness, indicating that the refractive index in the in-plane direction decreases with increasing the film thickness. The decrease in the molecular orientation for a thick film is reasonable, because the rate of solvent removal is slow. Since the solvent can be entrapped in a thick film for a long time as shown in Figure 2.2, the molecules are less oriented in the film plane. Similar results have been reported by another research group, Greener et al. (2005). According to them, a thin film shows a high value of birefringence because the stress builds up faster in the drying process than the stress relaxation [33].

In order to clarify the effect of film thickness on the birefringence, ATR measurements are performed focusing on the C-O-C stretching vibration in the pyranose ring and C=O stretching vibration in the carbonyl group. It should be noted that the same spectra were obtained for both surfaces (air and glass sides), indicating that the skin layer is not well-developed on the free surface (or the contribution of the skin layer on the birefringence can be ignored). As seen in Figure 2.5, the absorbances of the pyranose ring and the carbonyl

group decrease with increasing the film thickness. Considering that the penetration depth of IR beam ($d_p = \frac{\lambda_1}{2\pi\sqrt{\sin^2\theta - (n_2 - n_1)^2}}$) into the sample is approximately 2.2 μm at 1029 cm^{-1} and 1.2 μm at 1735 cm^{-1}, the film thickness itself does not affect the absorbance. The results indicate that the pyranose ring and the carbonyl group are aligned in the film plane, which is pronounced in a thin, *i.e.*, rapid evaporation film. The in-plane orientation of the carbonyl group will be responsible for the positive out-of-plane birefringence. In the case of a hot-stretched film of CTA, the carbonyl group orients perpendicular to the stretching direction. Consequently, the refractive index in the perpendicular direction is always higher than that in the stretching direction, leading to negative orientation birefringence. On the contrary, the carbonyl group preferably exists in a film plane for a solution-cast film, which is attributed to the in-plane orientation of the pyranose ring. As a result, the refractive index in the film plane is larger than that in the thickness direction, although the backbone chains of CTA are also in the film plane.

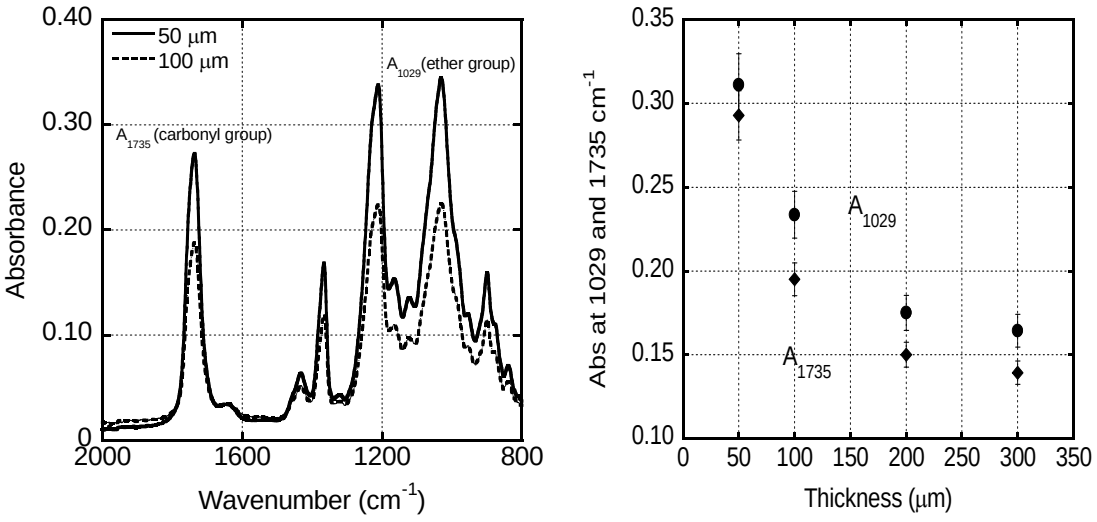

Figure 2.5 ATR spectra of CTA films with different film thicknesses and relation between film thickness and absorbances of pyranose ring (A_{1029}) (●) and carbonyl group (A_{1735}) (♦)

According to previous paper [22], the extraordinary wavelength dispersion for CDA is attributed to the contributions of the polarizability anisotropy of both hydroxyl and acetyl groups, in which the hydroxyl group provides positive birefringence with weak wavelength dispersion and the acetyl group gives negative one with strong wavelength dispersion. In this study, CTA also shows extraordinary wavelength dispersion suggesting that the contribution of the hydroxyl group cannot be ignored even if the amount is small.

In the case of CTA, the crystallization state has to be considered, because it is well known that CTA is a crystalline polymer [2,34]. As shown in Table 2.1, it is found that the degree of crystallization is almost constant irrespective of the film thickness. Furthermore, the degree of the crystallization is calculated to be 32 – 40 wt% based on the literature data [34], which seems to be extremely high for pure CTA. Therefore, WAXD measurements were also carried out as shown in Figure 2.6. Basically, CTA shows three sharp crystal peaks at 2θ of 9, 13 and 17 degree. As seen in the figure, it is found that any distinct peak is not detected in the diffraction pattern except for a broad peak ascribed to amorphous region. The result supports that the crystallites have a negligible effect on the out-of-plane birefringence of CTA.

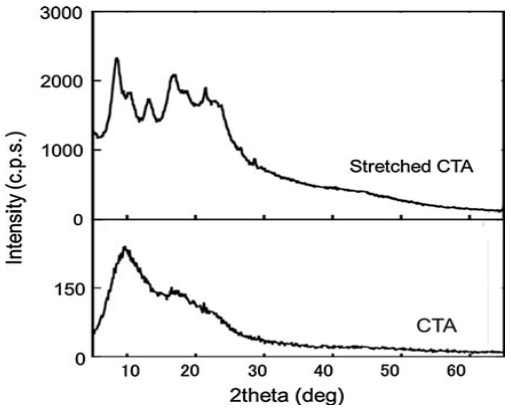

Figure 2.6 WAXD patterns for (bottom) a cast film with a thickness of 100 μm obtained from CH_2Cl_2/CH_3OH at a standard condition, and (top) a film stretched at a draw ratio of 1.5

Table 2.1 Thermal Properties of Solution-Cast Films Obtained at Various Conditions

Conditions				**Heat of Fusion (J/g)**	**T_m (°C)**
Thickness	**Evaporation Rate**	**Solvent**	**TCP**		
50 μm	Standard	CH_2Cl_2/CH_3OH	Not included	13.8	302
100 μm	Standard	CH_2Cl_2/CH_3OH	Not included	12.7	303
200 μm	Standard	CH_2Cl_2/CH_3OH	Not included	11.5	304
300 μm	Standard	CH_2Cl_2/CH_3OH	Not included	10.9	303
100 μm	Slow	CH_2Cl_2/CH_3OH	Not included	12.1	302
100 μm	Very slow	CH_2Cl_2/CH_3OH	Not included	11.3	303
100 μm	Standard	$CHCl_3/CH_3OH$	Not included	12.1	302
100 μm	Standard	CH_2Cl_2/CH_3OH	Included	10.2	294

It can be concluded from Figures 2.2-2.5, the achievable anisotropy is found to be a function of the evaporation rate. Therefore, further study is performed focusing the effect of evaporation rate.

2.3.2 Effect of evaporation rate

The evaporation rate is controlled by covering the petri dishes with an aluminium foil. The growth curves of the weight loss are shown in Figure 2.7. In the figure, the "standard" represents the cast film obtained from uncovered petri dishes as the same with the samples in Figure 2.2. The "slow" and "very slow" denote the cast films obtained with an aluminium foil having large and small holes, respectively. The thickness of all films is approximately 100 μm. As seen in the figure, the evaporation rate can be controlled by this technique. The initial slope of "standard" is three times larger than that of "very slow".

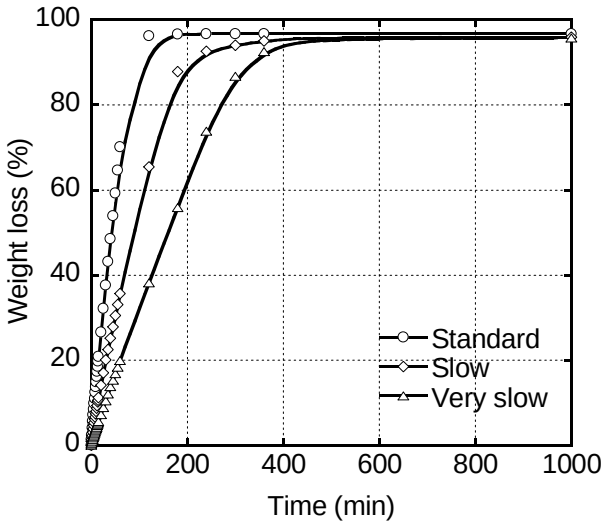

Figure 2.7 Growth curves of the weight loss (%) for CTA solutions at various evaporation rates; standard (○), slow (◊) and very slow (Δ).

The wavelength dispersion of out-of-plane birefringence of the samples is shown in Figure 2.8. All films show positive birefringence with extraordinary wavelength dispersion irrespective of the evaporation rate. However, the magnitude of the birefringence increases with increasing the evaporation rate. Therefore, a similar situation with a thick film occurs for the film evaporated slowly. The decrease in the birefringence for a film obtained by the

prolonged evaporation process suggests that stress, *i.e.*, molecular orientation, is relaxed. It is reasonable because the polymer chains are able to move randomly during the cast process.

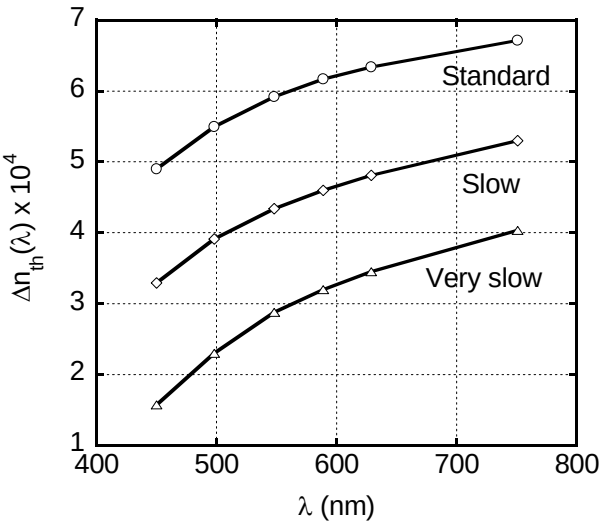

Figure 2.8 Wavelength dispersion of out-of-plane birefringence for films obtained at various evaporation rates; standard (○), slow (◊) and very slow (Δ).

The effect of the evaporation rate on the crystallization of CTA is also studied by DSC. As shown in Table 2.1, however, the heat of fusion, and thus, the degree of crystallization is not changed in this experimental condition.

2.3.3 Effect of solvent type

The species of solvents affects the evaporation rate and thus the out-of-plane birefringence as shown in Figures 2.9 and 2.10, respectively. As seen in Figure 2.9, the evaporation rate of the mixed solvent of CH_2Cl_2 and CH_3OH is faster than that of $CHCl_3$ and CH_3OH, because the vapor pressure of CH_2Cl_2 (47 kPa at 20 °C) is higher than that of $CHCl_3$ (21 kPa at 20 °C) at room temperature. Moreover, it is identified that the whole curve of the

$CHCl_3/CH_3OH$ solution is almost the same as that of the CH_2Cl_2/CH_3OH solution with an aluminium foil having small holes ("slow" in Figure 2.7). The result demonstrates that the retardant effect of the evaporation by CTA is almost the same for both solvents. This would be attributed to similar molecular interaction with CTA for both solvents.

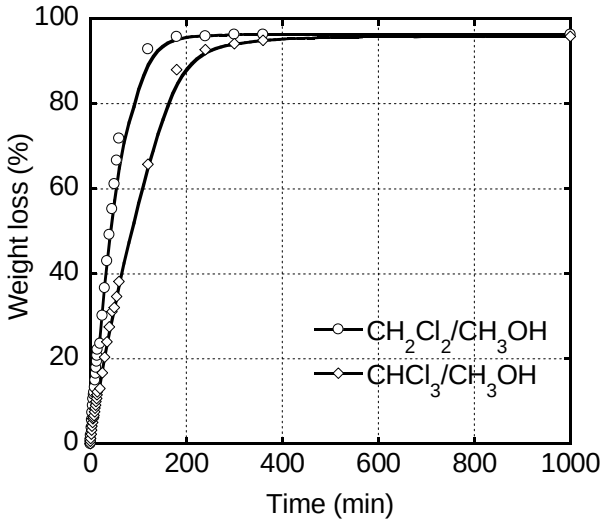

Figure 2.9 Growth curves of the weight loss (%) for CTA solutions using CH_2Cl_2/CH_3OH (○) and $CHCl_3/CH_3OH$ (◊) as solvents.

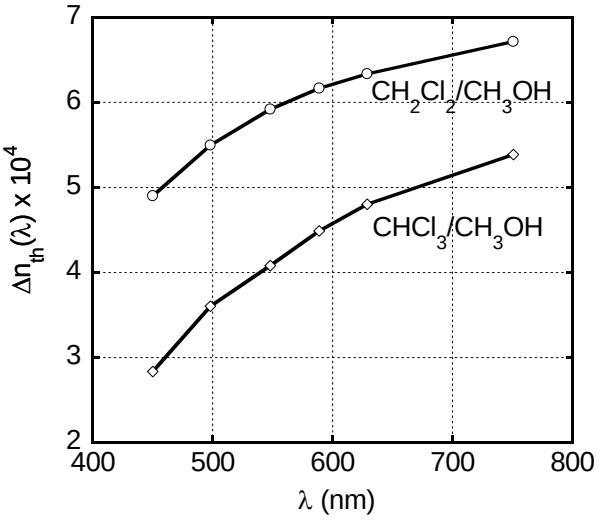

Figure 2.10 Wavelength dispersion of out-of-plane birefringence for the cast films obtained from CH_2Cl_2/CH_3OH (○) and $CHCl_3/CH_3OH$ (◊).

Because of the difference in the evaporation rate, the relaxation of molecular orientation of CTA is pronounced for the $CHCl_3/CH_3OH$ solution as long as the evaporation condition is the same. Therefore, the CTA film prepared by CH_2Cl_2/CH_3OH shows higher out-of-plane birefringence than that the film by $CHCl_3/CH_3OH$, as seen in Figure 2.10.

The out-of-plane birefringence at 588 nm is plotted against the initial slope of the weight loss in Figure 2.11. As seen in the figure, the birefringence of the film obtained from the $CHCl_3/CH_3OH$ solution is located on the line of the data from the CH_2Cl_2/CH_3OH solution. The result demonstrates that the out-of-plane birefringence is independent of the species of solvents, but depends on the evaporation rate.

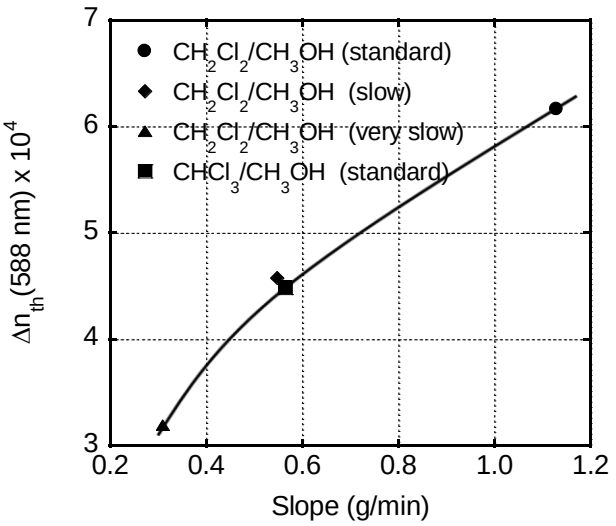

Figure 2.11 Out-of-plane birefringence at 588 nm for the cast films plotted against the initial slope of the weight loss (g); CH_2Cl_2/CH_3OH (standard) (●), CH_2Cl_2/CH_3OH (slow) (♦), CH_2Cl_2/CH_3OH (very slow) (▲) and $CHCl_3/CH_3OH$ (standard) (■).

2.3.4 Effect of plasticizer

Recently, it has been clarified that addition of specific plasticizers can control the orientation birefringence of a stretched film. In particular, it was found that orientation birefringence is enhanced by TCP for cellulose esters [23]. The phenomenon is explained by nematic interaction, *i.e.*, intermolecular orientation correlation [35,36]. Although TCP is a low mass compound in a liquid state, the molecules are forced to orient in the same direction with the polymer chains. Considering that the nematic interaction occurs when the size of a low mass compound is comparable with the segmental size of a matrix polymer [37-39], TCP has an appropriate size for CTA. To the best of our knowledge, however, the nematic interaction in solution-cast films has not been studied yet.

Figure 2.12 shows the out-of-plane birefringence of a CTA film containing 5 wt% of TCP with the data of pure CTA. As seen in the figure, addition of TCP greatly enhances the out-of-plane birefringence of CTA. Since the evaporation rate is not affected by the addition of TCP (but not presented here), the enhancement is attained by the orientation of TCP molecules in the film plane accompanied with CTA chains. Also in this experiment, the degree of crystallization is not changed as shown in Table 2.1.

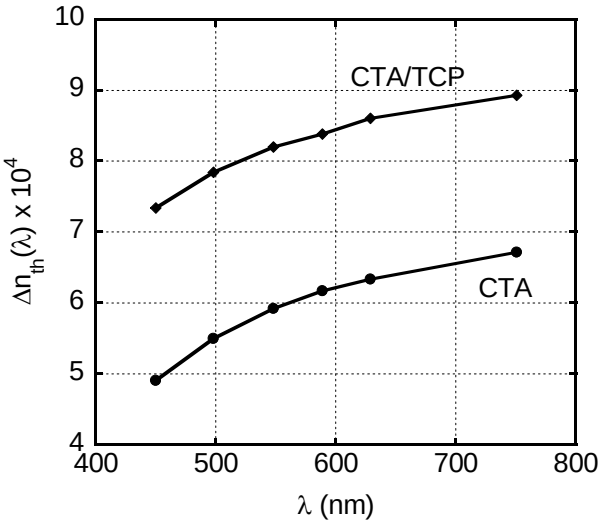

Figure 2.12 Wavelength dispersion of out-of-plane birefringence for CTA (●) and CTA/TCP (♦). The cast films with a thickness of 100 μm were prepared by CH_2Cl_2/CH_3OH at a standard condition.

In order to confirm the contribution of TCP to the birefringence, the CTA/TCP film is immersed in methanol for 24 h to remove TCP. Then, the out-of-plane birefringence is measured again after drying at room temperature under a vacuum condition. Prior to the measurement, it is confirmed that the methanol immersion does not affect the birefringence of the pure CTA. The removal of TCP is checked by FT-IR spectra, and the following experiment is performed after keeping the sample in the temperature-and-humidity controller for 24 hrs, as illustrated in Figure 2.13. The FT-IR spectrum for CTA/TCP shows a strong absorption peak around 780 cm^{-1}, which is not detected in CTA but appears in TCP spectrum. This peak is attributed to the vibration of C-H bond in meta-disubstituted benzene of TCP [23]. Therefore, the lack of this peak suggests that TCP has been completely removed out. After methanol immersion, the birefringence of CTA/TCP decreases approaching to that of pure CTA, as illustrated in Figure 2.14. The result demonstrates that TCP molecules oriented by nematic interaction enhance the out-of-plane

birefringence. In other words, the out-of-plane birefringence can be controlled by not only evaporation rate but also the species and amount of additives.

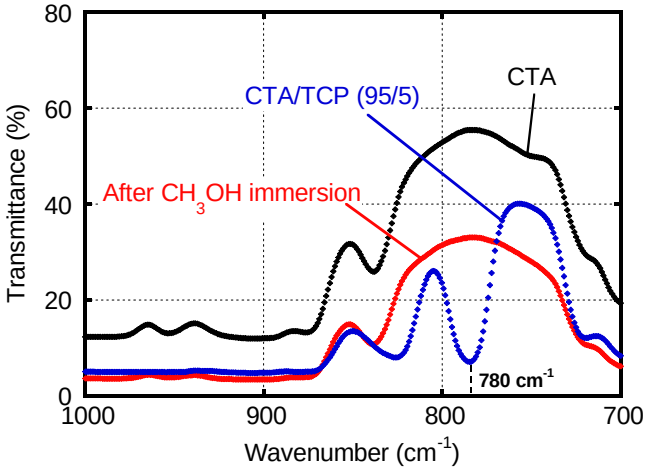

Figure 2.13 The FT-IR spectra for CTA and CTA/TCP before and after immersion in methanol.

As mentioned in introduction, the competition of molecular motion and deformation applied by the solvent evaporation determines the molecular orientation in a solution-cast film. In other words, CTA chains orient in the film plane by applied uniaxial compression deformation due to the solvent evaporation. At the same time, TCP molecules orient accompanied with the CTA chains. Therefore, the orientation relaxation of TCP molecules will be affected strongly by the existence of a solvent, although the relaxation time is reduced for both CTA and TCP. The experimental results indicate that the nematic interaction, *i.e.*, orientation of TCP molecules, ocuurs only at the final stage of evaporation. Therefore, a solvent that retards the evaporation rate at the final stage to obtain smooth surface will have a strong influence on the orientation of additives.

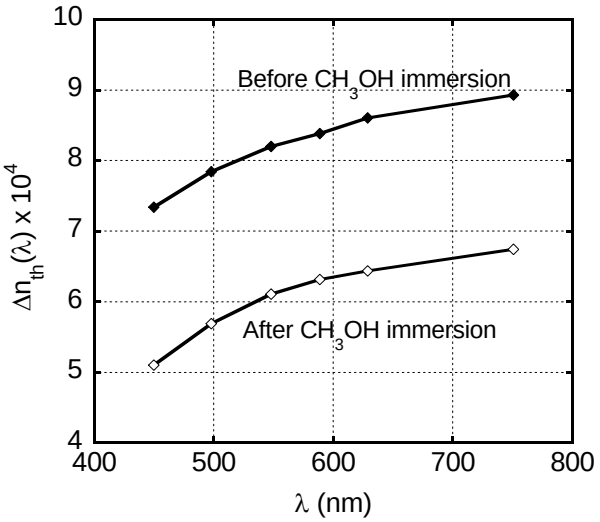

Figure 2.14 Wavelength dispersion of out-of-plane birefringence for CTA/TCP before (♦) and after immersion in methanol (◊).

2.3.5 Effect of hot-stretching

The hot-stretching was performed at the temperature where the tensile storage modulus at 10 Hz with a strain rate of 0.05 s^{-1} was 10 MPa (212 °C). The stress-strain curve is shown in Figure 2.15. The curve is a typical one for a viscoelastic body in a rubbery region.

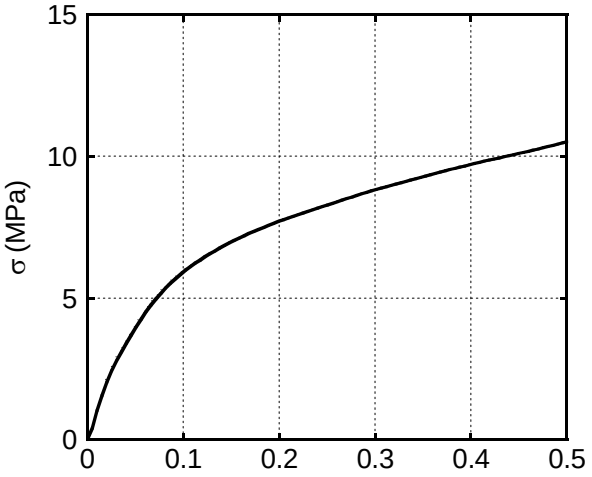

Figure 2.15 Stress (σ) – strain (ε) curve at 212 °C for CTA.

The refractive indices at 588 nm along three principle axes for films with various draw ratios are illustrated in Figure 2.16. In this experiment, the hot-stretching was performed in the *x* direction.

As mentioned, the solution-cast film is randomly oriented in the film plane, *i.e.*, $n_x = n_y$, but the principle refractive index in the thickness direction n_z is lower than n_x and n_y, which results in the positive out-of-plane birefringence. On the contrary, a hot drawn film shows negative in-plane birefringence.

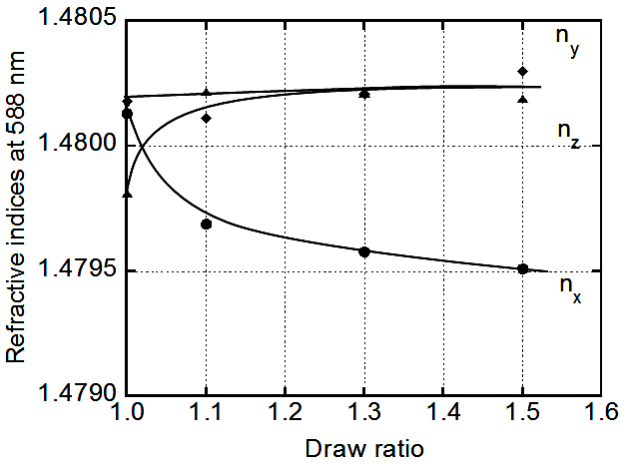

Figure 2.16 Refractive indices along three principle axes; n_x (●), n_y (♦) and n_z (▲) for CTA films stretched at various draw ratios.

The wavelength dispersion of in-plane and out-of-plane birefringences for the stretched films is shown in Figure 2.17. As seen in the figure, the order in the refractive indices changes with the draw ratio. When the draw ratio is around 1.035, n_z is almost the same as $(n_x + n_y)/2$ at 588 nm. Beyond this draw ratio, the out-of-birefringence of the unstretched sample shows extraordinary wavelength dispersion, whereas in-plane and out-of-plane birefringences for the stretched films exhibit ordinary wavelength dispersion. Moreover,

the out-of-birefringence of the stretched films is almost independent of the applied strain level, when the draw ratio is larger than 1.1.

The negative in-plane birefringence in CTA suggests that the direction of the polarizability anisotropy associated with the acetyl group is perpendicular to the main chain. This result corresponds to the previous reports [22,23,30,31].

Because the hot-stretching is carried out beyond the glass transition temperature, the degree of crystallinity has to be considered more seriously. The top pattern in Figure 2.6 shows the WAXD profile of a stretched film at a draw ratio of 1.5. As seen in the figure, several distinct peaks are clearly detected, which are attributed to the thermal history beyond the glass transition temperature with the flow induced crystallization during stretching. Therefore, the contribution of crystalline phase cannot be ignored especially after hot-stretching. It was found that the extraordinary wavelength dispersion of CAP becomes pronounced with increasing the draw ratio [22]. The result indicates that the acetyl group plays a more important role in the total birefringence with increasing the draw ratio. A similar situation is expected also for CTA, because the acetyl group is in the crystalline structure with the strong polarizability anisotropy in the direction perpendicular to the chain axis. In other words, the wavelength dispersion and the magnitude of birefringence for CTA, including solution-cast films, can be modified by controlling the crystalline state.

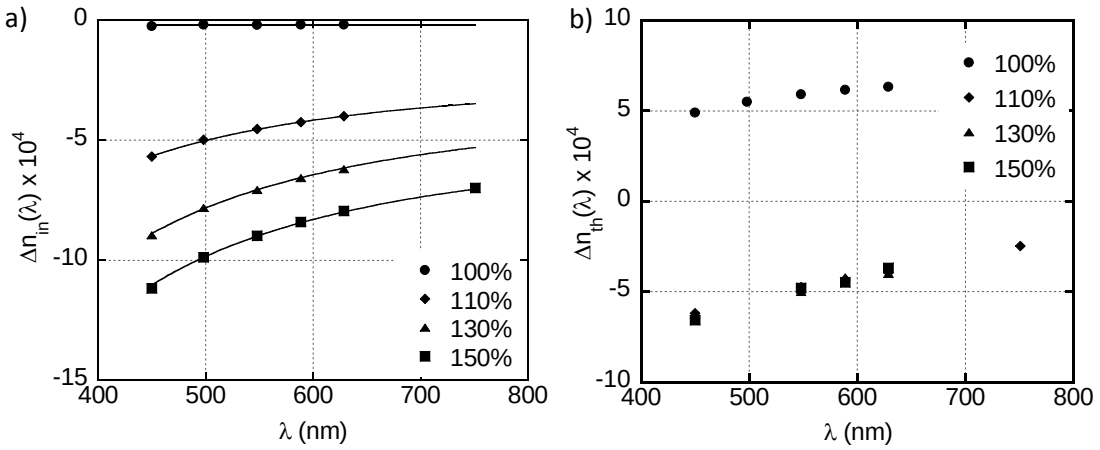

Figure 2.17 Wavelength dispersion of a) in-plane birefringence and b) out-of-plane birefringence for a cast film (●) and stretched films with draw ratios of 1.1 (♦), 1.3 (▲), and 1.5 (■). The cast films with a thickness of 100 μm were prepared by CH_2Cl_2/CH_3OH at the standard condition.

2.4 Conclusions

The orientation birefringence of CTA films produced by a solution-cast method is studied. Prior to stretching, the CTA film shows positive out-of-plane birefringence with extraordinary wavelength dispersion, whereas the stretched film shows negative birefringence. The positive birefringence is attributed to the in-plane orientation of the acetyl group in CTA, which is confirmed by ATR. A thin film shows marked birefringence, which is originated from the molecular orientation in the film plane due to the stress applied by the solvent evaporation. Similarly, prompt evaporation enhances the birefringence irrespective of the species of solvents. Moreover, it is found that the out-of-plane birefringence of CTA increases with the addition of TCP. This is attributed to the molecular orientation of TCP by the nematic interaction, *i.e.*, intermolecular orientation

correlation, between CTA and TCP. This will be a key technology in the field of high-performance optical films to improve the contrast of LCD, because there are numerous low-mass compounds having strong polarizability anisotropy.

References

[1] Edgar, K. J.; Buchanan, C. M.; Debenham, J. S.; Rundquist, P. A.; Seiler, B. D.; Shelton, M. C.; Tindall, D. *Prog. Polym. Sci.* **2001**, *26*, 1605-1688.

[2] Sata, H.; Murayama, M, Shimamoto S. *Macromol. Symp.* **2004**, 208, 323-333.

[3] Yamaguchi, M. Optical properties of cellulose esters and their blends. In *Cellulose: Structure and Properties, Derivatives and Industrial Uses*; Lejeune, A., Deprez, T., Eds.; Nova Science Publishers, Inc.: New York, 2010, pp 325-340.

[4] Yamaguchi, M.; Mohd Edeerozey, A. M.; Songsurang, K.; Nobukawa, S. *Cellulose* **2012**, *19*, 601-613.

[5] Tagaya, A.; Iwata, S.; Kawanami, E.; Tsukahara, H.; Koike, Y. *Jpn. J. Appl. Phys.* **2001**, *40*, 6117-6123.

[6] Tagaya, A.; Ohkita, H.; Mukoh, M.; Sakaguchi, R.; Koike, Y. *Science* **2003**, *301*, 812-814.

[7] Tagaya, A.; Ohkita, H.; Harada, T.; Ishibashi, K.; Koike, Y. *Macromolecules* **2006**, *39*, 3019-3023.

[8] Kuhn, W.; Grün, F. *Kolloid-Z* **1942**, *101*, 248-271.

[9] Treloar, L. R. G. *The physics of rubber elasticity*, Clarendon Press: Oxford. 1958.

[10] Read, B. E. *Structure and properties of oriented polymers*, Ward IM. Ed.; Applied Science Publishers: London, Chap. 4. 1975.

[11] Harding, G. F. Optical properties of polymers, Meeten GH, Ed.; Applied and Science: London, Chap. 2. 1986

[12] Marks, J. E.; Erman, B. *Rubberlike elasticity A molecular primer*, Wiley: New York. 1988.

[13] Hermans, P. H.; Platzek, P. *Kolloid-Z* **1939**, *88*, 68-72.

[14] Sosnowski, T. P.; Weber, H. P. *Appl. Phys. Lett.* **1972**, *21*,310-312.

[15] Croll, S. G. *J. Appl. Polym. Sci.* **1979**, *23*, 847-858.

[16] Prest, W. M.; Luca, D. J. *J. Appl. Phys.* **1979**, *50*, 6067-6072.

[17] Prest, W. M.; Luca, D. J. *J. Appl. Phys.* **1981**, *51*, 5170-5175.

[18] Cohen, Y.; Reich, S. *J. Polym. Sci. Polym. Phys. Ed.* **1981**, *19*, 599-608.

[19] Machell, J. S.; Greener, J.; Contestable, B. A. *Macromolecules* **1990**, *23*, 186-194.

[20] Lei, H.; Payne, A.; McCormick, A. V; Francis, L. F.; Gerberich, W. W.; Scriven, L. E. *J. Appl. Polym. Sci.* **2001**, *81*, 1000-1013.

[21] Greener, J.; Chen, J. *IDMC.* **2005**, Taipei, Taiwan.

[22] Yamaguchi, M.; Okada, K.; Mohd Edeerozey, A. M.; Shiroyama, Y.; Iwasaki, T.; Okamoto, K. *Macromolecules* **2009**, *42*, 9034-9040.

[23] Mohd Edeerozey, A. M.; Tsuji, M.; Shiroyama, Y.; Yamaguchi, M. *Macromolecules* **2011**, *44*, 3942-3949.

[24] Uchiyama, A.; Yatabe, T. *Jpn. J. Appl. Phys.* **2003**, *42*, 3503-3507.

[25] Uchiyama, A.; Yatabe, T. *Jpn. J. Appl. Phys.* **2003**, *42*, 5665-5669.

[26] Kuboyama, K.; Kuroda, T.; Ougizawa, T. *Macromol. Symp.* **2007**, *249-250*, 641-646.

[27] Uchiyama, A.; Yatabe, T. Jpn. J. Appl. Phys. **2003c**, *42*, 6941-6945.

[28] Koike, Y.; Yamazaki, K.; Ohkita, H.; Tagaya, A. *Macomol. Symp.* **2006**, *235*, 64-70.

[29] Yamaguchi, M.; Iwasaki, T.; Okada, K.; Okamoto, K. *Acta Materialia* **2009**, 57, 823-829.

[30] Mohd Edeerozey, A. M.; Tsuji, M.; Nobukawa, S.; Yamaguchi, M. *Polymers* **2011**, 3, 955-966.

[31] El-Diasty, F.; Soliman, M. A.; Elgendy, A. F. T.; Ashour, A. *J. Opt. A Pure Appl. Opt.* **2007**, *9*, 247-252.

[32] Yamaguchi, M.; Lee, S.; Mohd Edeerozey, A. M.; Tsuji, M.; Yokohara, T. *Eur. Polym. J.* **2010**, *46*, 2269-2274.

[33] Greener, J.; Lei, H.; Elman, J.; Chen, J. *J. SID.* **2005**, *13*, 835-839.

[34] Takahashi, A.; Kawaharada, T.; Kato, T. *Polym. J.* 1979, *11*, 671-675.

[35] Doi, M.; Watanabe, H. *Macromolecules* **1991**, *24*, 740-744.

[36] Watanabe, H.; Kotaka, T.; Tirrell, M. *Macromolecules* **1991**, *24*, 201-208.

[37] Urakawa, O.; Ohta, E.; Hori, H.; Adachi, K. *J. Polym. Sci. Polym. Phys. Ed.* **2006**, *44*, 967-974.

[38] Nobukawa, S.; Urakawa, O.; Shikata, T.; Inoue, T. *Macromolecules* **2010**, *43*, 6099-6105.

[39] Nobukawa, S.; Urakawa, O.; Shikata, T.; Inoue, T. *Macromolecules* **2011**, 44, 8324-8332.

Chapter 3

Three-Dimensional Orientation Control by Uniaxial Drawing of Cellulose Triacetate Film

3.1 Introduction

Cellulose triacetate (CTA), one of the biomass-derived materials, has found its applications in various films that are produced by a solution-cast method because of severe thermal degradation beyond the melting point [1-3]. In an optical film application, CTA has been utilized as a photographic film base and a polarizer protection film for years because of their attractive properties such as high transparency and excellent heat resistant [1-3]. It is well known that CTA films are mainly employed in liquid crystal display (LCD) at present and will be used for advanced systems such as 3D display and electro-luminescent display. In order to be used for polarizer protective and retardation films, birefringence control is extremely important. In the case of polarizer protective films, for example, the films have to be free from birefringence, and advanced methods to erase the birefringence have been proposed recently [4-6]. For retardation films, specific retardation, *i.e.*, the product of birefringence and thickness, should be provided.

It is well known that orientation birefringence is determined by the chain orientation and molecular polarizability. For example, a polymer showing positive birefringence has a large molecular polarizability, *i.e.*, refractive index, in the main chain direction. The value of birefringence is further controlled by the chain orientation by stretching a film. In general, refractive indices in the plane direction (n_x and n_y) can be controlled by uniaxial stretching, but it is not sufficient to control the refractive index of the film-thickness direction n_z. Therefore a special method should be used to control the refractive index n_z and to satisfy the relation of refractive indices.

Several approaches to obtain the three-dimensional characteristics of the refractive indices have been studied by several researchers. The most conventional method will be biaxial stretching which is, however, considerably an expensive method. Therefore, various approaches have been proposed. According to Arakawa, the desired film is obtained by slicing an extruded rod in which the molecule is oriented [7]. Yoshimi proposed a laminating method using a shrinkable film [8]. This method comprises of laminating a resin film, *i.e.*, the desired film, on one or both sides by a shrinkable polymer film. Then this laminate is stretched while being simultaneously heated so that the ability to shrink in the direction perpendicular to the stretching direction is passed on to the resin film. Three-dimensional control was also performed by film preparation under an electric or magnetic field [9]. After the polymer is oriented in the film-thickness direction in the solution, the polymer film is stretched. There is also a stacking method in which a stretched film with positive birefringence is stacked with a stretched film with negative birefringence [10].

Not only three-dimensional control but also the wavelength dispersion of birefringence has been important recently, because of the industrial importance for high performance retardation films. The property can provide a specific retardation, *e.g.*, a quarter or half of the wavelength, in the whole visible light. Most conventional polymers show ordinary dispersion of orientation birefringence as expressed by Sellmeier relation (equation 1). Therefore, various techniques are proposed to obtain the films showing extraordinary dispersion.

$$\Delta n(\lambda) = A + \frac{B}{\lambda^2 - {\lambda_{ab}}^2} \tag{1}$$

where λ_{ab} is the wavelength of a vibrational absorption peak in ultraviolet region, and A and B are the Sellmeier coefficients.

Up to now, several methods such as copolymerization with appropriate monomers [11], doping of anisotropic crystal [12] and blending with another polymer [13-15] or a low-mass compound (LMC) [16-17] have been proposed to control the birefringence in polymeric materials. In a polymer blending method, miscible polymer pairs showing intrinsic birefringence of different signs are mixed on a molecular scale are usually employed to avoid light scattering.

In our preceding papers [16,18,19], transparent films of cellulose acetate propionate (CAP) film show positives in-plane birefringence that increases with increasing wavelength, *i.e.*, extraordinary wavelength dispersion which was explained in detail in our previous papers. Furthermore, also in our previous studies [20], CTA films that have been successfully prepared using solution-cast process show good uniformity in thickness, high transparency, and adequate mechanical properties. The sign of the

optical anisotropy of out-of-plane birefringence in a solution-cast CTA film is opposite to in-plane orientation birefringence in a hot-stretched one. Moreover, the wavelength dispersion of the out-of-plane birefringence is found to be extraordinary for a solution-cast film. My previous study also found that the out-of-plane birefringence and its wavelength dispersion can be modified by addition of a certain plasticizer such as tricresyl phosphate (TCP). The enhancement of positive out-of-plane birefringence in CTA can be achieved by TCP addition, of which a certain amount (5 wt%) of TCP shows a good miscibility with CTA and resulted in highly transparent films [17,20]. This is attributed to the molecular orientation of TCP by the nematic interaction, *i.e.*, intermolecular orientation correlation, between CTA and TCP.

In this study, both three-dimensional refractive indices and wavelength dispersion of birefringence are controlled by uniaxial stretching with addition of various plasticizers with strong polarizability anisotropy. As well known in the field of T-die extrusion, film shrinking to the width direction, known as neck-in behavior, is reduced by modifying rheological properties of a molten polymer. In particular, long-chain branched polymers and weakly crosslinked polymers, showing marked strain-hardening in the transient elongational viscosity, provide small level of neck-in. In other words, planar elongation (one direction elongation with a constant width) rather than uniaxial elongation occurs. Since CTA is a crystalline polymer with low level of crystallinity, it is expected to show planar deformation mode to some degree only by uniaxial stretching. The transversal birefringence due to the transverseal orientation of CTA chains is magnified by plasticizeres. For the purpose, two types of plasticizers are employed from the viewpoint of the molecular shape: tricresyl phosphate (TCP) and

triphenyl phosphate (TPP) as disk-shaped molecules and 4-cyano-4'-pentylbiphenyl (5CB) as a rod-shaped molecule. The mechanism of this peculiar phenomenon is discussed in detail by comparing with blends with CAP having no/little crystallinity.

3.2 Experimental

3.2.1 Materials

The polymeric materials used in this study were commercially available cellulose esters such as cellulose acetate propionate (CAP) and cellulose triacetate (CTA). CAP employed in this study was produced by Eastman Chemical, while CTA was produced by Acros Organics. The molecular characteristics are summarized in Table 3.1. The plasticizer used in this study was tricresyl phosphate (TCP), triphenyl phosphates (TPP) and 4-cyano-4'-pentylbiphenyl (5CB). TCP and TPP in this study are produced by Daihachi Chemical Industry. 5CB was supplied by Wako Pure Chemical Industries Ltd.

Table 3.1. Characteristics of materials.

Sample	Compositions, wt%			Molecular weights	
	Acetyl	Propionyl	Hydroxyl	M_n (x 10^5)	M_w (x 10^5)
CTA	43.6 (2.96)	–	0.9	1.3	3.5
CAP	2.5 (0.19)	46 (2.58)	1.8	0.77	2.1

[a](Parenthesis): degree of substitution.

Both CTA and CAP films were prepared using a solution-cast method. CTA or CAP and plasricizers (95/5 in weight) were dissolved into dichloromethane (CH_2Cl_2) and methanol (CH_3OH) in 9 to 1 weight ratio and stirred for 24 h at room temperature before casting. In order to study the effect of solvent, chloroform ($CHCl_3$) was also employed instead of dichloromethane in the same ratio. The solution containing 4 wt% of polymer was poured into a glass petri dish (80 mm dia x 15 mm H) with a flat bottom at room temperature to allow the solvent to evaporate. The thickness of the films obtained was about 100 μm, which was controlled by the amount of the polymer solution.

Subsequently, the films were hot-drawn using a dynamic mechanical analyzer (UBM, DVE-4) to prepare uniaxial oriented films at different temperatures. The initial distance between the clamps was 10 mm and the stretching rate was 0.5 mm/s. The stress-strain data generated during the stretching was also collected. The samples were quenched by cold air blowing after holding the samples at the draw temperature for various times in the chamber.

3.2.2 Measurements

The temperature dependence of oscillatory tensile moduli in the solid state, such as storage modulus E' and loss modulus E'' were measured from -50 to 250 ^{o}C by a dynamic mechanical analyzer (UBM, E-4000) using rectangular specimens of 5 mm in width and 20 mm in length. The frequency and heating rate used were 10 Hz and 2 ^{o}C/min, respectively.

The refractive index of the polymer films was evaluated by an Abbe refractometer (Atago, NRA 1T) at room temperature employing α-bromonaphthalene as a contact liquid.

The average refractive index with various wavelength was evaluated by a variable angle spectroscopic ellipsometry (VASE; J.A.Woollam Co. Inc.) with λ = 400 –800 nm and 40° incident angle.

The retardation of the drawn films was measured by an optical birefringence analyzer (Oji Scientific Instruments Inc., KOBRA-WPR). The measurements were performed as a function of the wavelength between 450 to 800 nm by changing color filters. Prior to the measurement, the drawn samples were placed in a temperature and humidity control chamber at 25 ^{o}C and 50 %RH.

Attenuated total reflection (ATR) measurements using an infrared absorption spectrometer (Perkin Elmer, Spectrum 100) were performed to study the molecular orientation in CTA films. The KRS-5 was employed as an ATR crystal.

Thermal analysis was conducted by a differential scanning calorimeter (DSC) (Mettler, DSC820) under a nitrogen atmosphere. The samples were heated from room temperature to 320 ^{o}C at a heating rate 20 ^{o}C/min. The amount of sample in an aluminum pan was approximately 10 mg in weight.

Wide-angle X-ray diffraction (WAXD) measurements were performed at room temperature using a powder X-ray diffractmeter (Rigaku, RINT2500) by refractive mode. Samples were mounted directly into the diffractmeter. The experiments were

carried out using CuKα radiation operating at 40 kV and 30 mA at a scanning rate of 1^o/min over 2θ (Bragg angle) range from 10^o to 60^o.

3.3 Results and Discussion

3.3.1 Characteristic of Films Prior to Stretching

The temperature dependence of oscillatory tensile moduli such as storage modulus *E'* and loss tangent *tan* δ for CTA, CAP and CTA blends is measured at 10 Hz to determine the stretching temperature. The results are shown in Figure 3.1. As seen in the figure, *E'* in CTA shows a plateau beyond the glass to rubber transition, in which the modulus is much higher than a rubbery plateau modulus for a typical polymer. This is attributed to the presence of crystallites. In case of CAP, *E'* decreases sharply, resulting in the peak of *tan* δ for CAP is narrower than that of pure CTA. The narrow peak of *tan* δ as observed in CAP is possibly due to CAP have no/little crystallinity. The glass transition temperature T_g, which is defined as the peak temperature of *tan* δ in this study, is around 209 °C for pure CTA. As for the blends, the T_g shifts to 180, 179 and 183 °C by the addition of 5 wt% of TCP, TPP and 5CB, respectively. There is no significant difference in the dynamic mechanical properties between CTA/TCP and CTA/TPP while CTA/5CB shows a slightly higher T_g with a broader peak than the other blends.

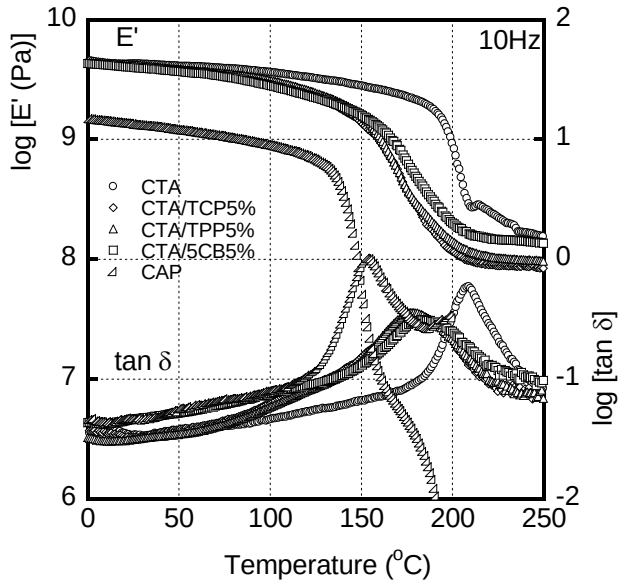

Figure 3.1 Temperature dependence of tensile storage modulus E' and loss tangent tan δ for various samples; CTA (○), CTA/TCP5% (◊), CTA/TPP5% (Δ), CTA/5CB5% (□) and CAP (◿ at 10 Hz.

The wavelength dispersion of the out-of-plane birefringence in the solution-cast films is shown in Figure 3.2. It is found that CTA shows positive birefringence ($n_z<n_x$, n_y) that increases with increasing wavelength, *i.e.*, extraordinary wavelength dispersion. As reported in our preceding paper [20], the pyranose ring and the carbonyl group are aligned in the film plane for a solution-cast film. Therefore, the in-plane orientation of the carbonyl group will be responsible for the positive out-of-plane birefringence. This is an anomalous phenomenon for a conventional polymer film. Generally, the carbonyl group in a hot-stretched CTA film orients perpendicular to the stretching direction. Consequently, the refractive index in the perpendicular direction is always higher than that in the stretching direction, leading to negative orientation birefringence. This phenomenon has been reported in our preceding papers with detailed characterization

[4,16-18,20,21]. Moreover, addition of LMCs greatly enhances the out-of-plane birefringence of CTA. The enhancement is attained by the orientation of LMC molecules in the film plane accompanied with CTA chains.

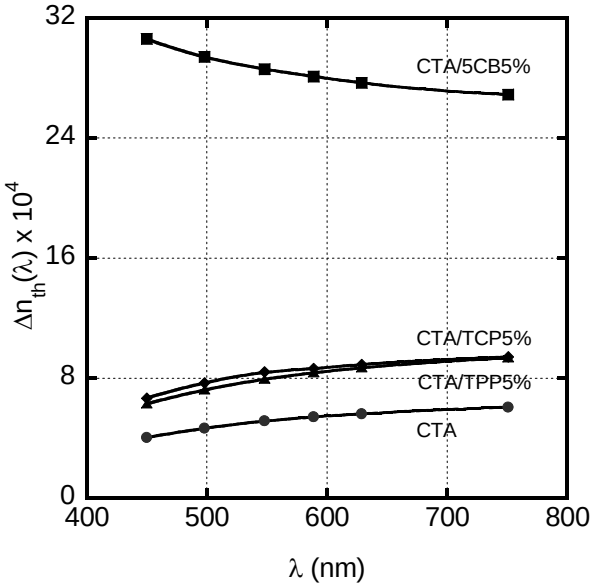

Figure 3.2 Wavelength dispersion of out-of-plane birefringence for CTA and the blends; CTA (●), CTA/TCP5% (♦), CTA/TPP5% (▲) and CTA/5CB5% (■)

3.3.2Characteristic of Films after to Stretching

The stress–strain curves of all samples stretched at temperatures above the glass transition temperature are shown in Figure 3.3. The curves for the samples stretched above the glass transition temperature show a rubber-like behavior without yield point. Moreover, the final stress applied on the plasticized CTA has almost a similar value to that for pure CTA.

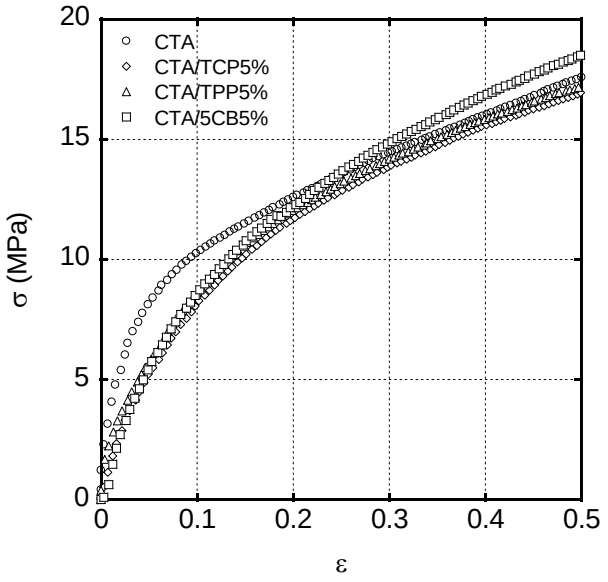

Figure 3.3 Stress–strain curves for CTA and the blends; CTA (○), CTA/TCP5% ◊), CTA/TPP5% (Δ) and CTA/5CB5% (□) stretched at the glass transition temperature.

Prior to the discussion of out-of-plane birefringence, the effect of LMCs on "in-plane" birefringence, *i.e.*, the refractive index difference between stretching and perpendicular directions in the film, of CTA is investigated. As well known, the cast-film prior to stretching has no in-plane birefringence because of random orientation of chain axis in the film plane.

Figure 3.4 shows the wavelength dispersion of the in-plane and out-of-plane birefringences for the stretched CTA films at a draw ratio of 1.5. As seen in Figure 3.4a, the pure CTA shows negative in-plane birefringence that decreases with increasing wavelength, *i.e.*, ordinary wavelength dispersion, as similar to most conventional polymers [4,11,18,19]. The negative orientation birefringence in CTA indicates that the direction of the polarizability anisotropy associated with the acetyl group is perpendicular to the main chain which aligns to the stretching direction. Consequently,

the refractive index in the oriented direction is lower than that in the perpendicular direction, *i.e.*, negative orientation birefringence.

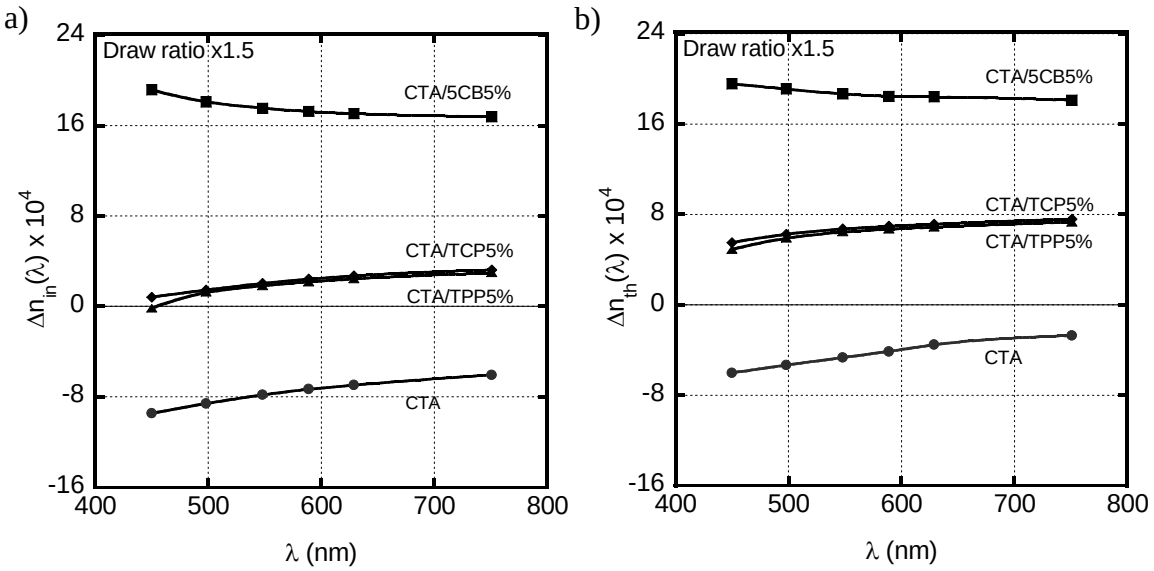

Figure 3.4 Wavelength dispersion of the in-plane and out-of-plane birefringences for the stretched CTA films; CTA (●), CTA/TCP5% (♦), CTA/TPP5% (▲) and CTA/5CB5% (■) at a draw ratio of 1.5.

Upon the addition of TCP, the negative in-plane birefringence of CTA does not increase instead changes drastically from negative to positive with extraordinary wavelength dispersion. The experimental results indicate that orientation of TCP molecules is forced to orient into the stretching direction accompanying the alignment of the polymer chains, which is known as mechanism described as nematic interaction [22-24]. The nematic interaction occurs in a miscible system when a low-mass compound has an appropriate size to move cooperatively with chain segments of a host polymer [25-27]. A similar result is obtained by TPP addition. The orientation birefringence of CTA changes from negative into positive ones with extraordinary

wavelength dispersion. This is reasonable because TPP has a similar chemical structure to TCP. The interaction between CTA and plasticizer is also performed by ATR measurements focusing on the C-O-C stretching vibration in the pyranose ring (1,029 cm^{-1}) and C=O stretching vibration in the carbonyl group (1,735 cm^{-1}), as shown in Figure 3.5. It is found that all plasticizers do not affect the intensity of the absorbances of the pyranose ring and the carbonyl group of pure CTA, indicating that there is no specific interaction such as chemical or electrostatic interactions between CTA and plasticizer.

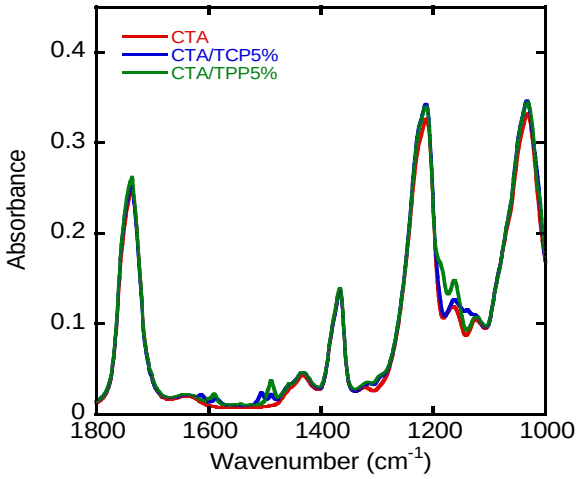

Figure 3.5 ATR spectra of CTA and the blends.

However, 5CB addition just changes the sign of CTA from negative to positive but still shows ordinary wavelength dispersion although the final stress applied on the plasticized CTA has almost a similar value to that for pure CTA. This is presumably to the large polarizability anisotropy of 5CB having ordinary wavelength dispersion with positive birefringence. This strong nematic interaction between CTA and 5CB will be also responsible for the large orientation birefringence.

The wavelength dispersion of the out-of-plane birefringence for the stretched films is shown in Figure 3.4b. As seen in the figure, out-of-plane birefringence for the stretched CTA film also shows negative out-of-plane-birefringence. Furthermore, the LMC also affects the out-of-plane birefringence. Addition of TCP and TPP increases the orientation birefringence of CTA and changes to positive birefringence with extraordinary wavelength dispersion. The results obtained for TCP and TPP correspond to the trend of in-plane birefringence in Figure 3.4a. Of course, that the out-of-plane birefringence for stretched films is originated from the orientation of LMC molecules. Moreover, addition of 5CB enhances the birefringence of CTA from negative to positive but still shows ordinary wavelength dispersion.

The wavelength dispersion of the out-of-plane birefringence of the stretched CAP and CAP/TCP is also investigated. The wavelength dispersion of the in-plane and out-of-plane birefringences of the stretched CAP and the blends is shown in Figure 3.6. The stretched CAP film shows positive birefringence with extraordinary dispersion. The results obtained for CAP correspond to the trend of in-plane birefringence, suggesting that the out-of-plane birefringence is simply originated from the chain orientation in the film plane. Addition of TCP increases both in-plane and out-of-plane birefringences of CAP.

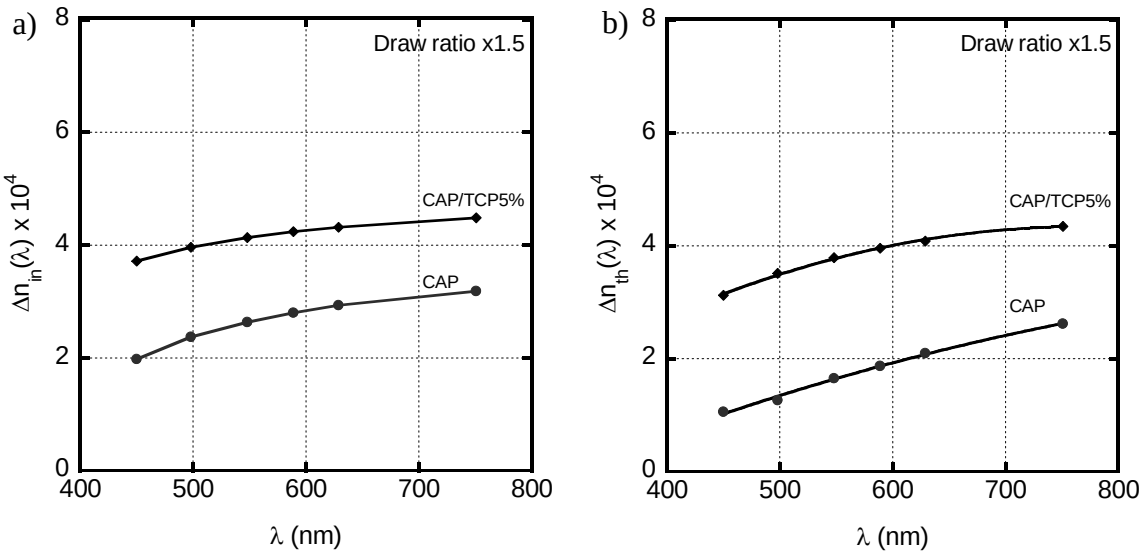

Figure 3.6 Wavelength dispersion of the in-plane and out-of-plane birefringences for the stretched CAP (●) and CAP/TCP5% (♦) films at a draw ratio of 1.5.

In order to study the contribution of LMC such as TCP and TPP to the orientation birefringence of the CTA blend, the drawn samples of the blend are immersed in methanol for 24 h to remove LMC. Then the orientation birefringence is measured again after drying at room temperature under a vacuum condition. After 24 h immersion, there is no considerable change in the dimension of the sample, suggesting that there is almost no alteration in degree of stretching upon the methanol immersion. The wavelength dispersion of in-plane and out-of-plane birefringences for the stretched films after methanol immersion is shown in Figure 3.7. As seen in the figure, the birefringences of the blends decrease and approach to those of pure CTA. The result demonstrates that the molecular orientation of CTA chains is not affected by the plasticizer addition.

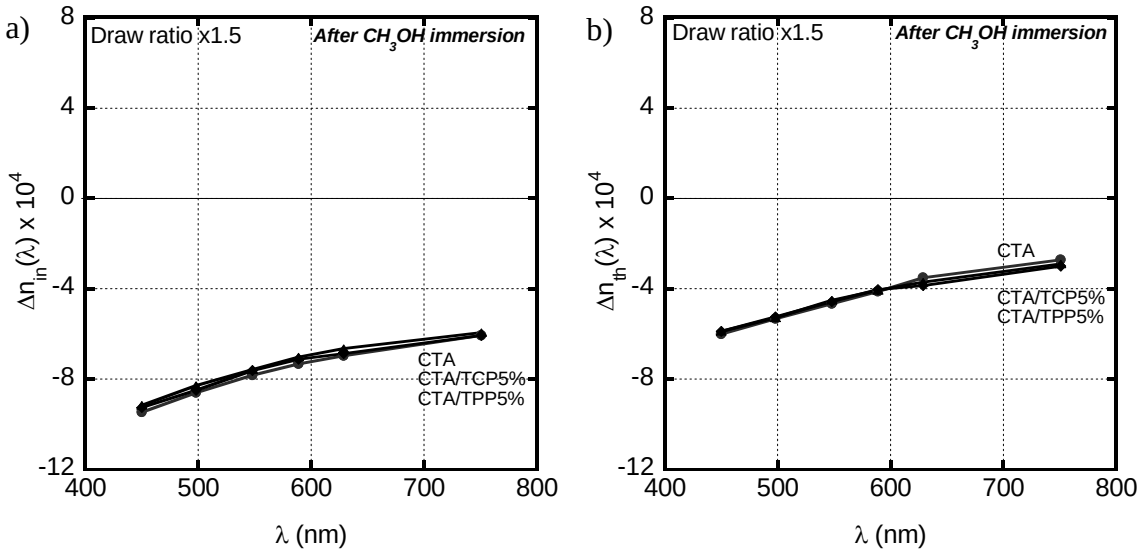

Figure 3.7 Wavelength dispersion of the in-plane and out-of-plane birefringences for the stretched CTA films; CTA (●), CTA/TCP5% (♦) and CTA/TPP5% (▲) at a draw ratio of 1.5 after methanol immersion.

The wavelength dispersion of average refractive index for CTA is illustrated in Figure 3.8, which is a typical one for conventional polymer.

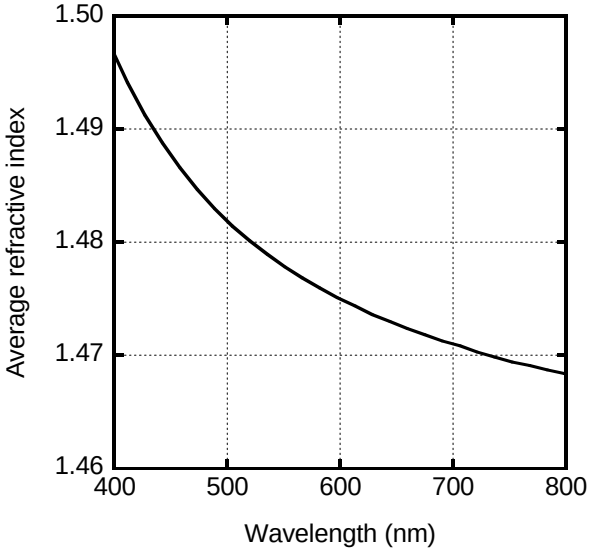

Figure 3.8 Wavelength dispersion of average refractive index for CTA

The normalized refractive indices along three principle axes for CTA and blend films after methanol immersion are illustrated in Figure 3.9. As seen in the figure, the refractive indices for the blends change from the previous one and approached to the pure CTA. The result suggests that the enhancement in birefringence in the blend is largely attributed to the orientation of LMC.

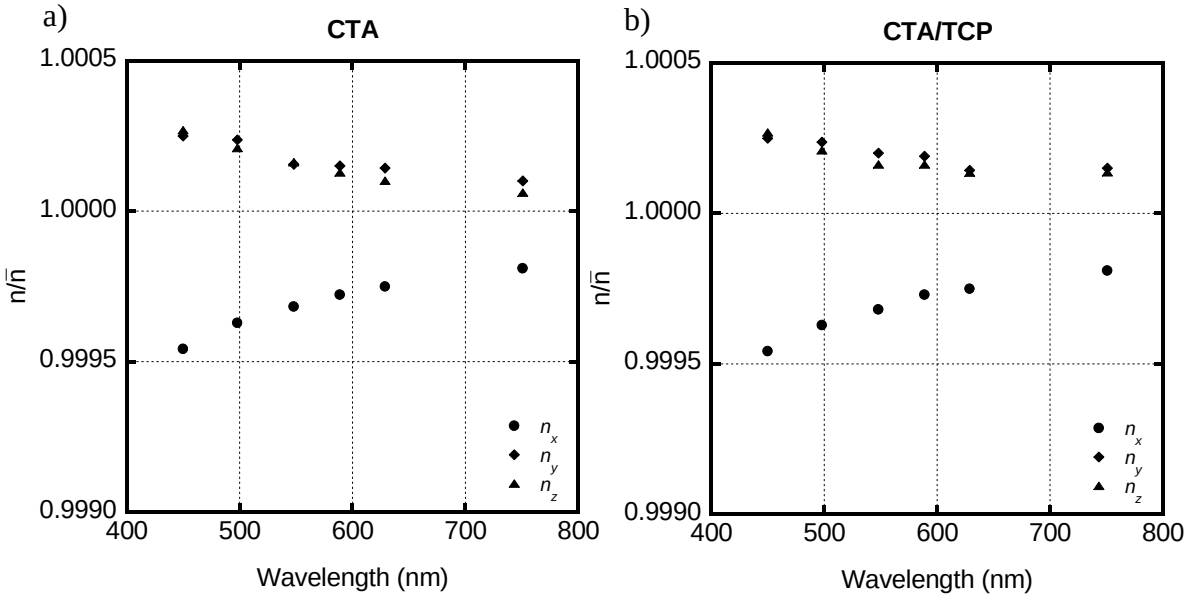

Figure 3.9 Normalized refractive indices along three principle axes for CTA and blend films after methanol immersion.

Accrodingly, it may be possible to control three-dimensional anisotropy by adding some certain disk-shaped plasticizers wherein a large molecular polarizability is introduced into the main chain to increase the in-plane birefringence and a large molecular polarizability and dipole moment are also introduced into the side chain to increase the out-of-plane birefringence.

In order to clarify the effect of plasticizer on the birefringence, the refractive indices along three principle axes are examined to understand three dimension

orientation in CTA. The refractive indices along three principle axes for films are illustrated in Figure 3.10. In this experiment, the hot stretching was performed in the *x* direction. For the CTA film (Figure 3.10), the refractive indices in the *y* and *z* directions overlap each other, indicating that the film is deformed uniaxially. However, for the blend samples, the refractive index in the *y* direction is different from that in the *z* direction. The normalized refractive indices along three principle axes for CTA and blend films are illustrated in Figure 3.11. As seen in the figure, the refractive indices in the *y* and *z* directions of the blend film are totally different, which will be due to the anisotropic dimension change in the width and thickness directions during stretching. The refractive indices along three principle axes for CAP and its blend are also examined, as illustrated in Figure 3.12. As seen in the figure, the refractive indices in the *y* and *z* directions overlap each other for CAP, so the films are uniaxially oriented. Moreover, the blends also show similar refractive indices in the *y* and *z* directions, which is different from CTA blend. This maybe because lateral reduction in the center part is prominent, uniaxial deformation takes place.

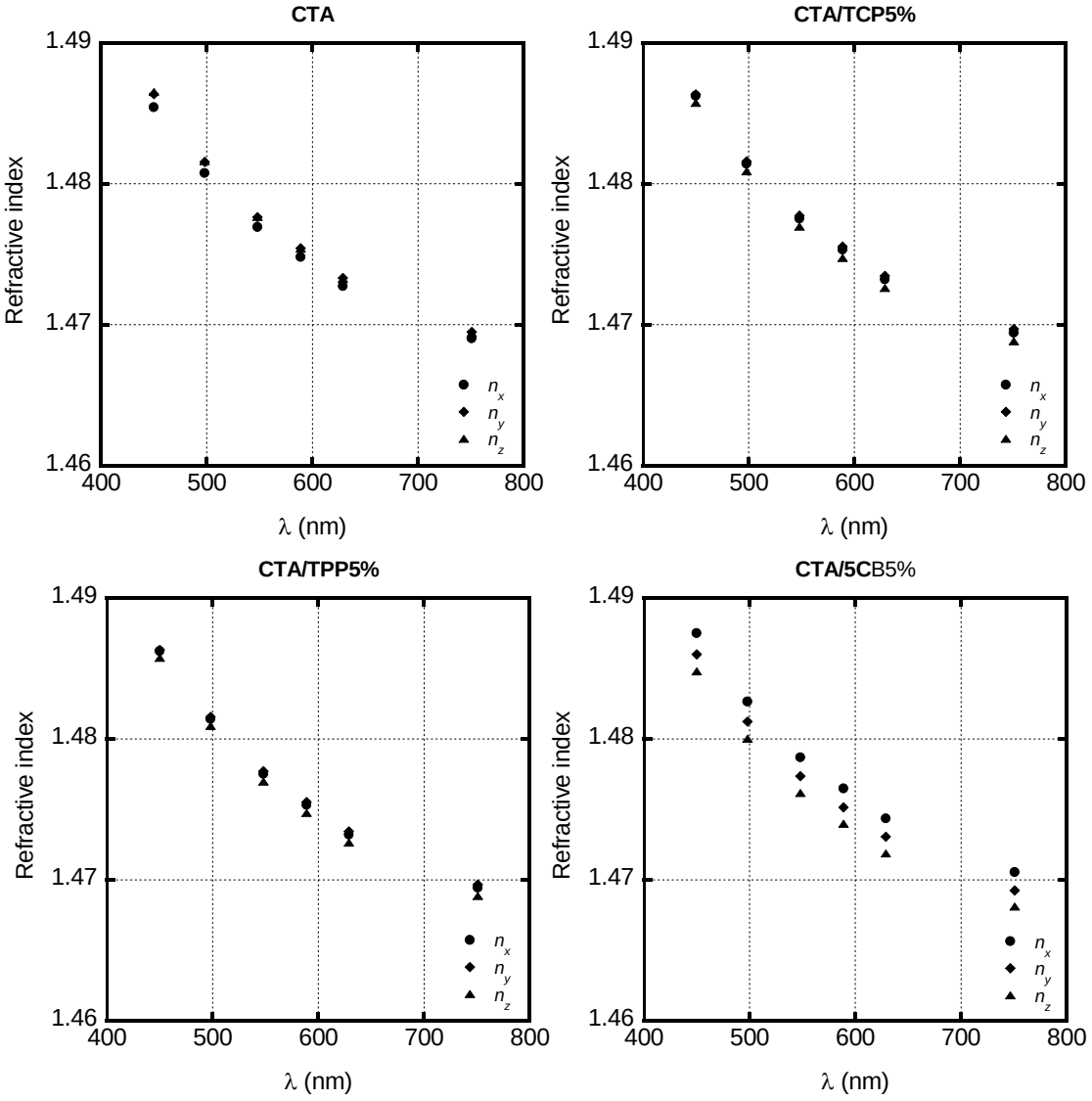

Figure 3.10 Refractive indices along three principle axes for CTA and the blends films

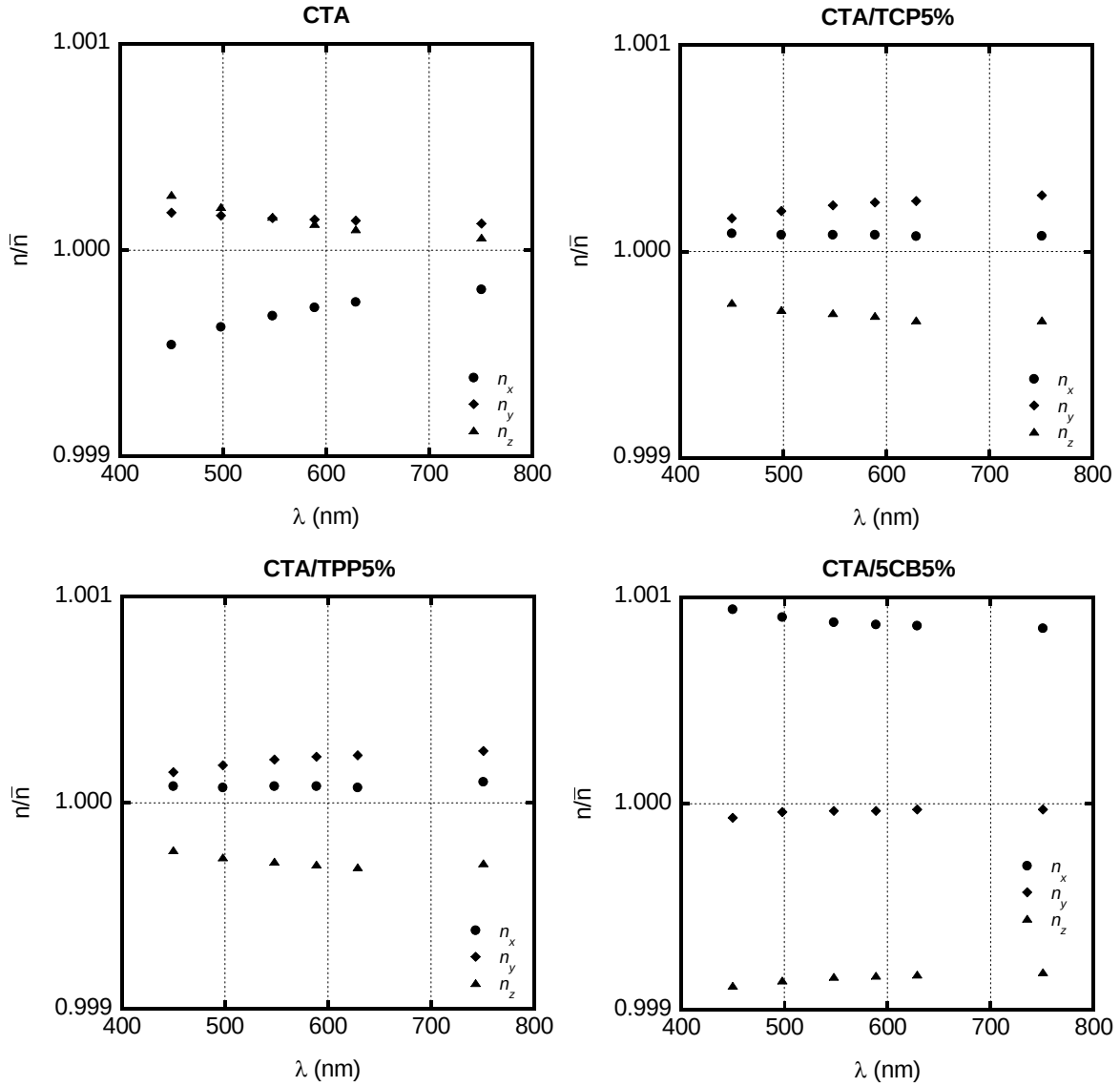

Figure 3.11 Normalized refractive indices along three principle axes for CTA and the blends films

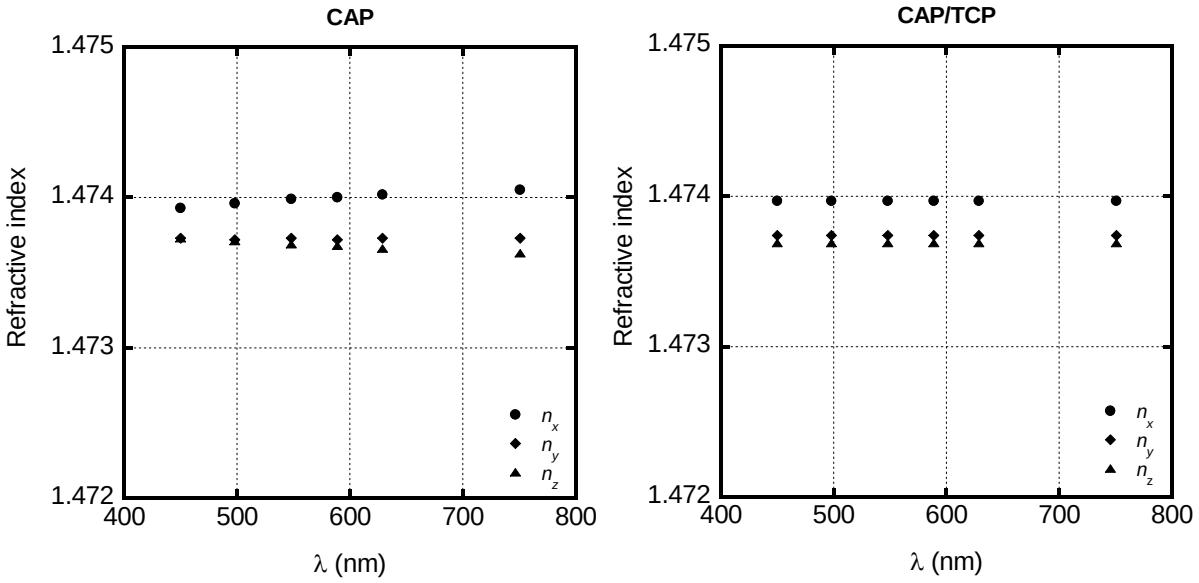

Figure 3.12 Refractive indices along three principle axes for CAP and its blend with TCP

In a T-die film extrusion, the molten is extruded through a slot die with a die gap and immediately stretched with a constant take-up velocity by a rotational chill roll. The die is designed to provide a constant exit velocity and uniform thickness in order to produce a film with uniform thickness. During the process, a film width decreases (lateral reduction) along the transverse direction, which is called neck-in. The thickness at the edge of an obtained film is thicker than that in the middle, known as edge bead phenomenon. The thicker portion, *i.e.*, edge bead, is usually trimmed out. It is known that neck-in level is decided by strain-hardening behavior in transient elongational viscosity. A molten polymer showing marked strain-hardening, such as long-chain branched polymer and crosslinked polymer, provides a wide film, *i.e.*, small neck-in.

CTA will show pronounced strain-hardening than CAP at hot-stretching because of the existence of crystallites, which act as crosslink points. As a result, the planar

elongational deformation takes place rather than uniaxial deformation especially in the center part of a film, which has been known at T-die film processing. According to the study on the T-die processing, a molten polymer showing marked strain-hardening in elongational viscosity is processed into film shape with wide width, *i.e.*, small reduction in the width direction [28-30].

Thus, the final film shape is also investigated. In case of the stretched CTA and the blends films, the width of the samples reduces (~10%) while thickness increases (~5%). On the contrary, the refractive indices in the *y* and *z* directions overlap each other for CAP and CAP/TCP, which is different from CTA blends. The width of the stretched CAP and CAP/TPP reduces (~30%) and also the thickness decreases (~10%). Thus, the films are uniaxially oriented. Because CAP has a low degree of crystallinity at the stretching temperature (no/little strain-hardening in elongational viscosity), the deformation occurs in a uniaxial mode rather than a planar elongation mode.

Generally, the ideally uniaxial drawn films shows, of course, uniaxial orientation, *i.e.*, $n_y = n_z$. However, the axial symmetry in the refractive indices is not observed by the addition of certain plasticizers such as TCP, TPP and 5CB ($n_x < n_y \neq n_z$), as shown in Figure 3.11. This phenomenon can be explained by the planar orientation, *i.e*, in-plane orientation, of the plasticizer molecules.

The planar orientation is the deformation mode of stretching with a constant width. Therefore, it contains the elongation in the *y*-direction, *i.e.*, perpendicular to the stretching *x*-direction in the film plane. This deformation mode is pronounced when a molten material shows strain-hardening behavior in the elongational viscosity, *i.e.*, the rapid increase in the elongational stress with the time or strain.

Figure 3.13 shows schematic illustration for dispersion state of disk-shaped and rod-shaped molecules. Because of the deformation mode in the *y*-direction, disk-shaped molecules tend to be embedded themselves in the film plane, resulting in the longer refractive index in the *y*-direction rather than that in the *z*-direction. In the case of rod-shaped molecules such as 5CB, the principal axis of the molecules is basically oriented in the *x*-axis, *i.e.*, stretching direction. Besides, the deformation mode in the *y*-axis leads to the plane orientation of the molecules. As a result, the refractive index in the *y*-direction becomes larger than that in the *z*-direction, as illustrated in Figure 3.10 and Figure 3.11.

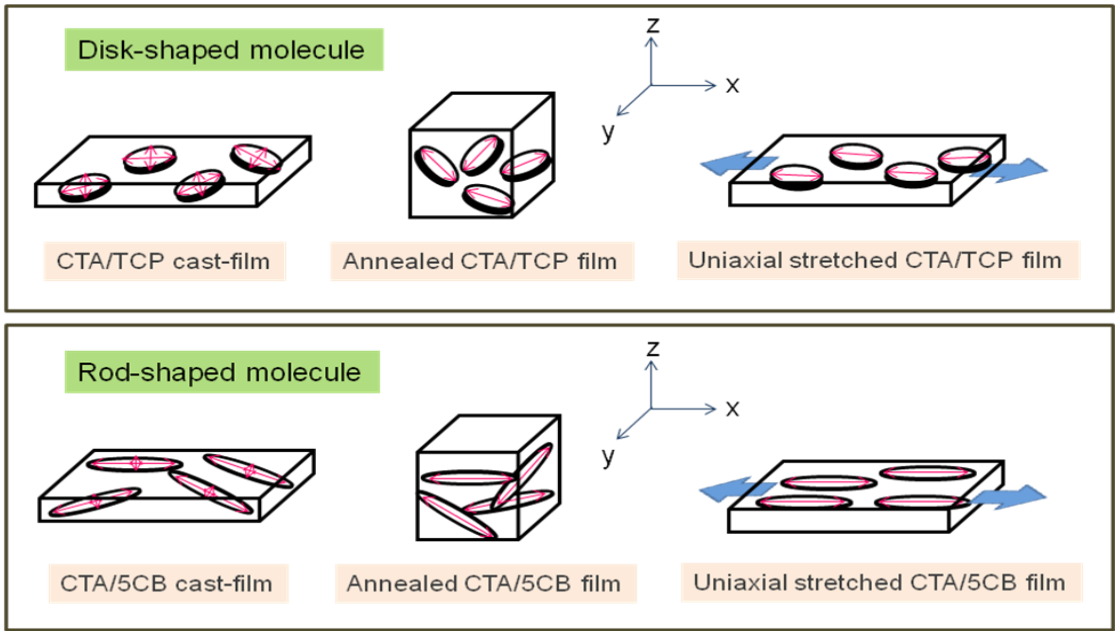

Figure 3.13 Schematic illustration for dispersion state of disk-shaped and rod-shaped molecules

3.4 Conclusions

The novel method to control three-dimensional refractive indices and wavelength dispersion of birefringence by uniaxial stretching with addition of various plasticizers with strong polarizability anisotropy is investigated. CTA and its blends show planar deformation mode to some degree only by uniaxial stretching. The transversal birefringence due to the transverseal orientation of CTA chains is magnified by plasticizeres. This phenomenon can be explained by the planar orientation of the plasticizer molecules. Disk-shaped molecules (TCP and TPP) and also a rod-shaped molecule and (5CB) enhance both in-plane and out-of-plane birefringences for CTA.

References

[1] Edgar, K. J.; Buchanan, C. M.; Debenham, J. S.; Rundquist, P. A.; Seiler, B. D.; Shelton, M. C.; Tindall, D. *Prog. Polym. Sci.* **2001**, *26*, 1605-1688.

[2] Sata, H.; Murayama, M, Shimamoto S. *Macromol. Symp.* **2004**, 208, 323-333.

[3] Yamaguchi, M. Optical properties of cellulose esters and their blends. In *Cellulose: Structure and Properties, Derivatives and Industrial Uses*; Lejeune, A., Deprez, T., Eds.; Nova Science Publishers, Inc.: New York, 2010, pp 325-340.

[4] Yamaguchi, M.; Mohd Edeerozey, A. M.; Songsurang, K.; Nobukawa, S. *Cellulose* **2012**, *19*, 601-613.

[5] Tagaya, A.; Ohkita, H.; Mukoh, M.; Sakaguchi, R.; Koike, Y. *Science* **2003**, *301*, 812-814.

[6] Tagaya, A.; Ohkita, H.; Harada, T.; Ishibashi, K.; Koike, Y. *Macromolecules* **2006**, *39*, 3019-3023.

[7] Arakawa, K. (Fuji Photo Film Co.) *Jpn. Kokai Tokkyo Koho (Patent)* **1990**, JP-A-160204.

[8] Yoshimi, H. (Nitto Denko Co.) *Euro. Pat. App.* **1992**, EP-A-2-482620

[9] Umemoto, S.; Fujimura, Y.; Yamamoto, H. (Nitto Denko Co.) *Jpn. Kokai Tokkyo Koho (Patent)* **1990**, JP-A-285303.

[10] Fujimura, Y.; Nagatsuka, T.; Yoshimi, H.; Umemoto, S.; Shimomura, T. *SID' 92 Digest* **1992**, 397.

[11] Uchiyama, A.; Yatabe, T. Jpn. J. Appl. Phys. **2003**, *42*, 6941-6945.

[12] Koike, Y.; Yamazaki, K.; Ohkita, H.; Tagaya, A. *Macomol. Symp.* **2006**, *235*, 64-70.

[13] Uchiyama, A.; Yatabe, T. *Jpn. J. Appl. Phys.* **2003**, *42*, 3503-3507.

[14] Uchiyama, A.; Yatabe, T. *Jpn. J. Appl. Phys.* **2003**, *42*, 5665-5669.

[15] Kuboyama, K.; Kuroda, T.; Ougizawa, T. *Macromol. Symp.* **2007**, *249-250*, 641-646.

[16] Yamaguchi, M.; Okada, K.; Mohd Edeerozey, A. M.; Shiroyama, Y.; Iwasaki, T.; Okamoto, K. *Macromolecules* **2009**, *42*, 9034-9040.

[17] Mohd Edeerozey, A. M.; Tsuji, M.; Shiroyama, Y.; Yamaguchi, M. *Macromolecules* **2011**, *44*, 3942-3949.

[18] Yamaguchi, M.; Iwasaki, T.; Okada, K.; Okamoto, K. *Acta Materialia* **2009**, 57, 823-829.

[19] Yamaguchi, M.; Lee, S.; Mohd Edeerozey, A. M.; Tsuji, M.; Yokohara, T. *Eur. Polym. J.* **2010**, *46*, 2269-2274.

[20] Songsurang, K.; Miyagawa, A.; Mohd Edeerozey, A. M.; Phulkerd, P.; Nobukawa, S.; Yamaguchi, M. *Cellulose* **2013**, *20*, 83–96.

[21] Mohd Edeerozey, A. M.; Tsuji, M.; Nobukawa, S.; Yamaguchi, M. *Polymers* **2011**, 3, 955-966.

[22] Doi, M.; Watanabe, H. *Macromolecules* **1991**, *24*, 740-744.

[23] Watanabe, H.; Kotaka, T.; Tirrell, M. *Macromolecules* **1991**, *24*, 201-208.

[24] Zawada, A. F., Fuller, G. G., Colby, R. H., Fetters, L. J., & Roovers, J. *Macromolecules*, **1994**, *27*, 6851-6860.

[25] Urakawa, O.; Ohta, E.; Hori, H.; Adachi, K. *J. Polym. Sci. Polym. Phys. Ed.* **2006**, *44*, 967-974.

[26] Nobukawa, S.; Urakawa, O.; Shikata, T.; Inoue, T. *Macromolecules* **2010**, *43*, 6099-6105.

[27] Nobukawa, S.; Urakawa, O.; Shikata, T.; Inoue, T. *Macromolecules* **2011**, 44, 8324-8332.

[28] Debroth, T.; Erwin, L. *Polym. Eng. Sci.* **1986**, *26*, 462-467.

[29] Debroth, T.; Erwin, L. *ANTEC86*, Boston, USA. **1986**, *32*, 893.

[30] Ito, H.; Doi, M.; Isaki, T.; Takeo, M. *J. Soc. Rheol. Japan* **2003**, *31*, 157-163.

Chapter 4

Optical Anisotropy of Cellulose Ester Films Prepared by Solution-Cast Method

4.1 Introduction

One of the most important applications of cellulose esters is optical films such as protective film and retardation film [1-6]. Cellulose triacetate (CTA) films prepared by the solution-casting method are widely used for this application. Besides CTA, various cellulose esters such as cellulose acetate propionate (CAP) and cellulose acetate butyrate (CAB) become candidates for the optical films these days because their films can be prepared by melt-extrusion, leading to good cost-performance. For the optical application, control of retardation, *i.e.*, the product of birefringence and film thickness, is the most important aspect in material design, and various methods have been proposed.

In the application as polarizer protective films, the films cover a polarizing film to protect the polarizer from mechanical damage, moisture, and oxidation. In order to keep the polarizing condition of the light after passing through the polarizer, the films have to be free from birefringence. A retardation film is defined as a film to provide a specific optical retardation. One of the most available applications is to compensate the birefringence arising from polarizers and/or liquid crystal cell, thus it is also known as a

compensation film. For the purpose, a retardation film is placed on the liquid crystal cell and/or polarizers to widen the viewing angle. Furthermore, quarter and half-wave plates are famous examples of a retardation film, which are used to change the anisotropic condition of the incident light. For the applications, not only birefringence at a specific wavelength but also the wavelength dependence of birefringence are significantly important.

Particularly, CTA has been utilized for the protective film although only a solution-cast can be applied to prepare the film due to the thermal degradation. The solution-cast method produces no birefringence in the plane, which is desirable for the protective film. However, molecular orientation in the thickness direction is different from that in the plane by the compressed pressure during the solvent evaporation, leading to the so-called "out-of-plane" birefringence.

In this study, the in-plane birefringence (Δn_{in}) and out-of-plane birefringence (Δn_{th}) are defined by the following equations.

$$\Delta n_{in} = n_x - n_y \tag{4.1}$$

$$\Delta n_{th} = \frac{n_x + n_y}{2} - n_z \tag{4.2}$$

Based on the Kuhn and Grün model, the orientation birefringence $\Delta n(\lambda)$ of an oriented polymer is expressed in the following relation [7-11].

$$\Delta n(\lambda) = \frac{2\pi}{9} \frac{\left(n(\lambda)^2 + 2\right)^2}{n(\lambda)} N \, \Delta\alpha(\lambda) \left(\frac{3\langle \cos^2 \theta \rangle - 1}{2} \right) \tag{4.3}$$

where λ, $n(\lambda)$, N, $\Delta\alpha(\lambda)$, and θ are the wavelength of light, the average refractive index, the number of chains in a unit volume, the polarizability anisotropy, and the angle that a segment makes with the stretch axis, respectively. The last bracketed term $\left(3\left\langle\cos^2\theta\right\rangle-1\right)/2$ is identically equal to the Hermans orientation function [12], whereas the other part in the right term is called as intrinsic birefringence determined by chemical structure. From equation (4.3), the above equation can also be written as

$$\Delta n(\lambda)=\Delta n^0(\lambda)F \tag{4.4}$$

where $\Delta n^0(\lambda)$ is the intrinsic birefringence and F is the orientation function.

Since the orientation function is independent of the wavelength, the following simple relation is derived,

$$\frac{\Delta n(\lambda)}{\Delta n(\lambda_0)}=\frac{\Delta n^0(\lambda)}{\Delta n^0(\lambda_0)}=const. \tag{4.5}$$

where λ_0 is the arbitrary standard wavelength.

According to equation (4.5), the wavelength dispersion of birefringence, *i.e.*, $\Delta n(\lambda)/\Delta n(\lambda_0)$, is a constant and determined by the chemical structure of a polymer. Furthermore, it is known that the polymeric materials decrease with increasing the wavelength in general, the so-called ordinary dispersion. This is attributed to a strong absorption in ultraviolet region for polymers. Therefore, the wavelength dispersion of the birefringence is contrary to that of an ideal quarter-wave retardation plate.

Since the intrinsic birefringence in eqs. 4.3 and 4.4 is a function of wavelength, the orientation birefringence is dependent upon the wavelength. Therefore, birefringence control is required in a wide range of visible light. In particular, the extraordinary

wavelength dispersion has been desired recently because of the industrial importance for high performance retardation films. The property can provide a specific retardation, *e.g.*, quarter or half of the wavelength, in the whole visible light. However, the wavelength dispersion of most polymers is represented by the following relation called the Sellmeier equation [7].

$$\Delta n(\lambda) = A' + \frac{B'}{\lambda^2 - \lambda_{ab}{}^2} \tag{4.6}$$

where λ_{ab} is the wavelength of a vibrational absorption peak in ultraviolet region and A' and B' are the Sellmeier coefficients. The equation indicates that the absolute value of birefringence decreases with increasing the wavelength, *i.e.*, ordinary wavelength dispersion.

At present, various techniques are proposed to obtain films showing extraordinary dispersion. One of the conventional methods is by piling two or more polymer films having different wavelength dispersions, in which the fast axis of one film is set to be parallel to the slow axis of the other films [13-15]. Although this technique is currently employed in industry to fabricate retardation films, it leads to poor cost-performance due to the complicated processing operation and results in a thick display. Therefore, it is more favorable to use a single film with extraordinary wavelength dispersion of birefringence. Blending with another polymer [16-18] or a low-mass compound [13,14], copolymerization with appropriate monomers [19], and addition of nonspherical materials having polarizability anisotropy [20] are promising techniques to provide the extraordinary dispersion.

For example, acetyl group provides negative orientation birefringence whereas

propionyl and butyryl groups contribute positive one with an intense fashion of the butyryl group. This situation is similar to the miscible blend systems showing extraordinary dispersion, such as PPO/PS and NB/SMA. Although some of the cellulose esters are currently employed for retardant films because of various attractive properties [2,4,21-23], only a few papers on wavelength dispersion of the orientation birefringence have been published to the best of my knowledge [22,24]. However, it is essential to understand the wavelength dispersion, especially the effect of chemical structure, molecular weight, and processing method and condition, for material design of a retardant film.

Since it was found that the in-plane birefringence of cellulose esters is generated by the ester groups, the effect of ester groups on the out-of-plane birefringence of a solution-cast film is investigated employing various cellulose esters such as CTA, cellulose acetate propionate (CAP) and cellulose acetate butyrate (CAB) in the study. It was clarified in our previous study that the in-plane birefringence of cellulose esters is not determined by the orientation of pyranose-ring but by the species and amounts of the ester groups [13]. However, it is essential to understand the out-of-plane birefringence, especially the effect of chemical structure (main chain and side chain), for material design of a retardant film.

4.2 Experimental

4.2.1 Materials

Materials employed in this study were commercially available cellulose esters such as cellulose triacetate (CTA), cellulose acetate propionate (CAP), and cellulose acetate butyrate (CAB). CTA was produced from Acros Organics and both CAP and CAB were produced by Eastman Chemical. The molecular characteristics are summarized in Table 4.1. The nomenclature used for the CAB is as follows; the last two digit numbers represent the weight percent of butyryl. For example, CAB17 is CAB with 17 wt% of butyryl content.

Table 4.1 Characteristics of the samples.[a]

Sample	Compositions, wt%			Molecular Weights	
	Acetyl	Propionyl/Butyryl	Hydroxyl	M_n (x 10^5)	M_w (x 10^5)
CTA	43.6 (2.96)	−	0.9	1.3	3.5
CAP	2.5 (0.19)	46 (2.58)	1.8	0.77	2.1
CAB17	29.5 (2.08)	17 (0.73)	1.1	0.62	2.7
CAB52	2.0 (0.17)	52 (2.64)	1.8	0.082	0.78

[a](Parentheses): degree of substitution.

The molecular weights of the samples were evaluated using a gel permeation chromatograph (Tosoh, HLC-8020) with TSK-GEL® GMHXL; chloroform was employed as the eluant, and its flow rate was 1.0 mL/min. The temperature was

maintained at 40 ºC and the sample concentration was 1.0 mg/mL. The number- and weight-average molecular weights vs. a polystyrene standard are shown in the Table 4.1.

The cellulose ester films were prepared using a solution-cast method by dichloromethane as a solvent. The initial concentration was 4 wt%. The films with approximately 100 μm thickness were obtained by evaporating the solvent at room temperature. The weight loss was monitored during the solution cast to control the evaporation speed.

4.2.2 Measurements

The temperature dependence of oscillatory tensile moduli in the solid state was measured from 0 to 250 °C by a dynamic mechanical analyzer (UBM, E-4000) using rectangular specimens with 5 mm in width and 20 mm in length. The frequency and heating rate used were 10 Hz and 2 °C/min, respectively.

The uniaxial oriented films were prepared by hot-drawing operation using a dynamic mechanical analyzer (UBM, DVE-4) at various temperatures and draw ratios. The initial distance between the clamps was 10 mm and the stretching rate was 0.5 mm/s. The drawn sample was quenched by blowing cold air in order to avoid relaxation of molecular orientation.

The refractive index of the polymer films was evaluated by Abbe refractometer (Atago, NRA 1T) at room temperature employing α-bromonaphthalene as the contact liquid.

The optical properties of CTA films were measured at room temperature by an optical birefringence analyzer (Oji Scientific Instruments, KOBRA-WPR). The retardation in the thickness direction (out-of-plane birefringence) R_{th} was determined by retardation measurements at an oblique incidence angle of 40° as a function of wavelength by changing color filters. The corresponding birefringence was calculated using the film thickness measured by a digital micrometer. Prior to the measurement, the cellulose ester films were placed in a temperature-and-humidity control chamber (Yamato, IG420) at 25 ºC and 50% RH for one day, because the moisture in the film affects the orientation birefringence [25]. Since a small amount of water which has strong interaction with acetyl or hydroxyl group cannot be eliminated even under a vacuum condition, this treatment is appropriate to obtain the reproducible data.

Attenuated total reflection (ATR) measurements using an infrared absorption spectrometer (Perkin Elmer, Spectrum 100) were performed to study the molecular orientation in CTA films. The KRS-5 was employed as an ATR crystal.

The melting point and heat of fusion of the obtained films were measured by a differential scanning calorimeter (Mettler, DSC820) at a heating rate of 20 ^{o}C/min.

Table 4.2 Melting points and average refractive index of film samples.

Sample	Melting Point and Heat of Fusion	Average Refractive Index
CTA	287 ^{o}C, 21.8 J/g	1.48 ± 0.01*
CAP	199 ^{o}C, 0.7 J/g	1.4738
CAB17	–	1.4758
CAB52	–	1.4737

4.3 Results and Discussion

4.3.1 Dynamic Mechanical Properties

Temperature dependence of the oscillatory tensile moduli such as storage modulus E' and loss tangent tan δ, was measured in order to decide the ambient temperature at hot drawing. Figure 4.1 exemplifies the dynamic mechanical spectra for various cellulose esters at 10 Hz. As seen in the figure, the glass transition temperature T_g, which is defined as the peak temperature in the tan δ curve, is around 148 °C. Furthermore, the storage modulus E' fall off sharply around T_g.

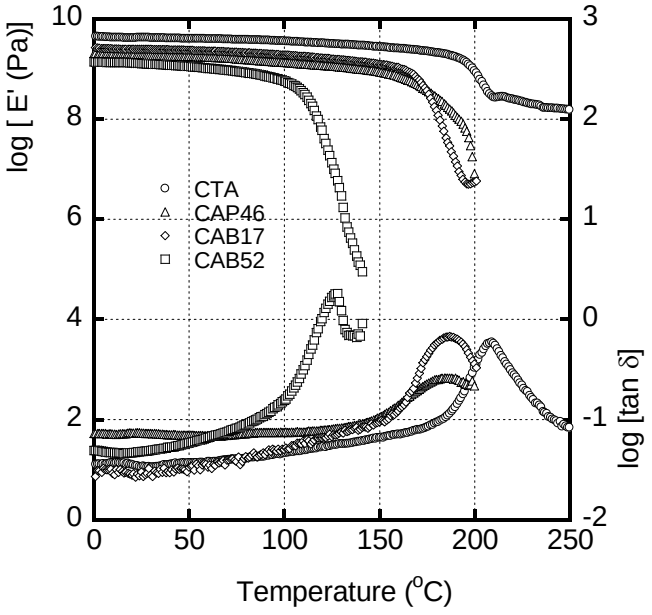

Figure 4.1 Temperature dependence of oscillatory tensile moduli such as storage modulus E' and loss tangent tan δ at 10 Hz, for a cellulose ester films; CTA (●), CAP46 (▲), CAB17 (♦), and CAB52 (■).

4.3.2 In-Plane and Out-of-Plane Birefringences

4.3.2.1 In-Plane Birefringence

Prior to discussion of the out-of-plane birefringence, the effect of ester group on "in-plane" birefringence, *i.e.*, the refractive index difference between stretching and perpendicular directions in the film, of cellulose esters is investigated. Figure 4.2 shows the wavelength dispersion of the in-plane birefringence for the stretched films at a draw ratio of 2.0. As seen in the figure, the in-plane birefringence seems to be dependent on the species and the contents of the ester groups. For example, CTA shows negative birefringence that decreases with increasing wavelength (ordinary wavelength dispersion), whereas the others exhibit positive birefringence with extraordinary wavelength dispersion. In the case of CAB, the in-plane birefringence increases with the butyryl content (as denoted by the numerals in the sample code (wt%)). The trend of the birefringence indicates that the butyryl group has positive polarizability anisotropy to the stretching direction. Furthermore, CAP46 exhibits positive birefringence, as similar to CAB. These experimental results indicate that the acetyl group contributes negative birefringence, whereas the propionyl and butyryl groups show positive birefringence. The flexible and bulky methylene part in ester groups would lead to the parallel orientation of the polarizability anisotropy along the flow direction. Furthermore, the interaction between the ester groups and the main chains may be important because the higher-order structure of cellulose esters [2,21,23] is strongly dependent on the species of the ester groups. Furthermore, the data for CAB52 and CAB46 represent that the positive contribution of the butyryl group is stronger than that of the propionyl group.

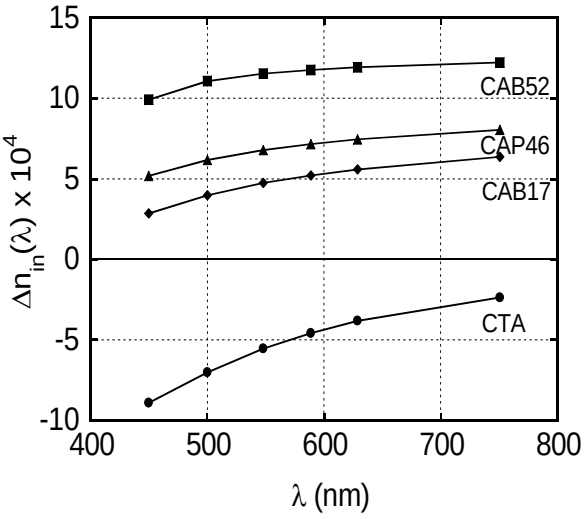

Figure 4.2 In-plane birefringence for various cellulose esters at a draw ratio of 2.0; CTA (●), CAP46 (▲), CAB17 (♦), and CAB52 (■). The number represents the weight fraction of ester group (propionyl or butyryl) for CAP and CAB.

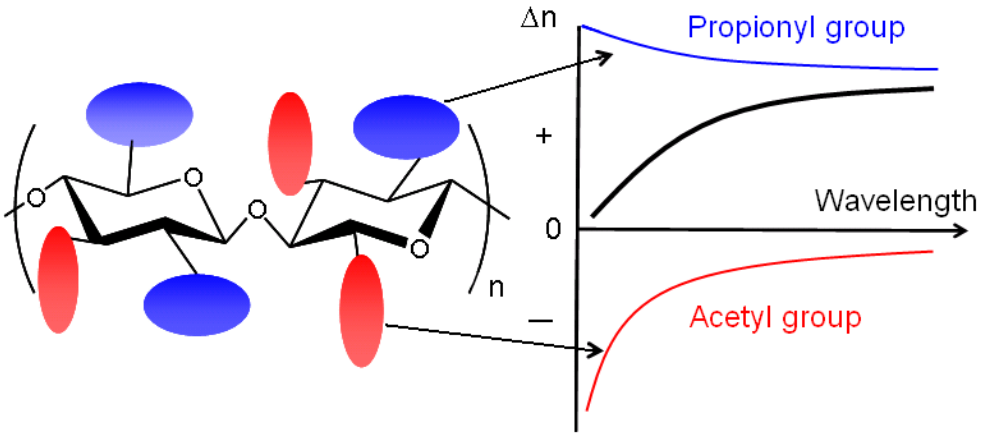

Figure 4.3 Schematic illustration of contribution of polarizability anisotropy of acetyl and propionyl groups and the obtained wavelength dispersion of orientation birefringence for CAP.

As well known, CAP has at least two ester groups having different polarizability anisotropies, that is, acetyl and propionyl groups. Since the orientation birefringence Δn is assumed to be expressed by a simple addition of the birefringence from each

component as discussed by Stein et al. [9], it is provided by the following relation:

$$\Delta n = \Delta n_F + \sum_i \phi_i \Delta n_i \tag{4.7}$$

where i refers i-th component, ϕ_i is the volume fraction, and Δn_F is the birefringence arising from form or deformation effects, which is negligible for cellulose esters owing to the homogeneous structure. Therefore, the orientation birefringence is determined by the summation of the birefringence arising from the acetyl group and that from the propionyl group as expressed in the following relation:

$$\Delta n(\lambda) = \Delta n_A{}^0(\lambda) F_A + \Delta n_P{}^0(\lambda) F_P \tag{4.8}$$

where $\Delta n_A{}^0(\lambda)$ and $\Delta n_P{}^0(\lambda)$ are the intrinsic birefringences, and F_A and F_P are the orientation functions of the acetyl and propionyl groups, respectively. The extraordinary wavelength dispersion of the orientation birefringence with positive sign for CAP is explained by the illustration in Figure 4.3. In the figure, the polarizability anisotropy of ester groups is represented by ellipsoids. As depicted in the figure, the addition of both components, denoted by a bold line, gives the extraordinary dispersion with positive orientation birefringence, when the wavelength dependence of the propionyl group is weaker than that of the acetyl group.

The normalized orientation birefringence is shown in Figure 4.4. It is demonstrated that the wavelength dependence of the normalized orientation function becomes weak as the butyryl content is increased. This is reasonable because the butyryl group has weak wavelength dependence.

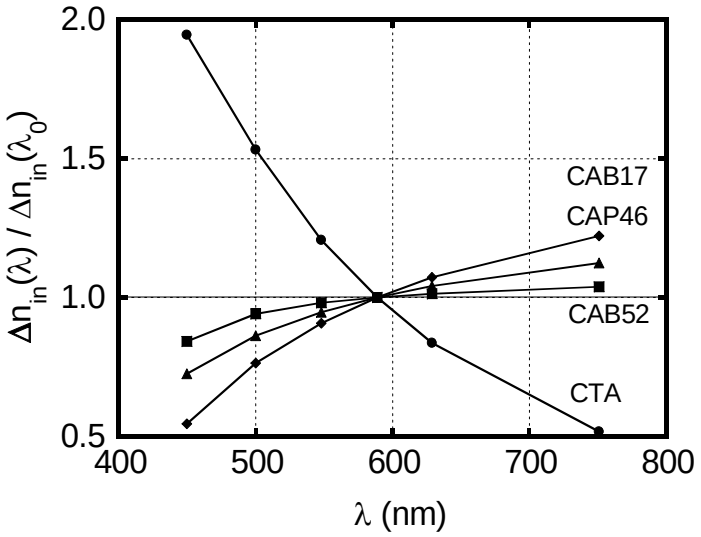

Figure 4.4 Normalized in-plane birefringence $\Delta n_{in}(\lambda)/\Delta n_{in}(\lambda_0 = 588\ nm)$ for various cellulose esters at a draw ratio of 2.0; CTA (●), CAP46 (▲), CAB17 (♦), and CAB52 (■). Hot-drawing was performed at the temperature where the tensile storage modulus is 10 MPa at 10 Hz.

Figure 4.4 also indicates that the slope of the orientation birefringence for CAP is larger than that for CAB52, although both contain a similar level of the degree of substitution of ester groups such as propionyl and butyryl ones. It suggests that the birefringence of the propionyl group shows strong dependence on the wavelength as compared with that of the butyryl group.

As a result, the following relation is expected.

$$-\left.\frac{d(\Delta n(\lambda))}{d\lambda}\right|_{\text{Acetyl}} > \left.\frac{d(\Delta n(\lambda))}{d\lambda}\right|_{\text{Propionyl}} > \left.\frac{d(\Delta n(\lambda))}{d\lambda}\right|_{\text{Butyryl}} \tag{4.9}$$

It is generally accepted that a wavelength dependence of the orientation birefringence of a polymeric material is well described by the following Sellmeier-type

relation [10,26,27];

$$\Delta n(\lambda) = A + \frac{B}{\lambda^2 - {\lambda_{ab}}^2} \tag{4.10}$$

where λ_{ab} is the coefficient having the relation with the wavelength of a strong vibrational absorption peak in ultraviolet region, and A and B are the Sellmeier coefficients. In the case of cellulose esters, equation 4.9 is predictable because λ_{ab} of the ester groups is in the following order; acetyl > propionyl > butyryl.

4.3.2.2 Out-of-Plane Birefringence

The wavelength dispersion of the out-of-plane birefringence of the samples is shown in Figure 4.5. The solution-cast films including CTA (butyryl content is zero) show positive birefringence although CTA shows negative in-plane birefringence. The out-of-plane birefringence increases with the butyryl content. Moreover, the out-of-plane birefringence of CAP46 is significantly smaller than CAB52, implying that the propionyl group exhibits lower birefringence. The results obtained for CAP and CAB correspond to the trend of in-plane birefringence in Figure 4.2, suggesting that the out-of-plane birefringence is simply originated from the chain orientation in the film plane. In contrast, the birefringence of CTA in Figure 4.5 is not consistent with that in Figure 4.2. In order to investigate the origin of the out-of-plane birefringence of CTA, the acetyl orientation is evaluated by a Fourier-transform infrared spectroscopy (FT-IR).

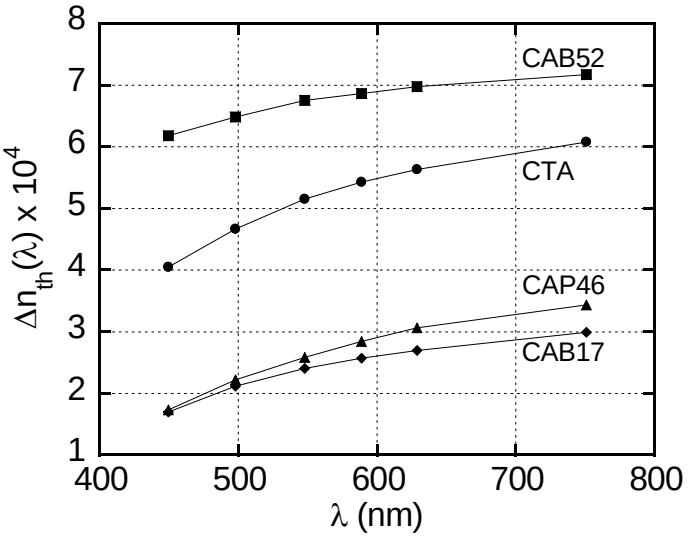

Figure 4.5 Out-of-plane birefringence for solution-cast films of various cellulose ester; CTA (●), CAP46 (▲), CAB17 (♦), and CAB52 (■).

Figure 4.6 compares the FT-IR spectra for carbonyl and ether in CTA films by using the attenuated total reflection (ATR) method. CTA films were prepared at two different evaporation rates (fast and slow), leading high and low chain orientations, respectively. The chain orientation which affects the intensity of ether band in the pyranose ring is enhanced by the prompt evaporation. Additionally, the carbonyl band become strong with evaporation rate, indicating that acetyl orientation in the plane also increases. Since the birefringence of CTA is mostly determined by the acetyl orientation, the positive birefringence for the out-of-plane is attributed to the in-plane alignment of acetyl group generated by the solution-cast method.

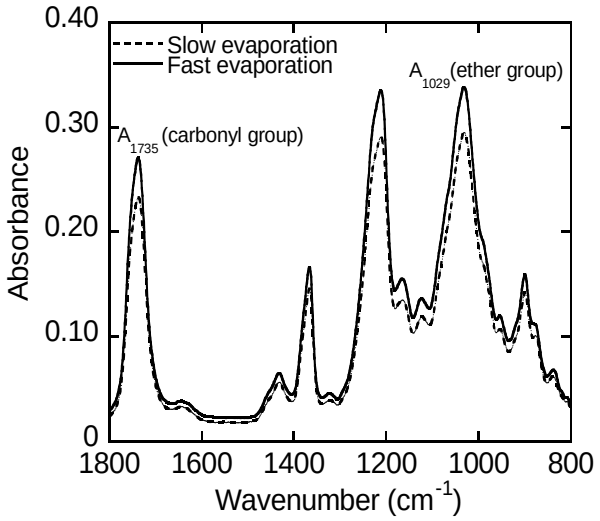

Figure 4.6 ATR spectra of CTA films prepared by the solution-cast method with different evaporation rates.

4.4 Conclusions

The birefringence of various types of cellulose esters and its dependence of the wavelength were studied. The species and contents of ester groups determine the sign and magnitude of the birefringence as well as the wavelength dispersion. Prior to stretching, the CTA film shows positive out-of-plane birefringence with extraordinary wavelength dispersion, whereas the stretched film shows negative birefringence. The in-plane and out-of-plane birefringences increase with increasing the wavelength for CAP and CAB, which is desired for a retardant film covering a broad wavelength. The difference in the sign of birefringence and the dependence of the wavelength for each ester group is responsible for the extraordinary dispersion. Furthermore, CAP shows strong dependence of the orientation birefringence as compared with CAB, because the propionyl group gives stronger wavelength dependence than the butyryl group.

References

[1] Edgar, K. J.; Buchanan, C. M.; Debenham, J. S.; Rundquist, P. A.; Seiler, B. D.; Shelton, M. C.; Tindall, D. *Prog. Polym. Sci.* **2001**, *26*, 1605-1688.

[2] Sata, H.; Murayama, M.; Shimamoto, S. *Macromol Symp.* **2004**, *208*, 323.

[3] Glasser, W. G. *Macromol. Symp.* **2004**, *208*, 371-394.

[4] Kamide, K. *Cellulose and Cellulose Derivatives*, Elsevier Science, Amsterdam, 2005.

[5] Yamaguchi, M. Optical properties of cellulose esters and their blends. In *Cellulose: Structure and Properties, Derivatives and Industrial Uses*; Lejeune, A., Deprez, T., Eds.; Nova Science Publishers, Inc.: New York, 2010, pp 325-340.

[6] Yamaguchi, M.; Lee, S.; Mohd Edeerozey, A. M.; Tsuji, M.; Yokohara, T. *Eur. Polym. J.* **2010**, *46*, 2269-2274.

[7] Kuhn, W.; Grün, F. *Kolloid-Z* **1942**, *101*, 248-271.

[8] Treloar, L. R. G. *The physics of rubber elasticity*, Clarendon Press: Oxford. 1958.

[9] Read, B. E. *Structure and properties of oriented polymers*, Ward IM. Ed.; Applied Science Publishers: London, Chap. 4. 1975.

[10] Harding, G. F. Optical properties of polymers, Meeten GH, Ed.; Applied and Science: London, Chap. 2. 1986

[11] Marks, J. E.; Erman, B. *Rubberlike Elasticity: A Molecular Primer*, Wiley, New York, 1988.

[12] Hermans, P. H.; Plotzek, P. *Kolloid-Z* **1939**, *88*, 68.

[13] Yamaguchi, M.; Okada, K.; Mohd Edeerozey, A. M.; Shiroyama, Y.; Iwasaki, T.; Okamoto, K. *Macromolecules* **2009a**, *42*, 9034–9040.

[14]Mohd Edeerozey, A. M.; Tsuji, M.; Shiroyama, Y.; Yamaguchi, M. *Macromolecules* **2011a**, *44*, 3942-3949.

[15]Yamaguchi, M.; Mohd Edeerozey, A. M.; Songsurang, K.; Nobukawa, S. *Cellulose* **2012**, *19*, 601-613.

[16]Uchiyama, A.; Yatabe, T. *Jpn. J. Appl. Phys.* **2003a**, *42*, 3503-3507.

[17]Uchiyama, A.; Yatabe, T. *Jpn. J. Appl. Phys.* **2003b**, *42*, 5665-5669.

[18]Kuboyama, K.; Kuroda, T.; Ougizawa, T. *Macromol. Symp.* **2007**, *249-250*, 641-646.

[19]Uchiyama, A.; Yatabe, T. Jpn. *J. Appl. Phys.* **2003c**, *42*, 6941-6945.

[20]Koike, Y.; Yamazaki, K.; Ohkita, H.; Tagaya, A. *Macomol. Symp.* **2006**, *235*, 64-70.

[21]Charles, K. J.; Buchanan, C. M.; Debenham, J. S.; Rundquist, P.A.; Seiler, B. D.; Shelton, M. C.; Tindall, D. *Prog. Polym. Sci.* **2001**, *26*, 1605.

[22]Yamaguchi, M.; Iwasaki, T.; Okada, K.; Okamoto, K. *Acta Materialia* **2009b**, 57, 823-829.

[23]Zugenmaier, P. *Macromol. Symp.* **2004**, *208*, 81.

[24]El-Diasty, F.; Soliman, M. A.; Elgendy, A. F. T.; Ashour, A. *J. Opt. A: Pure Appl. Opt.* **2007**, *9*, 247-252.

[25]Mohd Edeerozey, A. M.; Tsuji, M.; Nobukawa, S.; Yamaguchi, M. *Polymers* **2011b**, 3, 955-966.

[26]Ghosh, G. *Opt Commun*. **1999**, *162*, 95.

[27]Scharf, T. *Polarized Light in Liquid Crystals and Polymers*, Wiley, New York, 2006.

Chapter 5

General Conclusions

Cellulose esters are biomass-derived materials with great potential as optical films. Besides their relatively good cost-performance, cellulose esters also possess excellent physical properties suitable for optical film application such as high transparency and excellent heat resistance. However, to fulfill the optical function, it is necessary for films to show optical birefringence required for the particular application such as no birefringence for polarizer protective films and extraordinary wavelength dispersion that a birefringence increases with increasing wavelength over a wideband of wavelength for retardation films. Consequently, it is of great importance to produce films with a controlled birefringence, *i.e.*, having a certain birefringence property, in order to fulfill various requirements in practical applications.

Despite the potential exhibited by cellulose esters, most of the reported studies on the control of orientation birefringence deal with a more conventional polymer such as PMMA. Therefore, there is serious lack of study that deals with cellulose esters or any biomass-derived polymers on this subject. Several techniques such as polymer blending, copolymerization and anisotropic crystal or molecule doping have been reported to be useful for modifying the orientation birefringence in polymers.

The main objective of this research was to study the control mechanism of orientation birefringence in cellulose esters. At first, the information on the molecular orientation and the birefringence of a solution-cast film for cellulose triacetate was investigated. These were discussed in the Second chapter. In solution-cast process, CTA molecules are induced to align in the film plane. Furthermore, the birefringence in the thickness direction, called "out-of-plane birefringence", shows positive out-of-plane birefringence with extraordinary wavelength dispersion, which is an indispensable property for advanced displays such as 3D and electro-luminescent display while the stretched film shows negative birefringence. The level of the out-of-plane birefringence for cast films can be controlled by the preparation conditions, which is shown with the information on molecular orientation. Moreover, it is firstly demonstrated that the birefringence and its wavelength dispersion can be further modified by the addition of an appropriate low-mass compound such as tricresyl phosphate (TCP). During the evaporation, TCP molecules orient in the film plane accompanied with the orientation of CTA chains by intermolecular orientation correlation, called nematic interaction. This will be a key technology in the field of high-performance optical films to improve the contrast of LCD, because there are numerous low-mass compounds having strong polarizability anisotropy.

As a method to control three-dimensional refractive indices and wavelength dispersion of birefringence in cellulose esters, we proposed to use a low-mass compound (LMC). The LMCs used have high polarizability as well as good miscibility with the host polymer. The Third Chapter generally discusses the effect of LMC addition on the in-plane and out-of-plane birefringence before and after stretching of cellulose esters were

studied. Plasticizers such as tricresyl phosphate (TCP) and triphenyl phosphate (TPP) and 4-cyano-4'-pentylbiphenyl (5CB) were added to cellulose esters such as cellulose triacetate (CTA) and cellulose acetate propionate (CAP). Then their viscoelastic properties and wavelength dispersion of birefringence were studied. In this study, CTA is a crystalline polymer with low level of crystallinity, it is show planar deformation mode to some degree only by uniaxial stretching. The transversal birefringence due to the transverseal orientation of CTA chains is magnified by plasticizeres.

Chapter Four discusses the effect of the types and amounts of the substituent ester groups on the in-plane and out-of-plane birefringences and its wavelength dispersion were investigated. The types and amounts of ester groups determine the sign and magnitude of the birefringence as well as the wavelength dispersion. Prior to stretching, the CTA film shows positive out-of-plane birefringence with extraordinary wavelength dispersion, whereas the stretched film shows negative birefringence. A remarkable result was observed in CAB and CAP, *i.e.*, show extraordinary dispersion of in-plane and out-of-plane birefringences, which is the essential property for the retardation film application. It was also demonstrated that types and contents of ester groups, rather than the pyranose chain, determine the sign and magnitude of birefringence as well as its wavelength dispersion. These facts explain the extraordinary dispersion of birefringence observed in CAP and CAB, which is attributed to the combination of positive birefringence having weak wavelength dependence, and negative birefringence having strong wavelength dependence.

This reserach demonstrated that cellulose esters are highly potential materials as an ideal optical film. Cellulose esters can be produced by solution-cast method which

provides the film without molecular orientation in the film plane. This is the reason why a solution-cast film is preferably employed for a protective film rather than a melt-extruded film. The level of the out-of-plane birefringence in cast films depends on the preparation conditions, which is predictable considering the evaporation rate. Certain types of cellulose esters such as CTA and CAP were also found to exhibit the positive out-of-plane birefringence with extraordinary wavelength dispersion, a property essential for wideband retardation films. As the type and amount of substitution groups can be varied the esterification process, from the viewpoint of material design, cellulose esters are highly flexible and offer boundless possibility. It is also demonstrated that three-dimensional refractive indices and wavelength dispersion of birefringence in cellulose esters can be altered by the addition of a small amount of low-mass compounds. This would open up possibilities of developing biopolymer-based optical films with birefringence suited for various functions in optical devices. Besides them, some possibilities are suggested for the future development cellulose esters such as the effect of processing condition and effect of low mass compound. Further, the fact that mechanism of the peculiar phenomenon of solution-cast film is also dependent on the contribution of crystalline phase leads to further understanding of the information on the molecular orientation of polymer. Finally, suitable technique should be improved and reviewed carefully to support to large scale industries with some effort to develop high performance cellulose ester films for optical films and new LCD device with good cost-performance.

Achievements

Publications

1. **Kultida Songsurang**, Azusa Miyagawa, Mohd Edeerozey Abd Manaf, Panitha Phulkerd, Shogo Nobukawa, Masayuki Yamaguchi.
   Optical Anisotropy in Solution-Cast Film of Cellulose Triacetate. *Cellulose*, **2013**, 20, 83-96.

2. **Kultida Songsurang**, Hikaru Shimada, Shogo Nobukawa, Masayuki Yamaguchi. Three-Dimensional Orientation Control by Uniaxial Drawing of Cellulose Triacetate Film. *To be submitted*

3. **Kultida Songsurang**, Hikaru Shimada, Shogo Nobukawa, Masayuki Yamaguchi. Optical Anisotropy of Cellulose Ester Films Prepared by Solution-Cast Method. *To be published*

4. Masayuki Yamaguchi**,** Mohd Edeerozey Abd Manaf, **Kultida Songsurang**, Shogo Nobukawa.
   Material Design of Retardation Films with Extraordinary Wavelength Dispersion of Orientation Birefringence – A review. *Cellulose*, **2012**, 19, 601-613.

Book Chapter

1. **Kultida Songsurang**, Hikaru Shimada, Shogo Nobukawa, Masayuki Yamaguchi. "Optical Anisotropy of Cellulose Esters and Its Application to Optical Functional Films" in "Handbook of Sustainable Polymers: Processing and Applications", to be published by Stanford publisher –Singapore. *Accepted*

Presentations

International Conferences

Reviewed

1. **Kultida Songsurang**, Shogo Nobukawa, Masayuki Yamaguchi
   Control of Orientation Birefringence of Cellulose Triacetate with Aromatic Compound
   Annual Meeting of Plastic Engineering (ANTEC2012), April 2-4, 2012, Orlando, USA.

2. **Kultida Songsurang**, Shogo Nobukawa, Masayuki Yamaguchi
   Optical Properties in Solution-Cast Film of Cellulose Triacetate
   4th International Conference on Biodegradable and Biobased Polymers (*BIOPOL-2013*), October 1-3, 2013, Rome, Italy.

3. **Kultida Songsurang**, Shogo Nobukawa, Masayuki Yamaguchi
   Novel Method to Control the Optical Anisotropy for Cellulose Derivative
   International Conference on Material Science and Material Engineering (MSME2014), March 14-16, 2014, Chicago, USA.

4. **Kultida Songsurang**, Shogo Nobukawa, Masayuki Yamaguchi
   Optical Anisotropy in Solution-Cast Film of Cellulose Esters
   Annual Meeting of Plastic Engineering (ANTEC2014), April 28-30, 2014, Las Vegas, Nevada, USA.

Non-reviewed

5. **Kultida Songsurang**, Mohd Edeerozey Abd Manaf, Shogo Nobukawa, Masayuki Yamaguchi
   Rheological and Optical Properties of Cellulose Esters - Control of Orientation Birefringence of Cellulose Triacetate
   8th International Symposium on Advanced Materials in Asia Pacific (ISAMAP), November 3-5, 2011, Busan, Korea.

6. **Kultida Songsurang**, Shogo Nobukawa, Masayuki Yamaguchi
   Control of Out-of-Plane Birefringence of Solution-Cast Film
   4th International Workshop on Polymer Engineering and Processing, March 15, 2011, Nomi, Japan.

7. **Kultida Songsurang**, Shogo Nobukawa, Masayuki Yamaguchi
   Orientation Birefringence in Solution-Cast Films of Cellulose Triacetate
   International Symposium on Advanced Materials 2013, October 17-18, 2013, Ishikawa, Japan.

Domestic Conferences

Non-reviewed

1. **Kultida Songsurang**, Mohd Edeerozey Abd Manaf, Shogo Nobukawa, Masayuki Yamaguchi
   Control of Orientation Birefringence of Cellulose Triacetate
   60th Symosium on Macromolecules, September 28-30, 2011, Okayama, Japan.

2. **Kultida Songsurang**, Shogo Nobukawa, Masayuki Yamaguchi
   Optical Retardation of Solution-Cast Films for Cellulose Triacetate
   62nd SPSJ Annual Meeting, May 29-31, 2013, Kyoto, Japan.

3. **Kultida Songsurang**, Shogo Nobukawa, Masayuki Yamaguchi
   Out-of-Plane Birefringence of Cellulose Esters
   62nd Symosium on Macromolecules,SPSJ, September 11-13, 2013, Kanazawa, Japan.

4. **Kultida Songsurang**, Shogo Nobukawa, Masayuki Yamaguchi
   Optical Anisotropy of Cellulose Ester Films Prepared by Solution-Cast Method
   61st Rheology symposium, September 25-27, 2013, Yamagata, Japan.

Other Publications

1. **Kultida Songsurang**, Jatuporn Pakdeebumrung, Narong Praphairaksit, Nongnuj Muangsin.
   Sustained Release of Amoxicillin from Ethyl Cellulose-Coated Amoxicillin/Chitosan-Cyclodextrin-Based Tablets. *AAPS PharmSciTech*, **2011**, 12, 35-45.

2. **Kultida Songsurang**, Nalena Praphairaksit, Krisana Siraleartmukul, Nongnuj Muangsin.
   Electrospray Fabrication of Doxorubicin-Chitosan-Tripolyphosphate Nanoparticles for Delivery of Doxorubicin. *Archives of Pharmacal Research*, **2011**, 34, 583-592.

3. **Kultida Songsurang**, Phruetchika Suvannasara, Chuttree Phurat, Songchan Puthong, Krisana Siraleartmukul, Nongnuj Muangsin.
   Enhanced anti-topoisomerase II activity by mucoadhesive 4-CBS-chitosan/poly (lactic acid) nanoparticles. *Carbohydrate Polymers*, **2013**, 98, 1335-1342.

4. **Kultida Songsurang**, Chuttree Phurat, Songchan Puthong, Krisana Siraleartmukul, Nongnuj Muangsin.
   Hydrophobic chitosan/poly (lactic acid) composite nanoparticles for controlled doxorubicin delivery. *International Journal of Nanomedicine, Submitted as the revised manuscript*

5. **Kultida Songsurang**, Chuttree Phurat, Songchan Puthong, Krisana Siraleartmukul, Nongnuj Muangsin.
   Encapsulation and Controlled Release of Sesamin-sesamolin via Alignate/kappa-Carrageenan Hydrogel Beads as Food Supplyments. *Foodchem, Submitted*

Awards

1. Grant for Researchers Attending International Conferences, Research Foundation for the Electrotechnology of Chubu (REFEC) to present at ISAMAP and IWNM 2011, Busan, Korea, November 2011.

2. Grant for Researchers Attending International Conferences, Research Foundation for the Electrotechnology of Chubu (REFEC) to present at MSME 2014, Chicago, USA, March 2013.

3. Grant for PhD student, Thailand Research Fund through the Royal Golden Jubilee Ph.D. Program (Grant No. PHD/0099/2554), June 2012- June 2014.

Enhanced Anti-Topoisomerase II Activity by Mucoadhesive 4-CBS–Chitosan/Poly (lactic acid) Nanoparticles

1. Introduction

Topoisomerase II (Topo II) is a enzyme that passes an intact helix through a transient double-stranded break in DNA to modulate the DNA topology using ATP and plays a key role in transcription, replication, and chromosome segregation [1]. DNA is a cellular target for a number of widely used antitumor agents, such as doxorubicin (DOX) as well as etoposide [2]. Moreover, antitumor agents also intercalate into DNA and form reactive metabolites that interact with many intracellular molecules. A considerable interest has therefore arisen in combining Topo II inhibitors with a mucoadhesive polymer for enhancement of the Topo II activity.

Recently, mucoadhesive biodegradable and biocompatible polymeric nanoparticles have become a topic of great interestin biomedical applications to increase the specificity and localization at the target site enhance the permeability property and improve the delivery efficiency [3-5]. Chitosan, one of the most promising biodegradable polymers, has gained increasing attention in the pharmaceutical field due to its favorable biological properties, *i.e.*, non-toxic, biocompatible and biodegradable [6,7]. Moreover, chitosan chains show good adhesive properties on mucosal surfaces, a property that can

be exploited for the development of bioadhesive delivery devices. In our previous work, we developed mucoadhesive chitosan by modification with 4-carboxybenzenesulfonamide (4-CBS) for stomach-specific drug delivery, specifically for the treatment of Helicobacter pylori infections. In that study, the mucoadhesive 4-CBS–chitosan was shown to have enhanced mucoadhesive and swelling properties in the simulated gastric fluid (SGF; 0.1 M HCl, pH 1.2). Furthermore, the modified chitosan displayed antibacterial activity against Escherichia coli and Staphylococcus aureus and appeared non-toxic to Vero, KB, MCF-7 and NCI-H187 cell lines in tissue culture [8].

Despite these advantageous characteristics of chitosan, its insolubility in either water or common organic solvents and its poor mechanical properties for supporting tissue cells have limited basic research and various bio-fabrication applications [9,10]. Several approaches have been taken to overcome the limitations of chitosan, i.e., graft polymerization [11], blending [12] and mixing with other polymers [13] such as poly (lactic acid) (PLA) [14], which can impart desirable mechanical properties to the resultant copolymer composite while retaining the desirable properties of chitosan.

The aim of this work was to prepare a mucoadhesive polymer composite for non-paraenterally administered routes, particularly in mucoadhesive sites. Therefore, the present work focuses on the preparation and in vitro dug release behavior; Topo II inhibitory activity; and evaluation of the cytotoxic activity of doxorubicin (DOX)-loaded 4-CBS–chitosan/PLA nanoparticles formed by electrospray ionization.

2. Experimental

2.1 Materials

Chitosan with a deacetylation level of 95% (Mw = 400 kDa) was purchased from Biolife (Thailand). The PLA, with a View the MathML source of 121.4 kg/mol and consisting of a 1:24 mole ratio of d-lactide:l-lactide, was purchased from NatureWorks 2000D (Thailand). The 4-CBS and 1-ethyl-3-(3-dimethylaminopropyl) carbodiimide hydrochloride (EDAC) were obtained from Sigma (St. Louis, USA). Cellulose dialysis tubing (Membrane Filtration Products, Inc., USA) with a 12–14 kDa molecular weight cut-off was used to purify all of the modified chitosan. The doxorubicin (DOX) hydrochloride, etoposide, PBR322 plasmid, sodium tripolyphosphate (TPP) and SDS were purchased from Sigma Aldrich. Human Topo II was purchased from Amersham (UK), andlactic acid was purchased from Union chemicals (Thailand). All other chemicals used in this work were of reagent grade.

2.2 Measurements

2.2.1 Preparation of 1:1 (w/w) DOX-loaded 4-CBS–CS/PLA nanoparticles

Firstly, the 4-CBS–chitosanwas prepared via the coupling reaction of 4-CBS to chitosan in the presence of EDAC as a coupling reagent as previously reported [8]. Then, the preparation of DOX-loaded 4-CBS–chitosan/PLA nanoparticles was formed by ionic cross-linking. Briefly, DOX was added to a solution of 1% (w/v) 4-CBS–chitosan/PLA at three different (w/w) ratios of 4-CBS–chitosan to PLA (1:1, 1:2, and 2:1), selected for two different amounts of DOX (1% and 2%, w/v) in 4:1 (v/v) dichloromethane: toluene, and subsequently electrosprayed into 80 mL of a 5% (w/v)

aqueous solution of TPP. An applied voltage of 10 kV, an 8-cm working distance, a 800-rpm stirring rate, 20 G needle, and a flow rate of 10 mL/h were used for the electrospray ionization process.

The DOX-loaded hydrophobic 4-CBS–chitosan/PLA colloidal nanoparticles formed spontaneously under mild agitation at room temperature, and after 30 min of stirring, the colloidal nanoparticles were harvested by centrifugation at 15,000 × g for 30 min. The supernatant was discarded, and the deposit was re-dispersed in distilled water for further use.

2.2.2 Characterization of the 4-CBS–chitosan/PLA nanoparticles with or without DOX loading

Samples for scanning electron microcopy (SEM) analysis were prepared by sprinkling the dried nanoparticles on one side of a double adhesive stub. The stub was subsequently coated with gold under vacuum conditions. The microcapsules were observed via SEM (Phillips XL30CP) operating in the range from 10 kV to 20 kV.

2.2.3 Evaluation of in vitro DOX release

The DOX release from the 4-CBS–chitosan/PLA nanoparticles was studied as a suspension in phosphate buffer (PBS) at pH 7.4 using the dialysis bag diffusion technique. Accurately weighed quantities (~10 mg) of nanoparticles were enclosed in a dialysis bag (molecular weight cutoff of 3.5 kDa) and dialyzed against 50 mL of PBS at pH 7.4 in a flask, which was shaken at 100 rounds per minute (rpm) and incubated at 37 ± 1 °C. At designated time points, 200 μL of the dialyzed PBS was removed for analysis

of the DOX content (spectrophotometrically at 480 nm, as detailed above) and replaced by an equal volume of fresh PBS. The amount of released DOX was determined over 30 days, correcting for the PBS replacements each time.

2.2.4 Inhibition of topoisomerase II (Topo II) activity

The 4-CBS–chitosan/PLA nanoparticles, with or without DOX-loading, were screened for in vitro inhibitory activity against Topo II activity in terms of the ability of the nanoparticles to inhibit the conversion of supercoiled PBR322 plasmid double-stranded (ds) DNA to its relaxed form by human Topo II.

The Topo II reaction was performed in 20 μL of reaction mixture containing 10 mM Tris–HCl (pH 7.9), 175 mM KCl, 0.1 mM EDTA, 5 mM MgCl2, 2.5% (v/v) glycerol, 1 mM ATP, 0.5 mM dithiothreitol, 30 μg/mL bovine serum albumin, 0.2 μg pBR322 plasmid DNA, 0.3 units (U) of human DNA Topo IIα and the test compound (100 μM) in a final volume of 50 μL. An addition of etoposide instead of the test sample was used as a positive control. The reaction mixtures were incubated at 37 °C for 30 min and terminated by the addition of 3 μL of an aqueous solution of 0.77% (w/v) SDS/77 mM EDTA. The samples were mixed with 2 μL of an aqueous solution of 30% (w/v) sucrose, 0.5% (w/v) bromophenol blue and 0.5% (w/v) xylene cyanol and subsequently resolved by electrophoresis on a 1% (w/v) agarose-TBE gel at 1.5 V/cm for 10 h. The gels were stained for 30 min in an aqueous solution of ethidium bromide (0.5 μg/mL) and rinsed. The DNA bands were visualized by UV transillumination and quantified using an image analyzer and Syngene software [15].

3. Results and Discussion

3.1 Preparation of the 4-CBS–chitosan/PLA complex

The first modification in this study was achieved via the covalent attachment of 4-CBS to chitosan using EDAC as the activating agent, as described previously [8]. The 4-CBS–chitosan was white in color and odorless. The polymer displayed a fibrous structure and was easily dissolved in 1% (v/v) acetic acid solution to form a high viscosity pale yellow gel. The obtained 4-CBS–chitosan was synthesized and verified by 1H NMR and FTIR measurements (data not shown) accordingly with the methodologies described in the previous work, Suvannasara et al. (2013). The 4-CBS–chitosan samples with % DS values of 4.1–13.3 were obtained by changing the weight ratio of 4-CBS to the primary amine groups (-NH2) of the CS from 0.05 to 1. The second modification was performed between 4-CBS–CS and PLA via a complexation method by mixing of aqueous 4-CBS–chitosan with SDS followed by solution mixing of the hydrophobic 4-CBS–chitosan complex with PLA (with or without the DOX to be encapsulated), and electrospray ionization was carried out to obtain the 4-CBS–chitosan/PLA composite nanoparticles. It was noticeable that the hydrophobic 4-CBS–chitosan complex appeared as a gel and could be dissolved in such low- or non-polar solvents as toluene, hexane and dichloromethane (data not shown), thus revealing the likely hydrophobic nature of the 4-CBS–chitosan complex. Therefore, the obtained hydrophobic 4-CBS–chitosan was likely compatible with PLA. Accordingly, the 4-CBS–chitosan/PLA composite was synthesized by the solution mixing method using the hydrophobic 4-CBS–chitosan prepared from complexation of 4-CBS–chitosan and SDS. For DOX-loaded 4-CBS–chitosan/PLA composites, 1% (w/v) DOX was added to a

solution of 1% (w/v) 4-CBS–chitosan/PLA in 4:1 (v/v) dichloromethane: toluene and electrosprayed into 80 mL of a 5% (w/v) aqueous solution of TPP.

3.2 Characterization of the 4-CBS–chitosan/PLA nanoparticles with or without DOX loading

Fig. 1 shows representative SEM images of the surface morphology of anhydrous 4-CBS–chitosan/PLA and DOX-loaded 4-CBS–chitosan/PLA nanoparticles at three different (w/w) ratios of 4-CBS to PLA (1:1, 1:2, and 2:1, w/w). The anhydrous 4-CBS–chitosan/PLA nanoparticles (Fig. 1a and b) were uniformly spherical in shape, with visible pores and an average particle size of 228 ± 39 nm. In the case of the DOX-loaded 4-CBS–chitosan/PLA nanoparticles (Fig. 1c–f), the majority of the particles were also spherical in form and devoid of aggregates, with a slightly larger size than that of the unloaded 4-CBS–chitosan/PLA nanoparticles except for 1% DOX-loaded (1:2, w/w) 4-CBS–chitosan/PLA. Therefore, the size of the particles decreased with increasing PLA ratio. Moreover, the size of the particles increased with increasing DOX ratio.

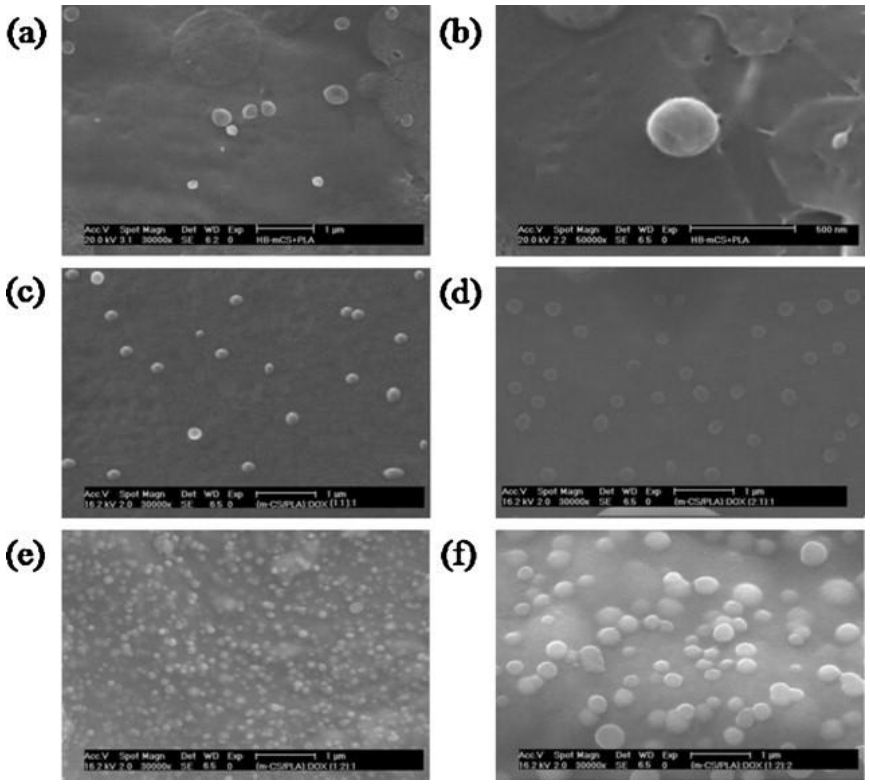

Fig. 1 SEM images of particles: (a) 4-CBS–chitosan/PLA at wide screen, (b) 4-CBS–chitosan/PLA (capture of one particle), (c) (4-CBS–chitosan/PLA)-DOX (1:1, w/w)-1%, (d) (4-CBS–chitosan/PLA)-DOX (2:1, w/w)-1%, (e) (4-CBS–chitosan/PLA)-DOX (1:2, w/w)-1% and (f) (4-CBS–chitosan/PLA)-DOX (1:2, w/w)-2%

3.3 In vitro DOX release profiles

The release of the DOX from encapsulated nanoparticles is another important factor that determines their suitability. The release behavior of DOX from hydrophobic chitosan/PLA (our previous study, data not shown) and 4-CBS–chitosan/PLA nanoparticles was evaluated in PBS (pH 7.4) by dialysis until 100% of the DOX had been released (Fig. 2).

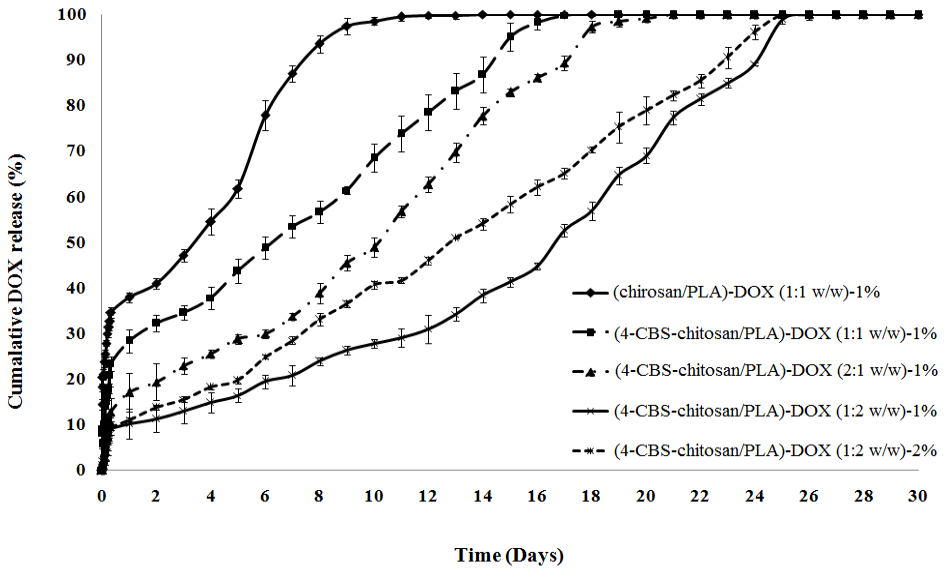

Fig. 2 Cumulative DOX release profile from (chitosan/PLA)-DOX (1:1, w/w)-1%, (4-CBS–chitosan/PLA)-DOX (1:1, w/w)-1%, (4-CBS–chitosan/PLA)-DOX (2:1, w/w)-1%, (4-CBS–chitosan/PLA)-DOX (1:2, w/w)-1% and (4-CBS–chitosan/PLA)-DOX (1:2, w/w)-2% nanoparticles at pH 7.4 and 37 °C.

3.3.1. Effect of CS/PLA and 4-CBS–CS/PLA with DOX

The release behavior of DOX from the nanoparticles can be described in a graph, and the release rate of DOX-loaded chitosan/PLA and 4-CBS–chitosan/PLA is shown in Fig. 2.

The cumulative release of DOX from (chitosan/PLA)-DOX (1:1, w/w)-1% exhibited the two release stages. In first stage, the drug was burst-released by approximately 35% within 8 h, followed by the slower release rate of the second stage over8 days and a slow sustained release rate to 100% by 12–14 days (data not shown). However, in the case of the 1:1 (w/w) DOX-loaded 4-CBS–chitosan/PLA nanoparticles,

also at 1% (w/v) in PBS pH 7.4, a much slower biphasic and sustained release of DOX was observed. In the first stage, the drug was released by approximately 20% within 8 h. In the second stage, the release rate was slower and was sustained up to 18 days.

It was clearly observed that (4-CBS–chitosan/PLA)-DOX (1:1, w/w)-1% showed a significantly prolonged release profile of DOX up to18 days compared with that of (chitosan/PLA)-DOX (1:1, w/w)-1%. Thus, 4-CBS–chitosan/PLA was selected for further studies to improve the release profile.

3.3.2. Effect of4-CBS–CS and PLA with DOX

The release rates for DOX-loaded (4-CBS–chitosan/PLA)-DOX (2:1, w/w)-1%, (4-CBS–chitosan/PLA)-DOX (1:2, w/w)-1% and (4-CBS–chitosan/PLA)-DOX (1:2, w/w)-2% nanoparticles are given in Fig. 2.

The in vitro release profiles of (4-CBS–chitosan/PLA)-DOX (2:1, w/w)-1%, (4-CBS–chitosan/PLA)-DOX (1:2, w/w)-1% and (4-CBS–chitosan/PLA)-DOX (1:2, w/w)-2% nanoparticles were investigated in phosphate buffer solution (PBS, pH 7.4) until 100% of the drug was released, and these formulations showed sustained release profiles. The (4-CBS–chitosan/PLA)-DOX (2:1, w/w)-1% nanoparticles exhibited nearly 50% and 80% release within 10 and 15 days, respectively, followed by continuing release. The release profiles of the (4-CBS–chitosan/PLA)-DOX (1:2, w/w)-1% nanoparticles exhibited nearly 50% and 80% release within 17 and 22 days, respectively, and DOX displayed subsequent sustained released. It was observed that the release rate of (4-CBS–chitosan/PLA)-DOX (1:2, w/w)-1%was slower than that of the (4-CBS–chitosan/PLA)-DOX (2:1, w/w)-1%nanoparticles. If the amount of PLA

was increased, the release rate was slower and the release was prolonged from 18 days to 26 days. Therefore, (4-CBS–chitosan/PLA)-DOX (1:2, w/w)-1% nanoparticles were selected for further studies.

With increases in the loaded DOX, the periods of release remained the same (26 days), but the release rate was faster due to the higher loading of DOX.

It was obvious that the cumulative release of DOX increased with the increasing amount of DOX in the formulation. The higher level of DOX corresponding to a lower level of the polymer in the formulation resulted in an increase in the cumulative percentage release. As additional drug was released from the nanoparticles, more channels were produced, thus contributing to faster drug release. In addition, higher drug levels in the nanoparticle formulation produced a higher drug concentration gradient between the nanoparticles and dissolution medium, and thus the cumulative release of drug was also increased [16].

3.3 Topo II activity assay

Topo II is a nuclear enzyme that catalyzes changes in the topological state of DNA by single-strand breaking and rejoining of (ds)DNA. This enzyme plays important roles in DNA metabolism, including replication, recombination, transcription and chromosome condensation. The DNA is a double helix with a mostly supercoiled structure. However, supercoiled DNA must be relaxed by the Topo II enzyme before processing during transcription, repair or replication. DOX is known to inhibit Topo II activity, and thus the ability of the DOX-loaded polymer nanoparticles to inhibit the relaxation of supercoiled pBR322 plasmid dsDNA by human Topo II was evaluated as a

measure of the release of functional DOX from the DOX-loaded hydrophobic chitosan/PLA (1:1, w/w) and 4-CBS–chitosan/PLA nanoparticles at three different (w/w) ratios of 4-CBS to PLA (1:1, 1:2, and 2:1, w/w).

As shown in Fig. 3, the % inhibition was classified into strongly or weakly active, depending on whether the% inhibition was lower or higher than the activity of the reference control of100 μM etoposide (63.4% inhibition). All formulations of DOX-loaded 4-CBS–chitosan/PLA nanoparticles displayed a strong Topo II inhibitory activity with greater than 63.4% inhibition at 100 μM. The (4-CBS–chitosan/PLA)-DOX (1:1, w/w)-1% (63.4%) displayed stronger Topo II inhibition than (hydrophobic chitosan/PLA)-DOX (1:1, w/w)-1% (59.4%) nanoparticles at 100 μM. The results suggest that 4-CBS–chitosan enhanced the anti-Topo II activity. Furthermore, (4-CBS–chitosan/PLA)-DOX (1:2, w/w)-2% showed the strongest Topo II inhibition (over 77.4%) compared with etoposide as the reference (63.4%). Accordingly, the DOX-loaded 4-CBS–chitosan/PLA nanoparticles would appear to release functional DOX, and therefore, if the nanoparticles are internalized into the cells (or if the DOX is released nearby and taken up by the target cells), this delivery could be a potentially potent inhibitor of Topo II activity.

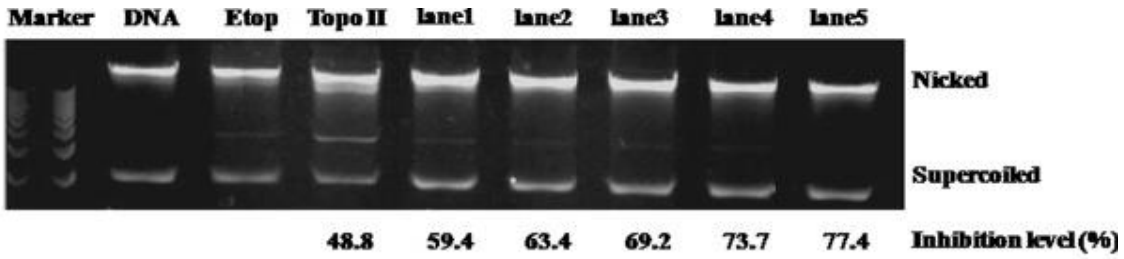

Fig. 2 Inhibitory effects of tested compounds on human DNA topoisomerase II (lane 1): (chitosan/PLA)-DOX (1:1, w/w)-1%, (lane 2): (4-CBS–chitosan/PLA)-DOX (1:1, w/w)-1%, (lane 3): (4-CBS–chitosan/PLA)-DOX (2:1, w/w)-1%, (lane 4): (4-CBS–chitosan/PLA)-DOX (1:2, w/w)-1%, (lane 5): (4-CBS–chitosan/PLA)-DOX (1:2, w/w)-2%.

4. Conclusions

The 4-CBS–chitosan/PLA nanoparticles were fabricated via electrospray ionization for the delivery of DOX as a model payload drug. The size distribution of the DOX-loaded 4-CBS–chitosan/PLA nanoparticles was relatively narrow (PDI of 0.455–0.705) and yielded a high EE (over 60%). The DOX-loaded 4-CBS–chitosan/PLA nanoparticles exhibited prolonged release of DOX and more sustained release, up to 26 days. The DOX-loaded 4-CBS–chitosan/PLA nanoparticles may be an advantageous alternative vehicle for sustained release formulation of DOX in the treatment of certain cancers.

References

[1] Kılıçay, E.; Demirbilek, M.; Türk, M.; Güven, E.; Hazer, B.; Denkbas, E. B. *Eur. J. Pharm. Sci.* **2011**, *44*, 310–320.

[2] Zunino, F.; Capranico, G. *Anti-Cancer Drug Des.* **1990**, *5*, 307–317.

[3] Andrews, G. P.; Laverty, T. P.; Jones, D. S. *Eur. J. Pharm. Biopharm.* **2009**, *71*, 505–518.

[4] Bernkop-Schnurch, A. *Adv. Drug Deliv. Rev.* **2005**, *57*, 1569–1582.

[5] Dodou, D.; Breedveld, P.; Wieringa, P. A. *Eur. J. Pharm. Biopharm.* **2005**, 60, 1–16.

[6] Songsurang, K.; Pakdeebumrung, J.; Praphairaksit, N.; Muangsin, N. *AAPS PharmSciTech* **2011**, *12*, 35–45.

[7] Wan, Y.; Wu, H.; Yu, A.; Wen, D. *Biomacromolecules* **2006**, *7*, 1362–1372.

[8] Suvannasara, P.; Juntapram, K.; Praphairaksit, N.; Siralertmukul, K.; Muangsin, N. *Carbohyd Polym* **2013**, *94*, 244–252.

[9] Feng, H.; Dong, C. M. *Carbohyd. Polym.* **2007**, *70*, 258–264.

[10] Huang, Y.; Yu, H.; Guo, L.; Huang, Q. *J. Phys. Chem. B.* **2010**, *114*, 7719–7726.

[11] Liu, L.; Wang, Y.; Shen, X.; Fang, Y. *Biopolymers* **2005**, *78*, 163–170.

[12] Zhang, R.; Xu, W.; Jiang, F. *Fiber Polym.* **2012**, *13*, 571–575.

[13] Chouwatat, P.; Polsana, P.; Noknoi, P.; Siralertmukul, K.; Srikulkit, K. *J. Miner. Met. Mater. Soc.* **2010**, *20*, 41–44.

[14] Wu, Y.; Li, M.; Gao, H. *J. Polym. Res.* **2009**, *16*, 11–18.

[15] Lin, T.; Fang, J.; Wang, H.; Cheng, T.; Wang, X. *Nanotechnology* **2006**, *17*, 3718–3723.

[16] Zhao, C. L.; Holl, Y.; Pith, T.; Lambla, M. *Colloid. Polym. Sci.* **1987**, *265*, 823–829.

Acknowledgements

Firstly and foremost I would like to express the deepest gratitude to my supervisor, Prof. Masayuki Yamaguchi for intellectual support, supervision, and enthusiasm throughout the completion of my doctoral study. It has been an honor to be his Ph.D. student. I am most grateful for his teaching and advice, not only the research methodologies but also many other methodologies in life. I appreciate all his contributions of time, ideas, and funding to make my Ph.D. experience productive and stimulating. The joy and enthusiasm he has for her research was contagious and motivational for me, even during tough times in the Ph.D. pursuit. I would not have achieved this far and this thesis would not have been completed without all the support that I have always received from him.

Secondly, I would like to express my appreciation to Professor Minoru Terano and Assistant Professor Shogo Nobukawa, who provided me a lot of valuable support. I also deeply appreciate the members of my committee: Professor Noriyoshi Matsumi, Associate Professor Tatsuo Kaneko, and Associate Professor Toshiaki Taniike of JAIST, and Professor Dr. Akihiro Tagaya of Keio University for their helpful comments

I am profoundly grateful to Professor Mikio Miyake for his generous hospitality and support throughout my sub-theme research. I am particularly very grateful to Chulalongkorn University and the Thailand Research Fund through the Royal Golden Jubilee Ph.D. Program (Grant No. PHD/0099/2554) for financial support during my

doctoral study. Further, I would like to show my best gratitude to my supervisor at Chulalongkorn University, Associate Professor Nongnuj Muangsin for her help and valuable advice during my completion sub-theme research. Without these facilities and sponsorship, I would not have been able to achieve and complete my study.

I am particularly very grateful to the Doctoral Dual Degree Program (JAIST-CU) for financial support during my doctoral study. Without these facilities and sponsorship, I would not have been able to achieve and complete my study.

I am indebted to my many colleagues who supported me throughout my study. My special thanks are extended to all present and former members of Yamaguchi Laboratory especially to Mohd Edeerozey Abd Manaf, Azusa Miyagawa, Hikaru Shimada, and Yoshiharu Fukui for their help and cooperation during my preparation of the experimental data.

Finally, I would like to extend my deepest gratitude to my family. Without their constant love, assistance, and encouragement, I would not have finished this thesis. Thank you, all Thai members in JAIST especially to Panitha Phulkerd, Jiraporn Seemork, Monchai Siriprumpoonthum and everyone else for their love, emotional support and making me feel less lonely.

Kultida Songsurang

March, 2014

Ishikawa, Japan